Fluorescence-Based Detection Methodologies for Nitric Oxide Using Transition Metal Scaffolds

By
Scott A. Hilderbrand
B.A., Chemistry
New College of Florida, 1998

SUBMITTED TO THE DEPARTMENT OF CHEMISTRY IN PARTIAL
FUFILLMENT OF THE REQUIREMENTS FOR THE DEGREE OF

DOCTOR OF PHILOSOPHY IN INORGANIC CHEMISTRY
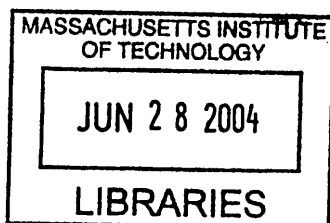AT THE
MASSACHUSETTS INSTITUTE OF TECHNOLOGY

June 2004

Signature of Author:_____
Department of Chemistry
February 4, 2004

Certified by:_____
Stephen J. Lippard
Arthur Amos Noyes Professor of Chemistry
Thesis Supervisor

Accepted by:_____
Robert W. Field
Chairman, Departmental Committee on Graduate Studies

This doctoral thesis has been examined by a committee of the Department of Chemistry as follows:

_____

Alan Davison
Committee Chairman
Professor of Chemistry

_____

Stephen J. Lippard
Arthur Amos Noyes Professor of Chemistry
Thesis Supervisor

_____

Daniel G. Nocera
W. M. Keck Professor of Energy and Professor of Chemistry

Fluorescence-Based Detection Methodologies for Nitric Oxide Using Transition Metal Scaffolds

By
Scott A. Hilderbrand

Submitted to the Department of Chemistry on February 4, 2004, in partial fulfillment of the requirements for the Degree of Doctor of Philosophy.

Abstract

Chapter 1. Fluorescence-Based Detection Methodologies for Nitric Oxide: A Review

This chapter presents a review of current fluorescence-based detection systems for nitric oxide. These systems include non-reversible organic fluorophore systems such as those based on the o-diamine functionality, fiber-optic probes, and transition metal based systems. None of these systems currently are capable of reversible detection of nitric oxide, although, the utilization of transition-metal nitrosyl chemistry is a promising avenue for development of such sensors.

Chapter 2. Cobalt Chemistry with Mixed Aminotroponimine Salicylaldimine Ligands: Synthesis, Characterization, and Nitric Oxide Reactivity

A new class of mixed aminotroponimine salicylaldimine ligands and their corresponding cobalt(II) complexes are reported. The H_2^{iPr}SATI-n (n = 3,4) ligands contain an aminotroponimine and a salicylaldimine fragment connected by an alkyl linker. In the H_2^{iPr}FATI-n (n = 3,4) ligands, a derivatized fluorescein moiety replaces the salicylaldimine fragment. The cobalt(II) complexes [Co(^{iPr}SATI-3)] and [Co$_2$(^{iPr}SATI-4)$_2$] were prepared and structurally characterized. The reaction of NO with both complexes ultimately results in the formation of a putative dinitrosyl species. The mononitrosyl, [Co(^{iPr}SATI-3)(NO)], is isolated and characterized. The NO reactivity of [Co(^{iPr}FATI-3)] and [Co$_2$(^{iPr}FATI-4)] mimic that observed for the salicylaldimine derivatives as monitored by solution IR spectroscopy. When monitored by fluorescence spectroscopy, the reaction of [Co(^{iPr}FATI-3)] with NO affords a 20% increase in the fluorescence emission intensity after 4 h, whereas with [Co$_2$(^{iPr}FATI-4)] a 3-fold enhancement of emission intensity is observed after 22 h.

4

Chapter 3. Carboxylate-Bridged Dimetallic Complexes as Potential Nitric Oxide Sensors

The suitability of carboxylate-bridged dimetallic complexes containing fluorophore conjugates for the detection of nitric oxide was investigated. The diiron(II) complex $[Fe_2(\mu-O_2CAr^{Tol})_4(Ds-pip)_2]$, reacts with NO within one minute, affording a 4-fold increase in fluorescence emission intensity. The diiron complex, however, is sensitive towards dioxygen. The air stable dicobalt analog was also synthesized and its reactivity studied. In solution, the dicobalt complex is in dynamic equilibrium between the paddlewheel $[Co_2(\mu-O_2CAr^{Tol})_4(Ds-pip)_2]$, and windmill $[Co_2(\mu-O_2CAr^{Tol})_2(O_2CAr^{Tol})_2(Ds-pip)_2]$, geometric isomers. Reaction of $[Co_2(\mu-O_2CAr^{Tol})_4(Ds-pip)_2]$ with excess NO proceeds by reductive nitrosylation. Reduction of the Co(II) to Co(I) corresponds to formation of the double dinitrosyl cobalt complex, $[Co(\mu-O_2CAr^{Tol})_2(NO)_4]$ and is accompanied by the release of the coordinated dansyl fluorophore, which is N-nitrosated in the process. Release of the Ds-pip fluorophore gives an overall 9.6-fold increase in fluorescence emission intensity. Although not water soluble or reversible, these complexes demonstrate the potential use of the ligand dissociation strategy to prepare fluorescence-based sensors for nitric oxide.

Chapter 4. Dirhodium Tetracarboxylate Scaffolds as Reversible Fluorescence-Based Nitric Oxide Sensors

The synthesis and characterization of dirhodium tetracarboxylate complexes with dansyl-imidazole (Ds-im) and dansyl-piperazine (Ds-pip) is reported. The fluorophores coordinate to the axial sites of the dirhodium core through the imidazole or piperazine N-atom and emit only weakly when excited at 365 or 345 nm for the Ds-im and Ds-pip complexes, respectively. The dinitrosyl complexes, $[Rh_2(O_2CR)_4(NO)_2]$ R = Me, Et, n-Pr, have been prepared and structurally characterized. The dinitrosyl adducts are air stable and lose NO on standing in solution. The fluorophore complexes were investigated for their ability to elicit a fluorescence response in response to NO. An immediate increase in fluorescence emission intensity of more than 15-fold is observed when NO is admitted to solutions containing $[Rh_2(O_2CMe)_4]$ and Ds-pip or Ds-im. In both systems the fluorescence response is reversible. Sequestration of the fluorophore complexes from an aqueous solution by an NO permeable membrane allows detection of aqueous NO.

Thesis Supervisor: Stephen J. Lippard
Title: Arthur Amos Noyes Professor of Chemistry

This thesis is dedicated to my family

Acknowledgements

Although trying at times, I am grateful for my time at MIT. Only now can I begin to appreciate fully the intense intellectual environment at MIT, which has driven me to expand my knowledgebase and has contributed to my development as a chemist.

First I must thank my advisor, Steve Lippard, for providing an environment conductive to learning and the advancement of science. Steve's intellectual insight, ideas, and overall enthusiasm were particularly helpful in directing my research and keeping me excited about the nitric oxide sensor project. I would also like to thank Professors Dan Nocera and Alan Davison, the other members of my thesis committee, for many valuable suggestions.

When I joined the lab as a first year graduate student in the fall of 1998, I received my initial indoctrination into lab culture from Kathy Franz. Kathy was instrumental in helping me in the lab and in particular with helping me get started on the NO sensor project. I also owe a great deal of gratitude to all of the other members (past and present) of the once fledgling neurochemistry subgroup. In particular, I would like to thank Shawn Burdette for sharing his expertise and knowledge of preparing functionalized fluoresceins. Other neurochemistry subgroup members; Caroline Woodroofe, Liz Nolan, Mi Hee Lim, Ben Davis, Matt Clark, and Chris Chang provided numerous hours of entertaining conversation, both scientific and casual. Matt Clark's synthetic organic prowess was particularly helpful in helping me strategize routes to new ligands for investigation. Chris Chang's ability to see the big picture and to provide useful strategic insight was greatly appreciated. Special thanks are also in order for Mi Hee Lim, to whom I am handing over the NO sensor project. I am confident that she will achieve great things in the coming years. I also thank all members of the Journal Club, you know who you are, for the good times and conversation. In addition, my desk mates, Emily Carson, Rayane Moreira, and Sungho Yoon were always ready for those early morning coffee breaks and provided hours of conversation. Finally, I thank all other members of the Lippard lab for helping to create an enjoyable and relaxed working environment.

I would like to thank my family whose support and encouragement is especially appreciated. My parents constantly offered help and advise at every turn during my tenure at MIT. Their help was particularly invaluable in helping me stay motivated when my research was not progressing at a pace with which I was happy. I owe the most gratitude to Sarah, my wife, for her unwavering support and understanding during my gradate career. Her support during the last months of my thesis preparation and constant reminders that it would all be finished soon enough will not be forgotten soon.

Table of Contents   **Page**

Chapter 1

Fluorescence-Based Detection Methodologies for Nitric Oxide: A Review 16

Chapter 2

Cobalt Chemistry with Mixed Aminotroponimine Salicylaldimine Ligands:

Synthesis, Characterization and Nitric Oxide Reactivity 59

8

Chapter 3

Carboxylate-Bridged Dimetallic Complexes as Potential Nitric Oxide Sensors 103

Chapter 4

Dirhodium Tetracarboxylate Scaffolds as Reversible Fluorescence-Based Nitric Oxide Sensors 151

List of Tables **Page**

List of Schemes **Page**

List of Figures   **Page**

Chapter 4

.

Chapter 1

Fluorescence-Based Detection Methodologies for Nitric Oxide:

A Review

Introduction

Nitric oxide (NO) is a neutral free radical gas molecule. NO has long been recognized as an environmental contaminant and is a potential health hazard in the atmosphere. It was not until the work Ignarro, Furchgott, and Murad that beneficial roles for NO were discovered in biological systems.[1-3] In the years since the groundbreaking discovery of NO signaling in biology, further work has demonstrated NO to be a ubiquitous messenger in the cardiovascular, immune, and nervous systems.[1,4-12] Even though NO is a relatively stable species with reported half-lives under physiological conditions of up to five seconds,[5,13,14] it readily reacts with a variety of species commonly found in biological systems. In living organisms, NO has a variety of targets including dioxygen and its derivatives, thiols, amines, and transition metals.[15] The reaction of NO with dioxygen and superoxide ion results in formation of the reactive nitrogen oxide species (RNOS) NO_2 and $ONOO^-$, respectively. Both products are more reactive than NO itself. In aqueous environments, the reaction of NO with dioxygen can also yield NO_2^-.

In vivo, NO is synthesized by the enzyme nitric oxide synthase (NOS). NOS catalyzes the transformation of L-arginine to L-citrulline in the presence of dioxygen, which releases NO (Scheme 1.1).[16,17] There are three isoforms of NOS found in humans. Nitric oxide from the first two forms, neuronal NOS (nNOS) and endothelial NOS (eNOS), regulates functions in the central nervous system (CNS) and vasculature. The other isoform, inducible NOS (iNOS), is activated only under certain conditions and produces higher concentrations of NO for a short period of time. The micromolar levels of NO produced by iNOS, which result in formation of RNOS, have been implicated in carcinogenesis and several neurodegenerative disorders such as Alzheimer's disease,

Parkinson's disease, multiple sclerosis, and Huntington's disease.[4,18,19] In lower concentrations, where formation of RNOS are minimal, NO has beneficial roles in vasodilation, in protection against bacterial invaders, and in long term potentiation (LTP).[1,9-12,15,20]

The concentration dependent lifetime of NO and its ability to diffuse passively through cellular membranes complicate efforts to decipher biological functions of NO. Under certain conditions NO has a lifetime of up to 10 minutes in solution.[21] During this time it has a diffusion range of 100-200 μm from its point of origin.[22] Such a diffusion range corresponds to an area that covers approximately two million synapses.[23] Thus NO produced by one cell can, in principle, have a variety of effects on both neighboring and more distant cells.

In the central nervous system, NO may play a role in LTP, the process by which neuronal connections are re-enforced and a basis for memory.[20] LTP requires a neurotransmitter that is capable of diffusing from the postsynaptic neuron to the presynaptic neuron (Figure 1.1). Studies have indirectly identified NO as a possible candidate for this retrograde neurotransmitter.[20,24,25] A submaximal presynaptic stimulus results in the activation of nNOS. The NO produced does not react in the postsynaptic neuron but is believed to diffuse back into the presynaptic neuron where it activates guanylate cyclase. The cGMP produced by guanylate cyclase starts a signal cascade that ultimately results in the release of more neurotransmitter by the presynaptic neuron. The net effect of this feedback loop is to strengthen the neuronal connection. However, there is currently no method to probe directly the involvement of NO in LTP.

Current Non-Fluorescent Detection Methods

To investigate adequately the role of NO in LTP, a suitable sensor is required. Over the past two decades, several NO sensors have been developed, all of which have their limitations. The Griess assay is one of the earliest NO detection methods and is not suited for in vivo NO detection. This assay provides an estimate of total NO production by measuring its conversion to nitrite ion and is incapable of giving real time measurements of NO.[26] Although they are more sensitive than the Griess assay, chemiluminescence methods require purging aqueous samples with an inert gas to transfer NO to an analyzer. They are therefore not easily adapted to in vivo detection.[27] Electrochemical-based sensors provide real time direct detection, but they only give information on NO concentrations directly at the electrode tip.[27-30] With these and any other invasive detection methods, it is necessary to puncture the cell to obtain measurements. EPR-based methodologies that use iron dithiocarbamate complexes as spin traps have been developed, but they only have μM sensitivity for NO.[31-34] A more detailed review of these non-fluorescence-based NO imaging techniques was recently published elsewhere.[35]

Although these methods have been invaluable for elucidation of NO related biochemistry, new methods with improved characteristics are needed. None of the current NO detection methodologies is ideally suited for elucidating the roles that NO may play in the central nervous system. In particular, new methodologies are needed that use non-invasive techniques, are capable of selective and direct detection of NO, provide both temporal and spatial information, and do not require complicated instrumentation that is not commonly found in biochemical research labs. One approach to overcome these

problems is through the use of fluorescence spectroscopy. The suitability of fluorescence-based sensors for in vivo work is amply illustrated by the Ca^{2+}[36,37] and by the Znpyr family of Zn^{2+}[38-40] sensors.

Early Fluorometric Imaging of NO

The first fluorescence-based NO sensors were originally prepared for the measurement of nitrite ion in solution. The sensor molecule, 2,3-diaminonaphthalene (DAN) undergoes diazotization at one of the amines under acidic conditions in the presence of nitrite ion. Following the diazotization, 2,3-naphthotriazole is formed (Scheme 1.2).[41] Following an aqueous workup, the triazole species can then be detected by fluorometric analysis. The optimal pH for triazole formation is 1.6 and the optimal fluorescence emission from the 2,3-naphthotriazole occurs at pH 11.65.[42] Nitrate ion can also be detected by this methodology if it is first reduced to nitrite ion.[43] Since NO in aqueous solution can lead to the formation of nitrite ion, DAN was also used to monitor nitrosative stress in *E. coli*.[44] Later, it was determined that nitrosation of DAN and ultimately triazole formation in *E. coli* is proceeded by formation of strong nitrosylating agents such as N_2O_3 or N_2O_4 that arise from the rapid reaction of NO with O_2.[45] Research with immortalized macrophages stimulated with *E. coli* lipopolysaccharide (LPS) and γ-interferon is also consistent with oxidation of NO to form N_2O_3 and N_2O_4.[46] Application of the NOS inhibitor, aminoguanidine, to LPS activated macrophages resulted in decreased nitrite formation as monitored by DAN using a protocol adapted from the literature.[47,48] In 1993, a procedure was developed in which NO could be monitored via RNOS and subsequent triazole formation with DAN at pH 7.4 followed by fluorometric analysis of the basified reaction mixture.[49] Formation of 2,3-naphthatriazole is pH-

dependent, presumably a result of the pH-dependence of the formation of the nitrosamine intermediate.[49] DAN, however, is not suited for detection of NO produced by stimulated porcine pulmonary artery endothelial cells, which contain eNOS in contrast to the iNOS in the macrophage cell lines.[50] DAN was not able to detect NO production from the stimulated endothelial cells, whereas other methodologies such as chemiluminescence analysis, which detects NO, NO_2^-, and NO_3^-, collectively known as NO_x, detected significant increases in NO_x levels.[50] In a 1995 study, mechanisms for the reaction of amines with N_2O_3 and N_2O_4, formed by the reaction of NO with O_2 were proposed (Scheme 1.3).[51] The study showed that NO_2^- does not react with amines in organic solvents or in neutral aqueous solutions.[51] Although DAN can be used to monitor NO production by means of reactive products formed by its reaction with O_2, it is not suited for observation of NO in living cells. Due to its non-polar nature, DAN leaks out of cells after loading.[52]

The first steps towards adapting the diamine based compounds for use in intracellular NO visualization were undertaken when, to solve the issue of sensor leakage from the cells after loading, DAN was derivatized by addition of an ester moiety (Scheme 1.4).[52] Ester derivatization is a well-known approach to forming trappable molecules that do not diffuse out of cells after loading.[53] Cell permeable DAN-1-EE is hydrolyzed into the non-permeable DAN-1 by intracellular esterases, thus trapping the probe inside the cell.[52] Once hydrolyzed inside the cell, DAN-1 was used to image NO production in activated vascular smooth muscle cells isolated from male Wistar rats. The formation of the DAN-1 triazole species was monitored by fluorescence microscopy by excitation of the 360 nm absorption band of the triazole and its emission at 447 nm was monitored

using a 420 nm long-pass emission filter. The absence of a proton on the DAN-1 triazole

results in removal of the pH dependence observed with 2,3-naphthatriazole, where the

fluorescence emission intensity was maximized at alkaline pH.[52] Although DAN-1 EE

can be used indirectly to visualize NO production inside living cells, it suffers from high

background fluorescence resulting from autofluorescence of intracellular components

when excited with UV light.[52]

The Diaminofluorescein Platform

To improve the fluorescence properties of the o-diamine-based compounds for

intracellular NO detection, fluorescein was used as a scaffold. Conversion of the anilinic

amine on fluoresceinamine to an amide results in increased fluorescence emission

intensity[54] and implies that conversion of the electron-donating amine to a less donating

group will restore the fluorescein fluorescence. To investigate this possibility, a series of

diaminofluoresceins (Figure 1.2) were prepared and their reactivity with NO in the

presence of O_2 was investigated.[55] Presumably the low quantum yields ($\Phi = 0.002\text{-}0.007$)

of the diaminofluorescein-based sensors are the result of photoinduced electron transfer

(PET) quenching of the fluorophore excited state by the free amine groups. Conversion of

the amines on a diaminofluorescein to a triazole results in enhanced fluorescence

emission ($\Phi = 0.53\text{-}0.92$). Of the diamines investigated, DAF-2 has the most desirable

fluorescence properties with a quantum efficiency of 0.005 for the diamine and 0.92 for

the triazole derivative.[55] The excitation band at 486 nm does not require UV light for

excitation, eliminating possible interference caused by autofluorescence.

The fluorescence emission intensity from the triazole forms of the DAF sensors

are dependent on pH, however. Fluorescence emission intensity from the triazole DAF-2

T decreases rapidly as the pH is lowered below 7.[55] This is due in part to the pK_a of

6.27±0.02 for the phenolic proton on DAF-2 T.[55] More recently, a new derivative DAF-

FM, which contains fluoro substituents at the 2' and 7' positions of the xanthene ring and

is N-methylated, was prepared to address the issue of pH dependence.[56] Fluorination

lowers the pK_a responsible for the decrease in fluorescence intensity and adds to the

overall photostability of the fluorophore.[57] The pH instability may also arise from the

triazole proton, as previously observed with 2,3-naphthatriazole. Introduction of a N-

methyl group will result in formation of a triazole that does not have a triazole proton

after reaction with NO and O_2.[56] With these modifications, the pK_a of the phenolic OH of

DAF-FM T is lowered to 4.38±0.05 and the fluorescence intensity is stable above pH

5.8.[56] The DAF sensors can be converted to their diacetate derivatives, which results in

formation of a lactone ring, giving a nonpolar dye that can penetrate the cell membrane

and enter the cytosol (Figure 1.3). This uptake is followed by hydrolysis of the acetates

by intracellular esterases, trapping the sensor inside the cell in a manner similar to DAN-

1 EE. Sensors based on the o-diamine functionality have become the most widely used

fluorescence-based imaging agents for intracellular NO.

Other o-Diamine NO Sensors

Several related o-diamine based sensors have been prepared in recent years,

including a series of diaminorhodamine analogs to the DAF sensors.[58,59] The rhodamine-

based sensors do not display the same pH dependent fluorescence and have stable

emission intensity above pH 4. The detection limit of DAR-4M is 7 nM NO, which is

slightly higher than the 3 nM detection limit observed for DAF-FM.[56,58] Probes based on

the anthracene, coumarin, acridine, and BODIPY fluorophores have also been

synthesized (Figure 1.4).[60,61] These sensors are synthetically more accessible and should not have a substantial pH dependence of their fluorescence emission intensity. Additional derivatives, 5,6-diamino-1,3-naphthalene disulfonic acid[62] and 1,2-diaminoanthraquinone,[63] have been investigated, but offer no significant improvement over the existing o-diamine based sensors. Even though the o-diamine based sensors react with NO^+ equivalents such as N_2O_4 or N_2O_3, they can still be used to monitor intracellular NO, although it may be difficult to draw accurate conclusions due to the lack of direct reaction with NO. The following section gives details on the various cellular systems in which o-diamine based NO sensors and in particular DAF-2, have been used to detect biological NO.

Biological NO Detection with o-Diamine Based Sensors

Initial work demonstrated the utility of DAF-2 for detection of intracellular NO. In non-activated macrophages, substantial fluorescence response due to triazole formation occurs 4.2 min after treatment with DAF-2. This increase reflects the substantial NO production from the macrophages even without stimulation from LPS.[55,64] It was also possible to image intracellular NO in activated aortic smooth muscle cells following incubation with DAF-2 diacetate as monitored by confocal laser scanning microscopy. In these studies, there was no indication of any cytotoxic effects as a result of administration of the probes.[55,64]

Methodologies for the use of DAF-2 diacetate to detect intracellular NO in non-activated endothelial cells have also been developed. The non-activated endothelial cells show low levels of NO synthesis from eNOS in contrast to the elevated NO synthesis by iNOS in macrophages. By incubation of endothelial cells with low (0.1 μM)

concentrations of DAF-2 coupled with subtraction of the initial DAF-2 autofluorescence from the measured total fluorescence, observation of basal NO production was possible.[65]

The validity of using o-diamine based sensors such as DAF-2 for quantitative intracellular measurements of NO has been questioned. Since it does not react directly with NO, but rather with a RNOS, the kinetic and thermodynamic properties behind the oxidation of NO by O_2 under physiological conditions may have a significant impact on the observed spatial and temporal intracellular fluorescence response. DAF-2 only directly observes the local distribution of the highly reactive species, N_2O_3 and N_2O_4, which are not necessarily the same as the intracellular distribution of NO. Additionally, other intracellular species such as superoxide (O_2^-) ion may have a dramatic effect on the observed fluorescence response of the DAF sensors. In the presence of either horseradish peroxidase and H_2O_2 or peroxynitrite, DAF-2 is oxidized to an unstable intermediate that combines directly with NO, bypassing the NO/O_2 chemistry.[66] By pre-forming this activated DAF species, addition of anaerobic NO results in a 7- to 10-fold increase in the amount of recovered DAF-2 T as compared to the analogous experiment with NO and O_2.[66] These data indicate that results from DAF-2 assays are difficult to interpret in environments where oxidants such as O_2^- are present in addition to NO. It is possible that intracellular oxidation of DAF-2 may result in increased NO-dependent fluorescence that could be confused with an increase in NO levels.[66]

Other Organic NO Sensors

Dichlorofluorescin has been used as a fluorometric assay for NO in a variety of intracellular applications.[67,68] It is difficult, however, to draw any concrete conclusions about the distribution and production of NO by using dichlorofluorescin.

Dichlorofluorescin is a more general fluorometric assay for intracellular oxidants, showing significant fluorescence response in the presence of oxidants such as H_2O_2, O_2^-, $ONOO^-$, NO, HOCl, and $^\bullet OH$ (Scheme 1.5).[69-71]

Another organic-based compound developed for detection of NO is rhodamine B hydrazide (RBH). The reaction of RBH with NO_2^- under acidic conditions (pH < 5), which favor formation of NO^+ equivalents, results in ultimate conversion of the nonfluorescent RBH to the fluorescent rhodamine B, with the shortest reaction time of 1 h being observed in pH 2 aqueous solution at 60° C (Scheme 1.6).[72] Exposure of RBH to NO in the presence of O_2 also elicits, presumably via a NO_2 or N_2O_3 reactive intermediate, an increase in fluorescence emission intensity; however, due to its indirect reactivity with NO, it has shortcomings similar to those observed with the o-diamine based sensors.

One novel approach for direct detection of NO is based on the modification of cheletropic traps used for EPR based NO detection. The fluorescent nitric oxide cheletropic traps (FNOCTs) start as a nonfluorescent dyes and add NO across a diene moiety giving a nitroxide radical species, which then must react with an external reductant such as ascorbate to give the corresponding hydroxylamine (Scheme 1.7).[73,74] The reaction of NO with the FNOCT in the presence of ascorbate gives a substantial increase in fluorescence, where the hydroxylamine product has a pH-dependent emission with a maximal intensity between pH 8-9.[73] The source of the pH-based fluorescence dependence was identified as protonation of the dimethylamino group, which was introduced to red-shift the fluorescence excitation wavelength of 315 nm in 1 to make it more amenable for use in living cells. Despite the pH dependence, the optical properties

of **1** are sufficient for intracellular studies (λ_{ex} = 380 nm, λ_{em} = 460 nm) and it can detect

sub-μM concentrations of NO. In addition to reactivity with NO, FNOCTs are also

sensitive to peroxynitrite. Addition of a small excess of peroxynitrite results in an

increase in fluorescence, whereas addition of a large excess leads to a diminution of

fluorescence emission intensity.[73] The details of the peroxynitrite reactivity are unclear.

The ability of FNOCTs to detect NO in living cells was demonstrated using alveolar

macrophages induced with LPS to produce large amounts of NO.[73] The requirement of an

external reductant and the potential issues involving interference by peroxynitrite may

limit the use of FNOCTs in certain biological applications such NO quantification.

Fiber-Optic NO Detection Systems

All of the purely organic fluorescence-based sensors developed so far rely on

destruction or formation of covalent bonds and are non-reversible. One way to engineer a

reversible sensor is to employ the use of transition metals, which are well known to bind

NO reversibly. This approach to developing NO sensors for biological imaging is

growing in popularity.

One strategy is the use of fluorophores attached to optical fibers coated in

colloidal gold. Gold films have previously been used to detect gaseous NO by monitoring

changes in the electrical resistance of the film in response to NO absorption.[75] For

modification into a fiber optic sensor, gold colloid coated optical fibers were treated with

a solution of 4-carboxy-2',7'-difluorofluorescein succinimidyl ester followed by

immersion of the sensor in a suspension of fluorescent carboxylate-modified polystyrene

microspheres. When the sensor is exposed to NO, the NO adsorbs on to the surface of the

gold colloid, which presumably causes the difluorofluorescein dye molecules to reorient

in relation to the gold film, resulting in a change in the transition dipole of the dye and affords a decrease in fluorescence emission intensity.[76] The fluorescent labeled polystyrene microspheres, which are unaffected by the presence of NO, are then used to determine the local NO concentration by ratiometric analysis. The sensor is reversible with a response time of 0.25 s or less for fluorescence quenching in the presence of NO and has a detection limit of 20 μM. Using this probe, a concentration of 190±70 μM NO was measured in macrophages activated with mouse interferon-γ and LPS.[76]

Related fiber optic sensors prepared using the heme domain of soluble guanylate cyclase (sGC) or cytochrome c' have also been investigated. These probes were prepared by a method similar to the 4-carboxy-2',7'-difluorofluorescein succinimidyl ester based colloidal gold sensor. Instead of immersing the gold coated optical fiber in the fluorophore, however, the fiber was soaked in either the heme domain of sGC or cytochrome c' both labeled with 4-carboxy-2',7'-difluorofluorescein.[77,78] In both cases, a decrease in fluorescence intensity from the dye conjugate was observed on binding of NO to the heme active site of the proteins. The origin of the fluorescence response of the dye is presumably due to protein conformational changes, which in turn alter the fluorescence emission intensity of the conjugated fluorophore.[79] Through the use of the fluorophore-protein adducts, detection limits of 1 and 8 μM NO have been achieved with the sGC and cytochrome c' based probes, respectively.[77,78] In addition to their reversibility, they are not affected by potentially interfering species NO_2^-, NO_3^{2-}, O_2, O_2^-, H_2O_2, and $ONOO^-$.[78,79] The probes were prepared with 100 μm optical fibers which are too large for intracellular measurements but could be miniaturized by use of sub-μm tips for intracellular NO detection. Although innovative, the low NO sensitivity and inability to give spatial

information, a disadvantage common to all fiber optic and electrochemical based sensors,

limits the utility of this approach for the detection of biologically generated NO.

Soluble Transition Metal Complexes

One of the first small molecule probes to utilize a fluorescence methodology

based upon transition metal chemistry was inspired by the active site of sGC. In the

resting state of sGC, the heme moiety contains a coordinated histidine. Upon reaction

with NO, a heme nitrosyl is formed, which results in dissociation of the coordinated

histidine.[80] The conformational change elicited by this reaction results in activation of the

enzyme. The iron(II) quinoline-pendant cyclam complex (Figure 1.5) contains two

distinct fragments, the iron(II) cyclam, which can be viewed as a simple model for the

heme center in sGC, and the pendant quinoline, which is analogous to the axial histidine

in the active site of sGC. When excited at 366 nm, the fluorescence emission intensity

from the Fe(II) complex at 460 nm is significantly enhanced in comparison to the free

ligand. Although no detailed studies were conducted, it was proposed that the observed

fluorescence enhancement was the result of electronic interactions between the lone pair

on the quinoline N-atom and the Fe(II) center.[80] This coordination induced fluorescence

enhancement is in contrast to the more commonly observed quenching properties of

transition metals with partially filled d-shells.[81] When exposed to NO in pH 7.4 aqueous

buffer, the 460 nm emission decreased markedly, with a detection limit of 1 μM NO.[80] No

interference was observed in the presence of NO_2^- or CN^-.[80] Because Fe(II) cyclam is

dioxygen-sensitive, however, the sensor may not function properly in an aerobic

environment. In addition, an increase in fluorescence emission intensity after analyte

binding is generally preferred over a decrease for biological imaging.

A new mechanism has recently been employed to develop fluorescence-based NO sensors. In this system, a nitroxyl radical coordinated to a Fe(II) dithiocarbamate complex is exchanged in the presence of NO to form an iron nitrosyl species with displacement of the nitroxyl moiety. EPR was employed to detect the liberated nitroxyl.[82] Modification of the nitroxyl ligand with a fluorophore, such as acridine, allows the use of fluorescence detection methodologies. The fluorescence emission intensity from the acridine moiety in acridine-TEMPO is quenched by the nitroxyl radical, and when the nitroxyl coordinates to the Fe(II) dithiocarbamate, the fluorescence intensity is restored. Exposure of the Fe(II) dithiocarbamate complex with acridine-TEMPO to NO affords an iron nitrosyl, releasing the acridine-TEMPO. The result is diminution of the acridine fluorescence emission intensity (Scheme 1.8).[83] With this system it was possible to detect 100 nM NO, however, it displays the less desirable decrease in fluorescence upon analyte binding and, as a consequence of using an Fe(II) dithiocarbamate complex, the system may be susceptible to competition from dioxygen.

This strategy has also been applied to prepare a ratiometric NO sensor containing fluorescamine and coumarin derivatives (Scheme 1.9).[84] In this case, a Fe(II) methoxycoumalinomethyl-cyclam (Mmc-cyclam) scaffold was used to bind either the fluorescamine-PROXYL conjugate, or NO. In an aqueous pH 7.4 buffered solution of 40 μM FeMmc-cyclam (λ_{ex} 360 nm, λ_{ex} 410 nm) and 40 μM fluorescamine-PROXYL (λ_{ex} 385 nm, λ_{ex} 470 nm) excitation of the coumarin at 360 nm resulted in fluorescence resonance energy transfer (FRET) to the fluorescamine moiety, and emission at 470 nm was observed. When this system was exposed to the NO-releasing agent NOC-7, over time a decrease in fluorescamine emission intensity along with an increase in coumarin

emission intensity occured.[84] A detection limit of less than 100 nM NO was reported. Owing to the use of a Fe(II) cyclam, the sensor may be susceptible to interference from O_2 and the reaction of NO with the metal center is apparently too slow to trap NO released in biological environments.[85]

Reductive Nitrosylation and Emission by Fluorophore Dissociation

From prior research in our laboratory focusing on the reactivity of NO with Fe,[86] Mn,[87] and Co[88-90] tropocoronand complexes, we discovered that fluorescence-based NO sensors might be available by using the related aminotroponiminate scaffold. The dansyl-containing aminotroponimine ligands, H^{R}DATI, were prepared in four steps in 20-50% yields starting with 2-tosyloxytropone (Scheme 1.10).[91] The corresponding Co(II) complexes of these ligands are accessible by addition of $CoCl_2$ to 2 equiv of the ligand, previously deprotonated with sodium or potassium hydride. The Co(II) complexes are not dioxygen sensitive in either the solution or solid state. Although they are air stable, the complexes are susceptible to hydrolysis in the presence of trace amounts of water. The Co(II) complex of the related $H_2^{iPr}DATI$-4 ligand (Figure 1.6) is prepared in a manner similar to that employed for the non-linked complexes.[91,92]

Structural studies of [Co(^{Bz}DATI)$_2$] (5), [Co(^{iPr}DATI)$_2$] (7), and [Co(^{tBu}DATI)$_2$] (8) revealed a pseudo-tetrahedral geometry (Figure 1.7). The dihedral angles of 73.8°, 76.1°, and 81.4° between the 5-member chelate rings in 5, 7, and 8, respectively, are a consequence of the differing steric requirements imposed by the R groups on the ligands. The dihedral angle of 62.2° in [Co(^{iPr}DATI-4)] (6) (Figure 1.7), however, is significantly smaller than the corresponding values in 5, 7, and 8 due to the added strain provided by the n-butyl linker between the two aminotroponiminate moieties.[91] The two dansyl

moieties in **6** are parallel and have an average separation of 3.5(1) Å, a value consistent with π-π stacking interactions.[93]

The H^{R}DATI and H$_2$DATI-4 ligands display typical dansyl fluorescence behavior. When excited at 350 nm, a broad emission centered at 500 nm occurs for each ligand. The Co(II) complexes **5-8**, have significantly quenched emission when compared to the free ligands, as evidenced by the approximately 20-fold diminution in the fluorescence intensity of **3** when compared to free H^{iPr}DATI in CH$_2$Cl$_2$ (Figure 1.8).[91] This observed transition metal quenching of fluorescence is a well known phenomenon and can occur by energy or electron transfer between the fluorophore excited state and the empty or partially filled d-orbitals of the metal.[94,95]

The reactions of **5**, **7**, and **8** with excess NO in CH$_2$Cl$_2$ are slow. Several hours after exposure of **7** to NO, IR bands form at 1838 and 1760 cm^{-1}. The appearance of these NO stretching bands is consistent with the formation of a dinitrosyl complex.[96-103] Although it was not possible to crystallize the nitrosyl complexes of in **5**, **7**, and **8**, the structure of the related non-dansylated dinitrosyl, [Co(i-Pr$_2$ATI)(NO)$_2$], which has similar IR bands at 1809 and 1730 cm^{-1}, strongly supports the conclusion that **5**, **7**, and **8** are pseudotetrahedral dinitrosyl species. When the reaction of **7** with NO was followed by ^{1}H NMR spectroscopy, signals for the free ligand, H^{iPr}DATI appear over time. The reaction proceeds by a reductive nitrosylation mechanism whereby [Co(^{R}DATI)$_2$], two NO molecules, and an electron form a dinitrosyl species in which the cobalt has been reduced to Co(I) (eq 1).[91] The resulting species is designated {Co(NO)$_2$}^{10}, where the superscript

denotes the sum of the metal d electrons and the unpaired π^* electrons on the nitrosyl ligands.[104]

When **7** is exposed to excess NO in CH_2Cl_2, a slow increase in fluorescence emission intensity at 505 nm occurs.[91] After 6 h a fluorescence emission intensity increase of 6-fold is observed. The related complex **6**, which has a more strained tetrahedral geometry induced by the n-butyl linker, reacts with NO in a similar fashion and displays moderate increases in fluorescence intensity. The fluorescence emission intensity of **6** at 505 nm doubles in the first 3 min after exposure to NO and reaches a greater than 4-fold increase after 6 h (Figure 1.9).[91] The initial reactivity of this complex is significantly faster than that observed with **7**. This difference in reaction rate may be the result of the added steric strain imparted by the linker, which further distorts the geometry of the cobalt from idealized tetrahedral geometry. The detection limit for **6** of 50-100 µM NO, however, is insufficient for detection of biological NO.

Summary

Over the past 15 years, many different approaches toward the development of NO sensors suitable for biological applications have been investigated. These approaches range from electrochemical- and EPR-based techniques to those that make use of fluorescence spectroscopy. The advancement of our understanding of NO in biology and the ability to design ever improving fluorescence-based sensors is remarkable considering the many challenges associated with handling and observing the reactive diatomic gas, nitric oxide. Early research adapting the fluorescence-based nitrite sensor DAN for NO detection was only the beginning. This work ultimately led to development of the diaminofluorescein sensors and a plethora of other o-diamine-based sensors that are

capable of detecting sub-μM NO in living cells. Despite their advances, the o-diamine-based sensors have limitations, in particular, the necessity for O_2 to react with NO to form more reactive nitrosylating species such as N_2O_3. Other organic based sensors such as dichlorofluorescin, the FNOCTs, and RBH have been developed and investigated for their NO sensing abilities. All of these organic sensors whether they react directly with NO or not are incapable of reversible binding and detection of NO.

Some of the more recent advancements in NO detection rely on strategies that employ transition metals. These systems are based on the use of nitrosyl forming reactions as signaling events, which ultimately alter the fluorescence emission properties of an attached fluorophore. One successful strategy utilizes sGC or the cytochrome c' labeled with a fluorescent reporter to prepare fiber optic probes capable of reversible NO detection. Other approaches use small molecule transition metal complexes such as the Co(II) dansyl-aminotroponiminate complexes, which are capable of detecting NO over a wide spatial field like the o-diamine sensors, but react with NO directly. The potential exists for further modification and development of small molecule transition metal complexes. The goal is to obtain reversible, direct detection of NO by fluorescence methodologies.

References

(1) Furchgott, R. F. *Angew. Chem. Int. Ed.* **1999**, *38*, 1870.

(2) Ignarro, L. J.; Buga, G. M.; Wood, K. S.; Byrns, R. E.; Chaudhuri, G. *Proc. Natl. Acad. Sci. USA* **1987**, *84*, 9265.

(3) Palmer, R. M. J.; Ferrige, A. G.; Moncada, S. *Nature* **1987**, *327*, 524.

(4) Wink, D. A.; Vodovotz, Y.; Laval, J.; Laval, F.; Dewhirst, M. W.; Mitchell, J. B. *Carcinogenesis* **1998**, *19*, 711.

(5) Moncada, S.; Palmer, R. M. J.; Higgs, E. A. *Pharmacol. Rev.* **1991**, *43*, 109.

(6) Kerwin, J. F., Jr.; Lancaster, J. R., Jr.; Feldman, P. L. *J. Med. Chem.* **1995**, *38*, 4343.

(7) Feldman, P. L.; Griffith, O. W.; Stuehr, D. J. *J. Chem. Eng. News* **1993**, *71*, 26.

(8) Bredt, D. S.; Snyder, S. H. *Annu. Rev. Biochem.* **1994**, *63*, 175.

(9) Murad, F. *Angew. Chem. Int. Ed.* **1999**, *38*, 1856.

(10) Ignarro, L. J. *Angew. Chem. Int. Ed.* **1999**, *38*, 1882.

(11) Butler, A. R.; Williams, D. L. H. *Chem. Soc. Rev.* **1993**, 233.

(12) Rubbo, H.; Darley-Usmar, V.; Freeman, B. A. *Chem. Res. Toxicol.* **1996**, *9*, 809.

(13) Lancaster, J. R., Jr. *Nitric Oxide Biology and Pathobiology*; Academic Press: San Diego, 2000.

(14) Furchgott, R. F.; Vanhoutte, P. M. *FASEB J.* **1989**, *3*, 2007.

(15) Pfeiffer, S.; Mayer, B.; Hemmens, B. *Angew. Chem. Int. Ed.* **1999**, *38*, 1714.

(16) Dredt, D. S.; Hwang, P. M.; Snyder, S. H. *Nature* **1990**, *347*, 768.

(17) Leone, A. M.; Palmer, M. J.; Knowles, R. G.; Francis, P. L.; Ashton, D. S.; Moncada, S. *J. Biol. Chem.* **1991**, *226*, 23790.

(18) Laval, F.; Wink, D. A. *Carcinogenesis* **1994**, *15*, 443.

(19) Calabrese, V.; Bates, T. E.; Stella, A. M. G. *Neurochem. Res.* **2000**, *25*, 1315.

(20) Schuman, E. M.; Madison, D. V. *Science* **1991**, *254*, 1503.

(21) Bonner, F. T.; Stedman, G. In *Methods in Nitric Oxide Research*; Feelisch, M., Stamler, J. S., Eds.; John Wiley & Sons: New York, 1996; pp 3-18.

(22) Lancaster, J. R. *Nitric Oxide: Biol. and Chem.* **1997**, *1*, 18.

(23) Wood, J.; Garthwaite, J. *Neuropharm.* **1994**, *33*, 1235.

(24) Schuman, E. M.; Madison, D. V. *A. Rev. Neurosci.* **1994**, *17*, 153.

(25) Boehme, G. A.; Bon, C.; Lemaire, M.; Reibaud, M.; Piot, O.; Stutzmann, J.-M.; Doble, A.; Blanchard, J.-C. *Proc. Natl. Acad. Sci. USA* **1993**, *90*, 9191.

(26) Schmidt, H. H.; Kelm, M. In *Methods in Nitric Oxide Research*; Feelisch, M., Stamler, J., Eds.; John Wiley & Sons: New York, 1996; pp 491-497.

(27) Hampl, V.; Walters, C.; Archer, S. L. In *Methods in Nitric Oxide Research*; Feelisch, M., Stamler, J. S., Eds.; John Wiley & Sons: New York, 1996; pp 309-318.

(28) Mao, L.; Tian, Y.; Shi, G.; Liu, H.; Jin, L.; Yamamoto, K.; Tao, S.; Jin, Y. *Anal. Lett.* **1998**, *31*, 1991.

(29) Bedioui, F.; Villeneuve, N. *Electroanalysis* **2003**, *15*, 5.

(30) Ciszewski, A.; Milczarek, G. *Tanlanta* **2003**, *61*, 11.

(31) Kotake, Y.; Tanigawa, T.; Tanigawa, m.; Ueno, I.; Allen, D. R.; Lai, C.-S. *Biochim. Biophys. Acta* **1996**, *1289*, 362.

(32) Komarov, A. M.; Lai, C.-S. *Biochim. Biophys. Acta* **1995**, *1272*, 29.

(33) Yoshimura, T.; Fujii, S.; Yokoyama, H.; Kamada, H. *Chem. Lett.* **1995**, 309.

(34) Fujii, S.; Yoshimura, T. *Coord. Chem. Rev.* **2000**, *198*, 89.

(35) Nagano, T.; Yoshimura, T. *Chem. Rev.* **2002**, *102*, 1235.

(36) de Silva, A. P.; Gunaratne, H. Q. N.; Gunnlaugsson, T.; Huxley, A. J.; McCoy, J. T.; Rademacher, C. P.; Rice, T. E. *Chem. Rev.* **1997**, *97*, 1515.

(37) Lakowicz, J. R. *Principles of Fluorescence spectroscopy*; Kluwer Academic/Plenum Publishers: Boston, 1999.

(38) Walkup, G. K.; Burdette, S. C.; Lippard, S. J.; Tsien, R. Y. *J. Am. Chem. Soc.* **2000**, *122*, 5644.

(39) Burdette, S. C.; Walkup, G. K.; Spingler, B.; Tsien, R. Y.; Lippard, S. J. *J. Am. Chem. Soc.* **2001**, *123*, 7831.

(40) Burdette, S. C.; Frederickson, C. J.; Bu, W.; Lippard, S. J. *J. Am. Chem. Soc.* **2003**, *125*, 1778.

(41) Wiersma, J. H. *Anal. Lett.* **1970**, *3*, 123.

(42) Damiani, P.; Bruini, G. *Talanta* **1986**, *33*, 649.

(43) Sawicki, C. R. *Anal. Lett.* **1971**, *4*, 761.

(44) Ralt, D.; Wishnok, J. S.; Fitts, R.; Tannenbaum, S. R. *J. Bacteriology* **1988**, *170*, 359.

(45) Ji, X.-B.; Hollocher, T. C. *Appl. Environ. Microbiol.* **1988**, *54*, 1791.

(46) Kosaka, H.; Wishnok, J. S.; Miwa, M.; Leaf, C. D.; Tannenbaum, S. R. *Carcinogenesis* **1989**, *10*, 563.

(47) Misko, T. P.; Moore, W. M.; Kasten, T. P.; Nickols, G. A.; Corbett, J. A.; Tilton, R. G.; McDaniel, M. L.; Williamson, J. R.; Currie, M. G. *Eur. J. Pharm.* **1993**, *233*, 119.

(48) Misko, T. P.; Schilling, R. J.; Salvemini, D.; Moore, W. M.; Currie, M. G. *Anal. Biochem.* **1993**, *214*, 11.

(49) Miles, A. M.; Chen, Y.; Owens, M. W.; Grisham, M. B. *Methods* **1995**, *7*, 40.

(50) Kleinhenz, D. J.; Fan, X.; Rubin, J.; Hart, C. M. *Free Rad. Biol. Med.* **2003**, *34*, 856.

(51) Nagano, T.; Takizawa, H.; Hirobe, M. *Tet. Lett.* **1995**, *36*, 8239.

(52) Kojima, H.; Sakurai, K.; Kikuchi, K.; Kawahara, S.; Kirino, Y.; Nagoshi, H.; Hirata, Y.; Akaike, T.; Maeda, H.; Nagano, T. *Biol. Pharm. Bull.* **1997**, *20*, 1229.

(53) Tsien, R. Y. *Nature* **1981**, *290*, 527.

(54) Munkholm, C.; Parkinson, D.-R.; Walt, D. R. *J. Am. Chem. Soc.* **1990**, *112*, 2608.

(55) Kojima, H.; Kakatsubo, N.; Kikuchi, K.; Kawahara, S.; Kirino, Y.; Nagoshi, H.; Hirata, Y.; Nagano, T. *Anal. Chem.* **1998**, *70*, 2446.

(56) Kojima, H.; Urano, Y.; Kikuchi, K.; Higuchi, T.; Hirata, Y.; Nagano, T. *Angew. Chem. Int. Ed.* **1999**, *38*, 3209.

(57) Sun, W.-C.; Gee, K. R.; Klaubert, D. H.; Haugland, R. P. *J. Org. Chem* **1997**, *62*, 6469.

(58) Kojima, H.; Hirotani, M.; Nakatsubo, N.; Kikuchi, K.; Urano, Y.; Higuchi, T.; Hirata, Y.; Nagano, T. *Anal. Chem.* **2001**, *73*, 1967.

(59) Kojima, H.; Hirotani, M.; Urano, Y.; Kikuchi, K.; Higuchi, T.; Nagano, T. *Tet. Lett.* **2000**, *41*, 69.

(60) Platter, J. M.; Greig, I.; Helfrich, M. H.; Ralston, S. H. *J. Chem. Soc. Perkin Trans. 1* **2001**, 2553.

(61) Zhang, X.; Wang, H.; Li, J.-S.; Zhang, H.-S. *Anal. Chim. Acta* **2003**, *481*, 101.

(62) Zhang, X.; Wang, H.; Liang, S.-C.; Zhang, H.-S. *Tantala* **2002**, *56*, 499.

(63) Schuchmann, S.; Albrecht, D.; Heinemann, U.; Halbach, O. v. B. u. *Nerobiol. of Disease* **2002**, *11*, 96.

(64) Nakatsubo, N.; Kojima, H.; Kikuchi, K.; Nagoshi, H.; Hirata, Y.; Maeda, D.; Imai, Y.; Irimura, T.; Nagano, T. *FEBS Lett.* **1998**, *427*, 263.

(65) Leikert, J. F.; Räthel, T. R.; Müller, C.; Vollmar, A. M.; Dirsch, V. M. *FEBS Lett.* **2001**, *506*, 131.

(66) Jourd'Heuil, D. *Free Rad. Biol. Med.* **2002**, *33*, 676.

(67) Imrich, A.; Kobzik, L. *Nitric Oxide: Biol. and Chem.* **1997**, *1*, 359.

(68) Gunasekar, P. G.; Kanthasamy, A. G.; Borowitz, J. L.; Isom, G. E. *J. Neurosci. Methods* **1995**, *61*, 15.

(69) Hempel, S. J.; Buettner, G. R.; O'Malley, Y. Q.; Wessels, D. A.; Flaherty, D., M. *Free Rad. Biol. Med.* **1999**, *27*, 146.

(70) Setsukinai, K.-i.; Urano, Y.; Kakinuma, K.; Majima, H., J.; Nagano, T. *J. Biol. Chem.* **2003**, *278*, 3170.

(71) Myhre, O.; Andersen, J. M.; Aarnes, H.; Fonnum, F. *Biochem. Pharma.* **2003**, *65*, 1575.

(72) Rieth, T.; Sasamoto, K. *Anal. Commun.* **1998**, *35*, 195.

(73) Meineke, P.; Rauen, U.; de Groot, H.; Korth, H.-G.; Sustmann, R. *Chem. Eur. J.* **1999**, *5*, 1738.

(74) Baetz, M.; Korth, H.-G.; Sustmann, R. *Angew. Chem. Int. Ed. Engl.* **1997**, *1997*, 1501.

(75) Toda, K.; Ochi, K.; Sanemasa, I. *Sens. Actuators, B* **1996**, *32*, 15.

(76) Barker, S. L. R.; Kopelman, R. *Anal. Chem.* **1998**, *70*, 4902.

(77) Barker, S. L. R.; Clark, H. A.; Swallen, S. F.; Kopelman, R.; Tsang, A. W.; Swanson, J. A. *Anal. Chem.* **1999**, *71*, 1767.

(78) Barker, S. L. R.; Zhao, Y.; Marletta, M. A.; Kopelman, R. *Anal. Chem.* **1999**, *71*, 2071.

(79) Barker, S. L. R.; Kopelman, R.; Meyer, T. E.; Cusanovich, M. A. *Anal. Chem.* **1998**, *70*, 971.

(80) Katayama, Y.; Takahashi, S.; Maeda, D. *Anal. Chim. Acta* **1998**, *365*, 159.

(81) Varnes, A. W.; Dodson, R. B.; Wehry, E. L. *J. Am. Chem. Soc.* **1972**, *94*, 946.

(82) Katayama, Y.; Soh, N.; Koide, K.; Maeda, D. *Chem. Lett.* **2000**, *2000*, 1152

(83) Soh, N.; Katayama, Y.; Maeda, D. *Analyst* **2001**, *126*, 564.

(84) Soh, N.; Imato, T.; Kawamura, K.; Maeda, M.; Katayama, Y. *Chem. Commun.* **2002**, 2650.

(85) Katayama, Y.; Soh, N.; Maeda, D. *Bull. Chem. Soc. Jpn.* **2002**, *75*, 1681.

(86) Franz, K. J.; Lippard, S. J. *J. Am. Chem. Soc.* **1999**, *121*, 10504.

(87) Franz, K. J.; Lippard, S. J. *J. Am. Chem. Soc.* **1998**, *120*, 9034.

(88) Jaynes, B. S.; Ren, T.; Masschelein, A.; Lippard, S. J. *J. Am. Chem. Soc.* **1993**, *115*, 5589.

(89) Jaynes, B. S.; Doerrer, L. H.; Liu, S. C.; Lippard, S. J. *Inorg. Chem.* **1995**, *34*, 5735.

(90) Doerrer, L. H.; Bautista, M. T.; Lippard, S. J. *Inorg. Chem.* **1997**, *36*, 3578.

(91) Franz, K. J.; Singh, N.; Spingler, B.; Lippard, S. J. *Inorg. Chem.* **2000**, *39*, 4081.

(92) Franz, K. J.; Singh, N.; Lippard, S. J. *Angew. Chem. Int. Ed.* **2000**, *39*, 2120.

(93) Liu, Z.-H.; Duan, C.-Y.; Hu, J.; You, X.-Z. *Inorg. Chem.* **1999**, *38*, 1719.

(94) Fabbrizzi, L.; Licchelli, M.; Pallavicini, P. *Acc. Chem. Res.* **1999**, *32*, 846.

(95) Bergonzi, R.; Fabbrizzi, L.; Licchelli, M.; Mangano, C. *Coord. Chem. Rev.* **1998**, *170*, 31.

(96) Martin, R. L.; Taylor, D. *Inorg. Chem.* **1976**, *15*, 2970.

(97) Field, J. S.; Wheatley, P. J.; Bhaduri, S. J. *J. Chem. Soc. Dalton Trans.* **1974**, 74.

(98) Haymore, B. L.; Huffman, J. C.; Butler, N. E. *Inorg. Chem.* **1983**, *22*, 168.

(99) Kaduk, J. A.; Ibers, J. A. *Inorg. Chem.* **1977**, *16*, 3283.

(100) Reichert, B. E. *Acta Crystallogr., Sect. B* **1976**, *B32*, 1934.

(101) Roustan, J.-L.; Ansari, N.; Le Page, Y.; Charland, J.-P. *Can. J. Chem.* **1992**, *70*, 1650.

(102) Aresta, M.; Ballivet-Tkatchenko, D.; Bonnet, M. C.; Faure, R.; Loiseleur, H. *J. Am. Chem. Soc.* **1985**, *107*, 2994.

(103) Hendrickson, A. R.; Ho, R. K. Y.; Martin, R. L. *Inorg. Chem.* **1974**, *13*, 1279.

(104) Enemark, J. H.; Feltham, R. D. *Coord. Chem. Rev.* **1974**, *13*, 339.

$$[Co(^{iPr}DATI)_2] \xrightarrow[e^-, H^+]{2\ NO} [Co(NO)_2(^{iPr}DATI)] + H^{iPr}DATI$$
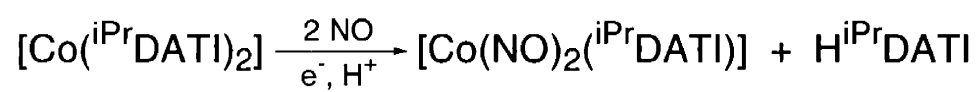
Equation 1.1.
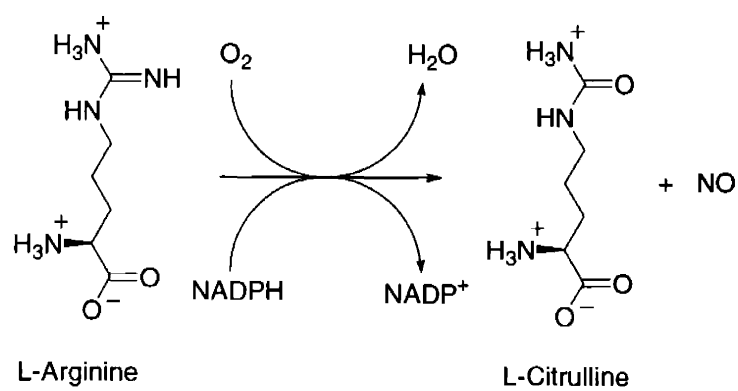
Scheme 1.1. Synthesis of NO from L-arginine
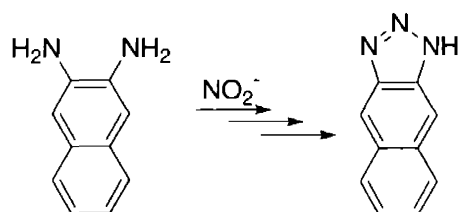
Scheme 1.2. Formation of the 2,3-naphthatriazole from NO_2^-.
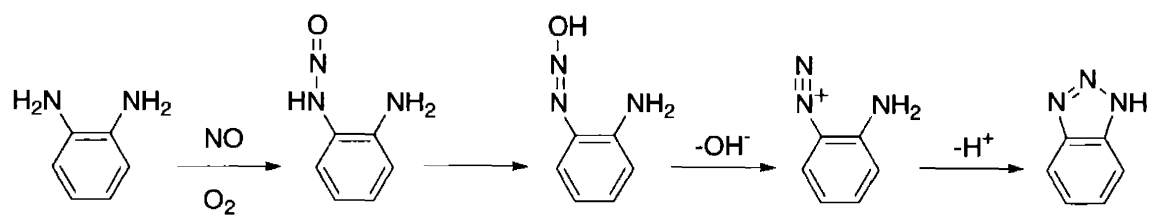
Scheme 1.3. Formation of the 1,2-triazole from NO and O_2.
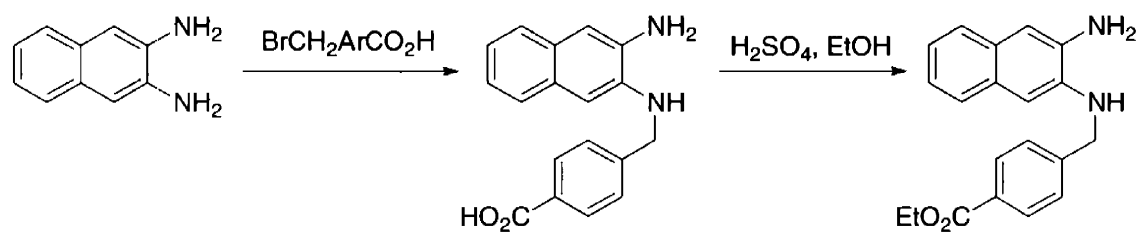
Scheme 1.4. Preparation of the cell-permeable DAN-1 EE
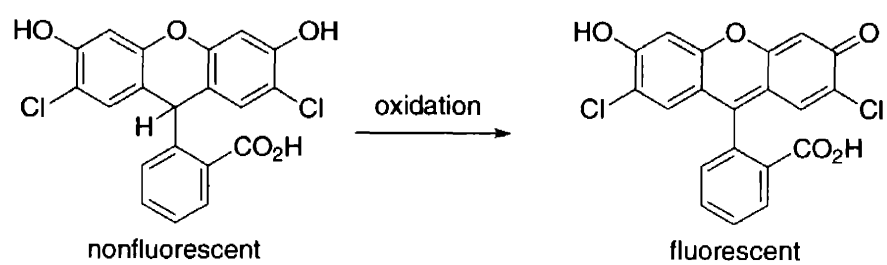
Scheme 1.5. The oxidation dichlorofluorescin to dichlorofluorescein.
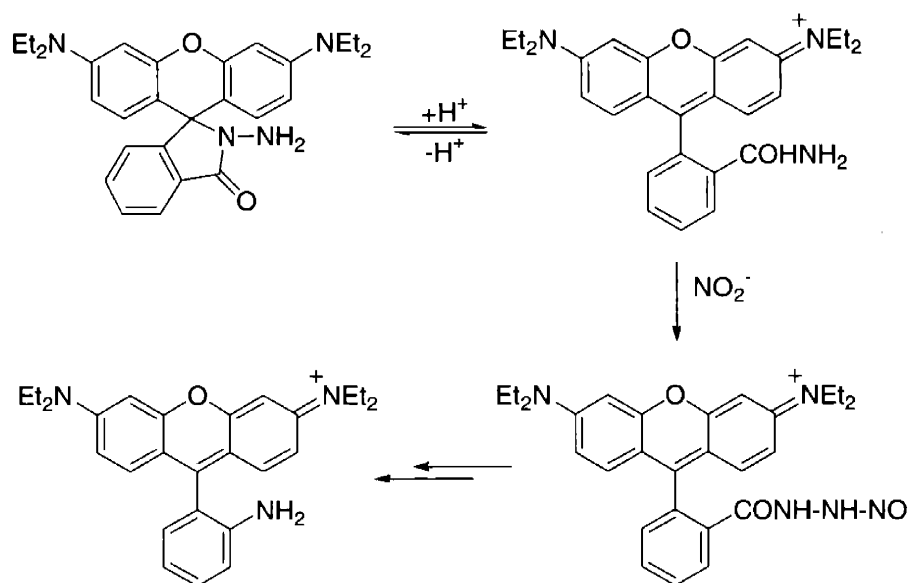
Scheme 1.6. The proposed mechanism for the conversion of RBH into a fluorescent species on reaction with NO_2^-.
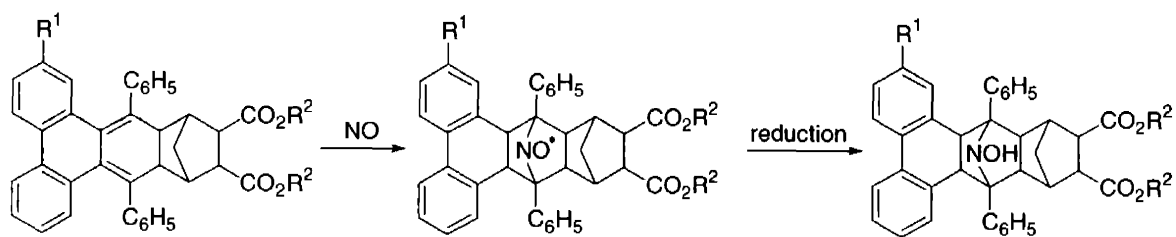
	R¹	R²
1	H	H
2	H	$CH_2CO_2CH_3$
3	$N(CH_3)_2$	H
4	$N(CH_3)_2$	$CH_2CO_2CH_3$

Scheme 1.7. Reaction of the FNOCTs to form fluorescent species.

highly fluorescent

nonfluorescent

NO
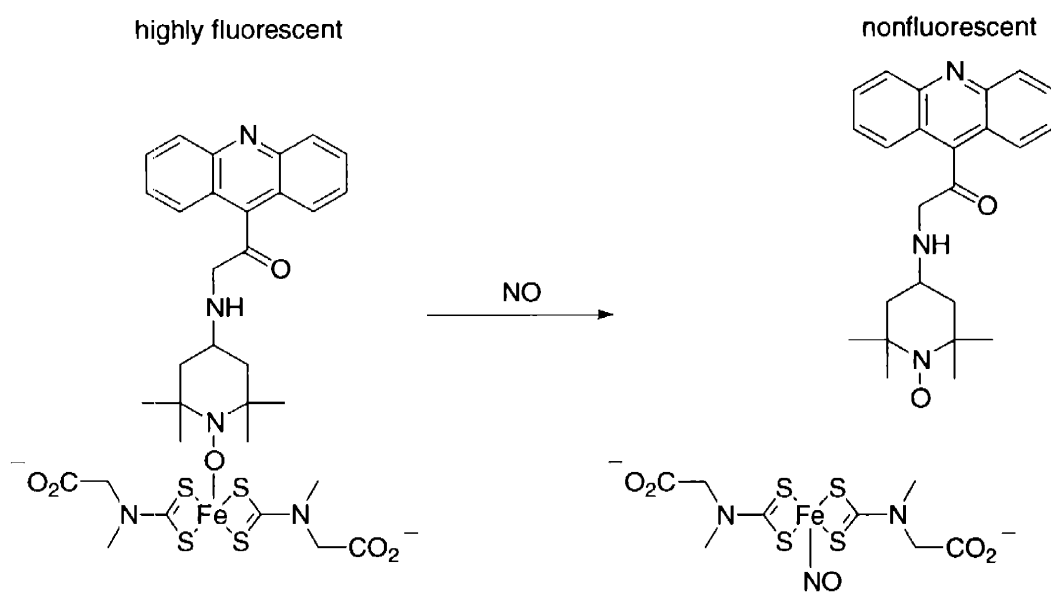
Scheme 1.8. Reaction of an Fe(dtc)$_2$-(acridine-TEMPO) conjugate with NO.
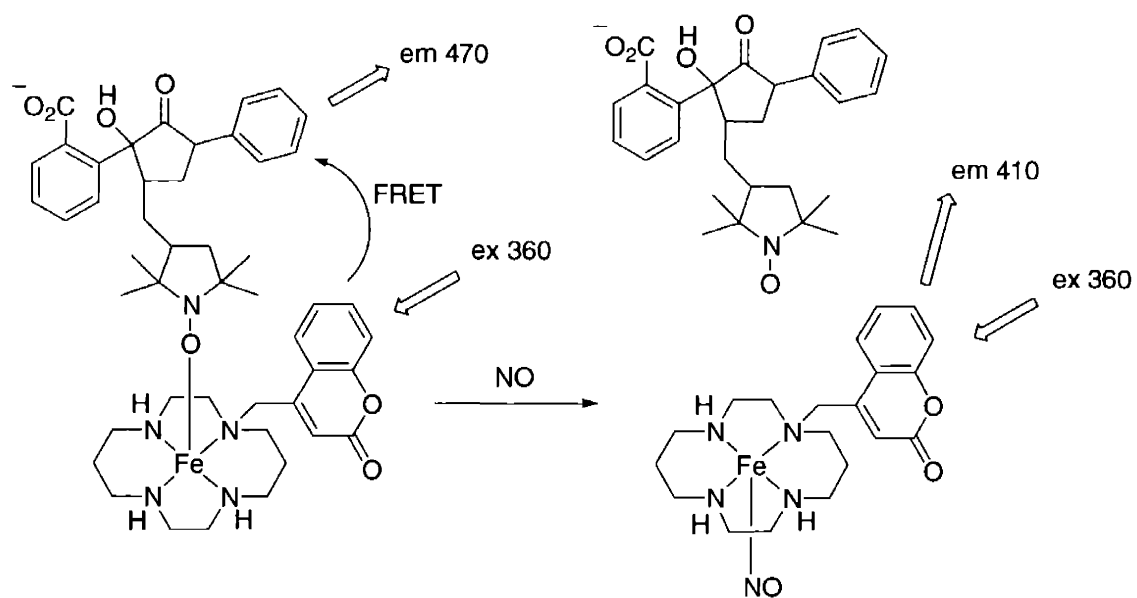
Scheme 1.9. An Fe(II)-cyclam-based ratiometric NO sensor.
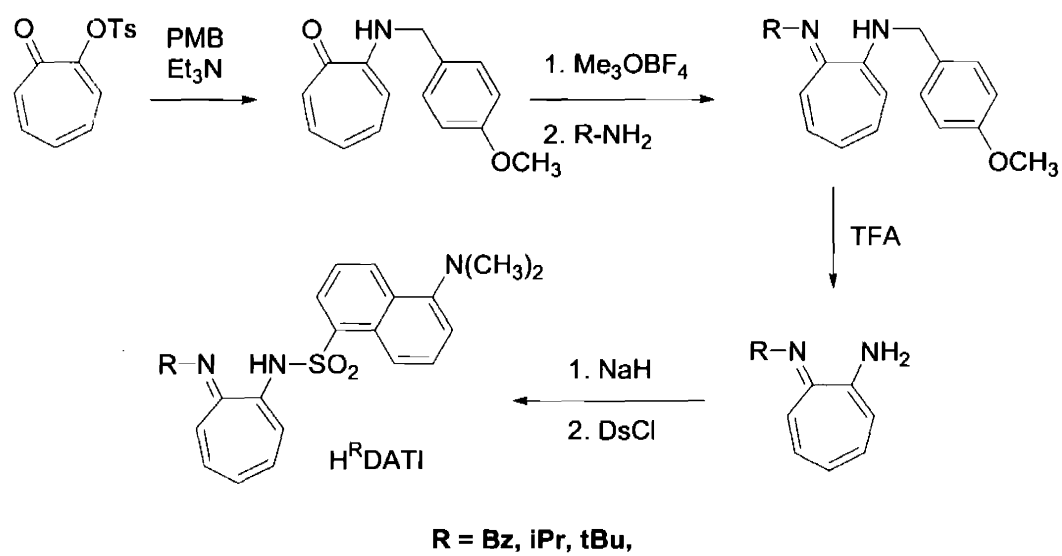
Scheme 1.10. Synthesis of the H^RDATI ligands.
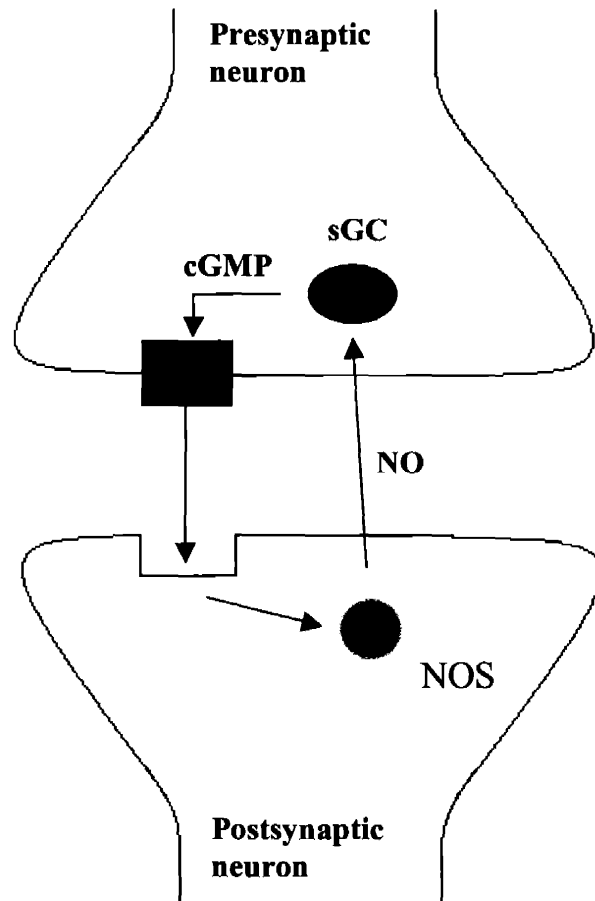
Figure 1.1. Illustration of the function of NO as a retrograde neurotransmitter where it is capable of diffusion from the postsynaptic neuron back to the presynaptic neuron.

	R_1	R_2	R_3	R_4	R_5
DAF-1	H	H	H	NH_2	NH_2
DAF-2	H	H	NH_2	NH_2	H
DAF-3	H	NH_2	NH_2	H	H
DAF-4	Cl	H	H	NH_2	NH_2
DAF-5	Cl	H	NH_2	NH_2	H
DAF-6	Cl	NH_2	NH_2	H	H
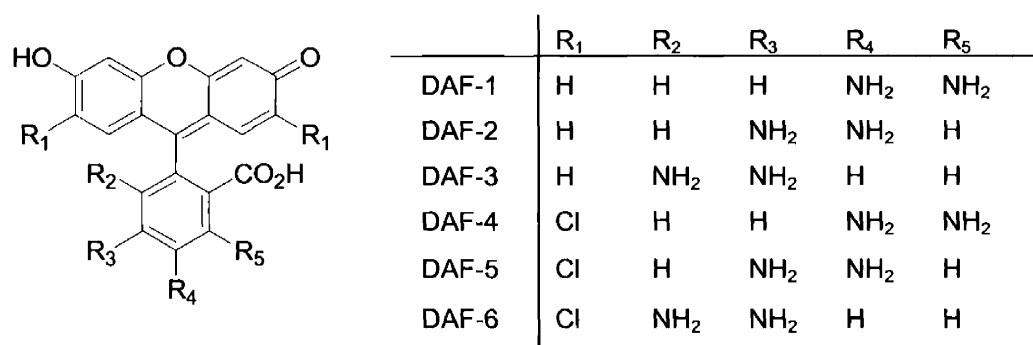
Figure 1.2. A family of diaminofluorescein derivatives.
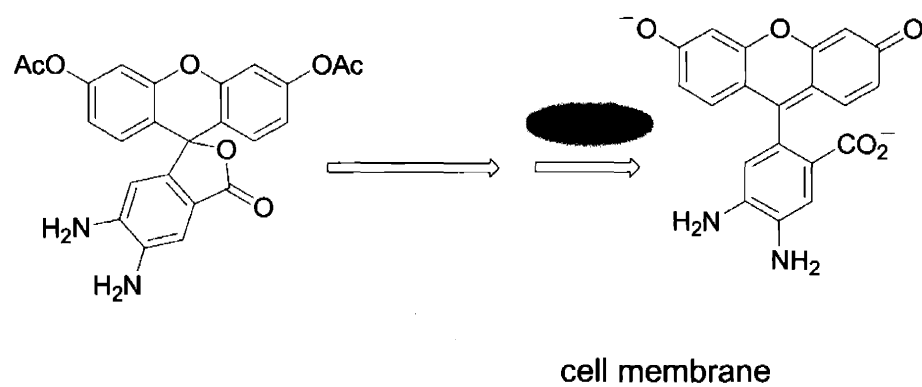
Figure 1.3. Schematic representation of DAF-2 DA, its diffusion across the cell membrane, and subsequent hydrolysis by intracellular esterases to afford DAF-2.
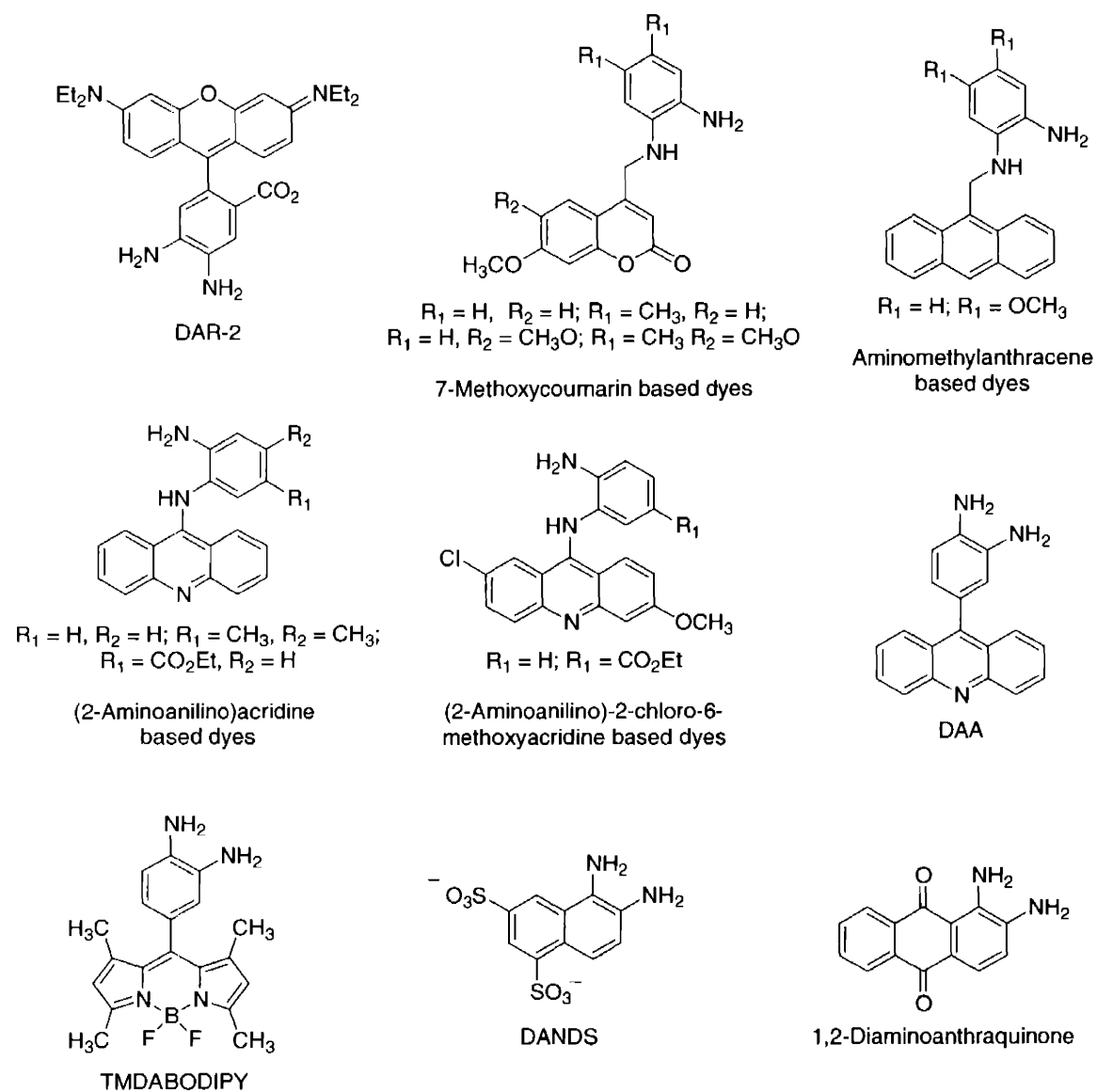
Figure 1.4. Fluorophore systems functionalized with an *o*-diamine moiety to act as NO sensors.
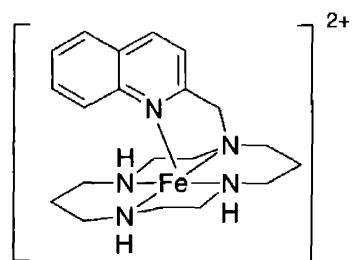
Figure 1.5. An Fe(II) quinoline pendant cyclam sensor, the design of which was based upon the active site of sGC.
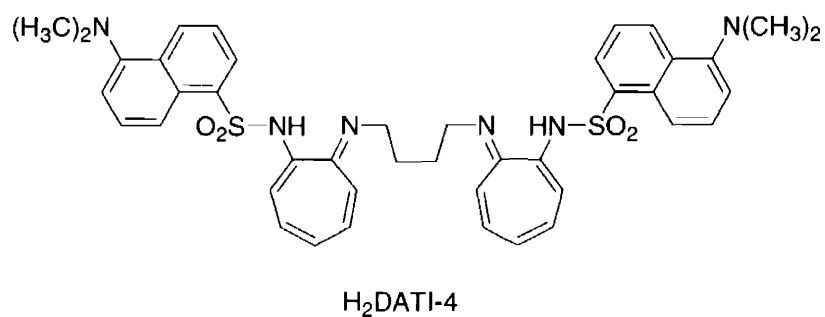
H₂DATI-4

Figure 1.6. The linked tropocoronand ligand, H₂DATI-4, prepared by an adaptation of the synthetic procedure used to make H₂^{iPr}DATI.
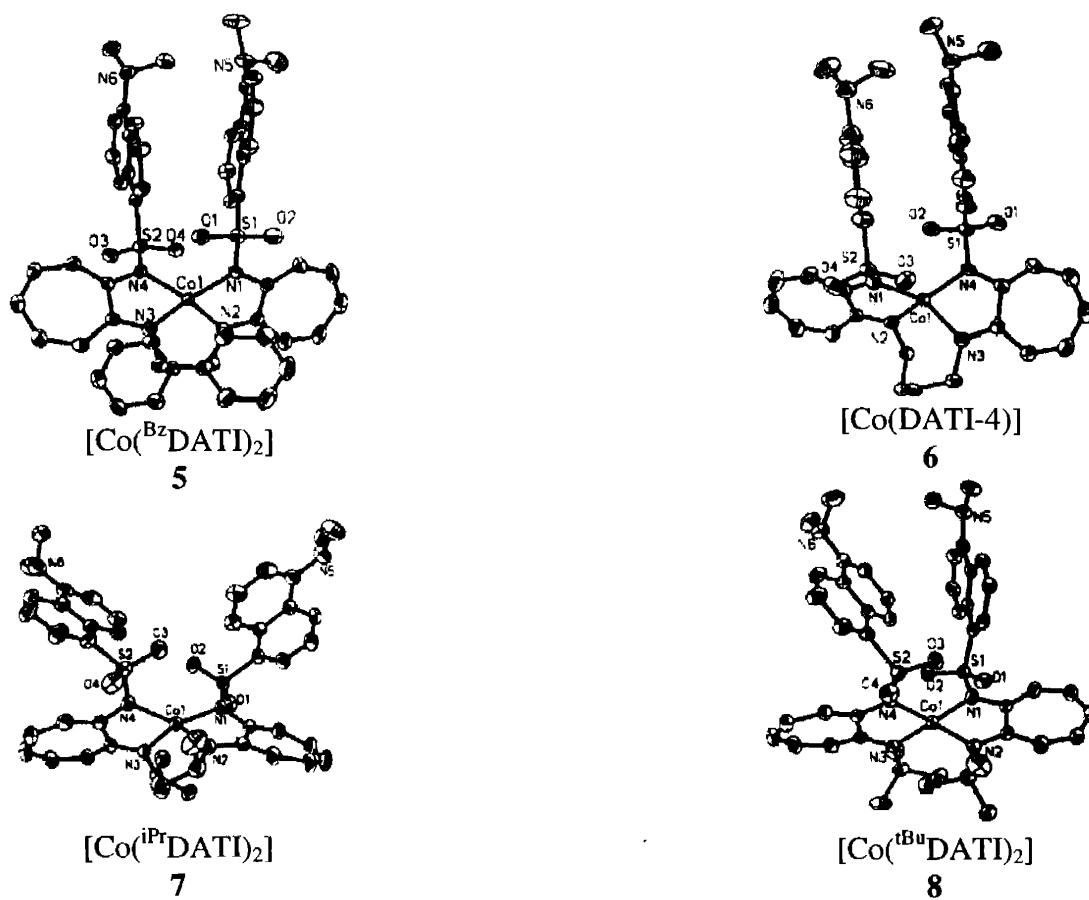
Figure 1.7. ORTEP diagrams showing 50% thermal ellipsoids for the cobalt complexes [Co(^{Bz}DATI)₂], [Co(DATI-4)], [Co(^{iPr}DATI)₂], and [Co(^{tBu}DATI)₂] as reported in reference 90.
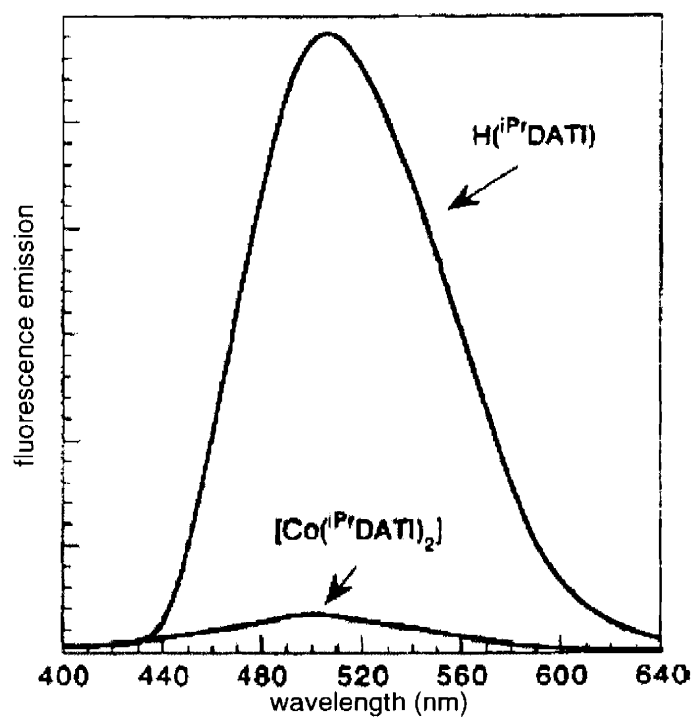
Figure 1.8. Comparison of the fluorescence emission intensity spectra of 46 μM CH₂Cl₂ solutions of H^{iPr}DATI and [Co(^{iPr}DATI)₂] as reported in reference 90. Fluorescence excitation is at 350 nm.
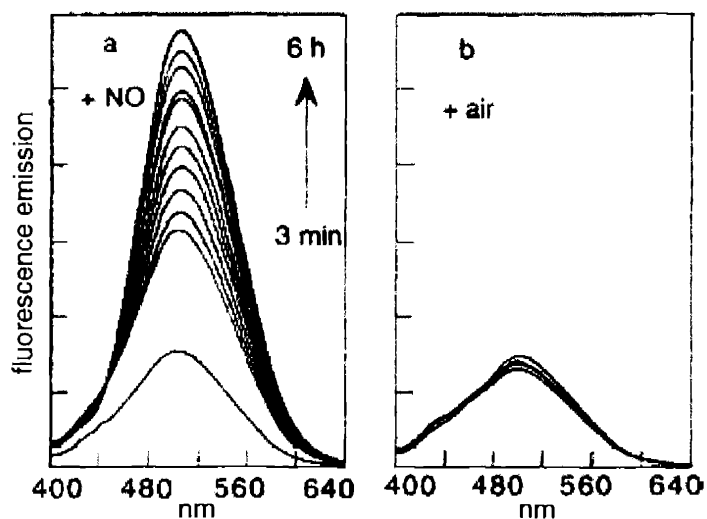
Figure 1.9. (a) Fluorescence emission intensity spectra showing the increase in intensity at 505 nm (excitation at 350 nm) when a 40 μM CH_2Cl_2 solution of [Co(DATI-4)] was exposed to 1 atm of NO gas. After 6 h, a greater than 4-fold increase in emission intensity is observed. (b) Fluorescence emission intensity spectra of a 40 μM CH_2Cl_2 solution of [Co(DATI-4)], showing no change in emission over a 6 h period. Previously reported in reference 91.

Chapter 2

Cobalt Chemistry with Mixed Aminotroponimine Salicylaldimine

Ligands: Synthesis, Characterization, and Nitric Oxide Reactivity

Introduction

Fluorescence detection methodologies are highly sensitive and have been employed to synthesize a variety of nitric oxide sensors, as described in Chapter 1. One strategy for preparing new fluorescent NO sensors is based on the NO chemistry of [Co(DATI-4)] and related compounds, previously prepared in our laboratory (Scheme 2.1). Upon reaction with excess NO, both [Co(^{iPr}DATI)$_2$] and [Co(^{iPr}DATI-4)] complexes show a steady increase in fluorescence emission intensity over several hours that is attributed to ejection of one of the dansyl moieties from the cobalt coordination sphere.[1] The reaction of NO with [Co(^{iPr}DATI-4)] is approximately 50-fold faster than with [Co(^{iPr}DATI)$_2$].[1] This increased reactivity is attributed to the added strain provided by the methylene linker on the pseudotetrahedral [Co(^{iPr}DATI-4)] complex. The reactions of both [Co(^{iPr}DATI)$_2$] and [Co(^{iPr}DATI-4)] with NO are too slow for use in biological systems, however, and neither complex is water-soluble.

New tactics are therefore needed to detect NO rapidly and directly in order to provide both temporal and spatial information. To achieve these goals, the use of fluorescence spectroscopy and transition metal-nitrosyl chemistry merits further investigation. Complexes that react directly and reversibly with NO, emitting light in the process, could ultimately be capable of detecting biological NO. In an extension of our previously reported dansyl aminotroponiminate work, we designed a new family of Co(II) complexes to address some of the shortcomings encountered.

In an effort to improve the reactivity and fluorescence properties, one of the aminotroponiminate moieties was replaced with a derivatized fluorescein having a coordination mode similar to that of salicylaldimines. Fluorescein has fluorescence

properties that are more amenable to biological sensing than the dansyl groups employed in the DATI complexes. Fluorescein typically has high quantum yields, approaching unity, and long wavelength excitation of 490 nm or greater. In addition, since fluorescein is more polar than dansyl, complexes with fluorescein-containing ligands are expected to be more water soluble than [Co(^{iPr}DATI)$_2$] and [Co(^{iPr}DATI-4)]. Owing to difficulties in purification and the preparation of large quantities of the fluorescein-containing complexes for characterization, salicylaldimine analogues were also synthesized for the purpose of characterization and investigation of their NO reactivity.

Experimental

General Considerations. Pentane, tetrahydrofuran (THF), and diethyl ether (Et$_2$O) were purified by passage through alumina columns under a N$_2$ atmosphere.[2] Dichloromethane (CH$_2$Cl$_2$), chloroform (CHCl$_3$), and acetonitrile (CH$_3$CN) were distilled from CaH$_2$ under a N$_2$ atmosphere. Anhydrous dimethylsulfoxide (DMSO), packaged under N$_2$, was purchased from Aldrich and used as received. Methanol (MeOH) used for fluorescence studies was distilled from magnesium and iodine under a N$_2$ atmosphere. All other solvents were purchased from Mallinckrodt or EM Science and used without further purification. Silica gel 60 (230-400 mesh, EM Science) was used for column chromatography. The starting material, 2-(isopropylamino)tropone, was prepared as previously described.[3] All other reagents were obtained commercially and used without further purification. IR spectra were recorded on a Bio Rad FTS-135 or a ThermoNicolet AVATAR 360 spectrophotometer. In situ IR spectra were recorded on a ReactIR 1000 instrument from ASI equipped with a 1-in.-diameter, 30-reflection silicon ATR (SiComp) probe. UV-visible spectra were recorded on a Hewlett-Packard 8435 spectrophotometer.

Unless otherwise mentioned, fluorescence emission intensity spectra were recorded at 25 ± 0.2 °C on a Hitachi F-3010 fluorescence spectrophotometer. Electrospray ionization (ESI) mass spectrometry was performed in the MIT Department of Chemistry Instrumentation Facility. NMR spectra were recorded on a Bruker DPX-400 spectrometer at ambient temperature and referenced to internal ^{1}H and ^{13}C solvent peaks. Nitric oxide (Matheson 99%) was purified by a method adapted from the literature.[4] The NO stream was passed through an Ascarite (NaOH fused on silica gel) column and a 6 ft coil filled with silica gel cooled to -78 °C with a dry ice/acetone bath.

2'-Carboxy-5-chloro-2,4-dihydroxybenzophenone (1). A portion of AlCl$_3$ (40.0 g, 300 mmol) was added to a solution of phthalic anhydride (20.0 g, 135 mmol) and 4-chlororesorcinol (18.8 g, 130 mmol) in 225 ml nitrobenzene and purged with N$_2$. After stirring overnight, the solution was poured into a vigorously stirred biphasic solution of 750 mL of hexanes and 1.0 L 0.5 M of aqueous HCl. The solution was allowed to stir for 2 h and the light tan precipitate that formed was filtered and washed with 200 mL of aqueous 0.1 M HCl and 300 mL of hexanes. The crude product was crystallized from hot McOH/H$_2$O (12.1 g, 32%). ^{1}H NMR (300 MHz, CD$_3$OD) δ 6.48 (1 H, s), 6.95 (1 H, s), 7.39 (1 H, dd, J = 7.2 1.5), 7.62-7.52 (2 H, m), 8.12 (1 H, dd, J = 1.2, 7.8). FTIR (KBr, cm^{-1}) 3390 (m br), 2828 (w), 2663 (w), 2547 (w), 1691 (s), 1615 (s), 1571 (m), 1488 (m), 1453 (w), 1419 (m), 1288 (s), 1219 (m), 1155 (s), 1141 (s), 925 (m), 894 (w), 862 (w), 772 (m), 738 (w), 709 (m), 682 (m), 649 (w), 615 (w), 590 (w), 538 (w). HRMS (ESI) MH$^+$: Calcd for C$_{14}$H$_{10}$ClO$_5$, 293.0217; Found, 293.0212.

7'-Chloro-4'-methylfluorescein dibenzoate (2). Benzophenone 1 (10.00 g, 34.1 mmol), 2-methylresorcinol (4.25 g, 34.1 mmol), and ZnCl$_2$ (0.90 g, 6.6 mmol) were

ground and melted at 200 °C. As the liquid was heated for 50 min, it turned into a brick red solid. The solid was cooled to room temperature, ground into a powder and boiled in 200 mL of 6 M aqueous HCl for 30 min. The dark red solid was then filtered, washed with deionized water, and dried. The crude 7'-chloro-4'-methylfluorescein was dissolved in 125 mL of pyridine and benzoic anhydride (30.5 g, 135 mmol) was added. After refluxing for 2.5 h, the orange solution was poured into 250 mL of deionized water. Upon cooling a light brown solid formed. The solid was filtered, dissolved in boiling toluene, filtered through activated charcoal, washed with 200 mL of hot toluene, and dried. Pure **2** was crystallized from hot toluene/EtOH (10.50 g, 52%). ^{1}H NMR (300 MHz, CD_2Cl_2) δ 2.37 (3 H, s), 6.74 (1 H, d, J = 8.7 Hz), 6.94 (1 H, d, J = 8.7 Hz), 7.00 (1 H, s), 7.30 (1 H, d, J = 7.5), 7.53-7.59 (4 H, m), 7.67-7.80 (4 H, m), 8.06 (1 H, d, J = 7.5 Hz), 8.20-8.24 (4 H, m). ^{13}C NMR (125 MHz, $CDCl_3$/DMF-d_7) δ 7.70, 79.73, 111.89, 111.98, 114.89, 117.012, 117.019, 117.86, 120.68, 122.74, 123.67, 123.76, 124.09, 124.55, 126.78, 127.16, 127.28, 127.33, 127.43, 127.49, 128.49, 128.62, 128.74, 129.16, 132.66, 132.94, 134.40, 147.13, 148.14, 149.43, 150.61, 162.09, 192.66, 166.88. FTIR (KBr, cm^{-1}) 3064 (w), 1771 (s), 1747 (s), 1600 (m), 1580 (m), 1482 (m), 1466 (w), 1451 (m), 1439 (w), 1409 (s), 1265 (s), 1242 (s sh), 1217 (s), 1180 (m), 1157 (s), 1081 (s), 1062 (s), 1022 (m), 710 (m), 693 (m). HRMS (ESI) MH$^+$: Calcd for $C_{35}H_{22}ClO_7$, 589.1054; Found, 589.1040.

7'-Chloro-4'-bromomethylfluorescein dibenzoate (3). 1,1'Azobis(cyclohexane-carbonitrile) (415 mg, 1.7 mmol) was added to a solution of **2** (10.00 g, 17.0 mmol), 1,3-dibromo-5,5-dimethylhydantoin (4.86 g, 17.0 mmol), and HOAc (300 μl, 5.3 mmol) in 400 mL of chlorobenzene. The light yellow solution was heated at 40 °C for 50 h and the solvent was removed under reduced pressure. Light orange crystals of **3** were obtained by

crystallization from hot toluene/EtOH (10.72 g, 94%). ^{1}H NMR (300 MHz, CD$_3$OD) δ

4.80 (2 H, s), 6.90 (1 H, d, J = 8.7 Hz), 7.02 (1 H, s), 7.08 (1 H, d, J = 8.7 Hz), 7.33 (1 H,

d, J = 7.5 Hz), 7.51 (1 H, s), 7.54-7.61 (4 H, m), 7.69-7.80 (4 H, m), 8.07 (1 H, d, J = 7.2

Hz), 8.22-8.27 (4 H, m). ^{13}C NMR (125 MHz, CDCl$_3$/DMF-d_7) δ 21.43, 80.98, 144.07,

117.40, 119.08, 119.56, 120.15, 122.90, 124.65, 125.63, 125.65, 126.40, 128.53, 128.56,

129.08, 129.27, 129.43, 129.52, 130.35, 130.47, 130.51, 131.16, 134.72, 134.94, 136.38,

149.15, 149.35, 150.35, 151.36, 152.90, 164.20, 168.66. FTIR (KBr, cm^{-1}) 3064 (w),

3035 (w), 1771 (s), 1746 (s), 1600 (m), 1580 (w), 1482 (m), 1466 (w), 1451 (m), 1439

(m), 1409 (s), 1265 (s), 1242 (s), 1217 (m), 1180 (m), 1157 (s), 1081 (s), 1062 (s), 1022

(m), 899 (m), 796 (w), 764 (w), 710 (m), 693 (m), 676 (w). HRMS (ESI) MNa$^+$: Calcd

for NaC$_{35}$H$_{20}$BrClO$_7$, 688.9979; Found, 688.9953.

7'-Chloro-4'-fluoresceincarboxaldehyde (4). Dibenzoate **3** (2.00 g, 3.0 mmol)

and NaHCO$_3$ (2.52 g, 30 mmol) in 75 mL of anhydrous DMSO were heated to 150 °C for

3 h. The deep red solution was stirred for an additional 1 h while cooling to 70 °C. An

orange precipitate formed as the solution was poured into 500 mL of 4 M HCl. After

stirring overnight, the mixture was extracted with CHCl$_3$ (4 x 150 mL) and the solvent

was removed to leave a dark orange-brown liquid. A light yellow solid precipitated upon

addition of 75 mL deionized water. Flash chromatography of the filtered and dried solid

on silica gel (33:1 CHCl$_3$/MeOH) yielded a light yellow solid. The light yellow solid was

dissolved in hot chlorobenzene and, upon cooling, **4** crystallized (207 mg, 18%). TLC

silica (9:1 CHCl$_3$/MeOH) R$_f$ = 0.57. ^{1}H NMR (300 MHz, CD$_2$Cl$_2$) δ 6.06 (1 H, s), 6.65 (1

H, d, J = 8.7 Hz), 6.81 (1 H, s), 6.90 (1 H, d, J = 8.7), 7.05 (1 H, s), 7.19 (1 H, d, J = 7.2

Hz), 7.67-7.70 (2 H, m), 8.03 (1 H, d, J = 6.9 Hz), 10.65 (1 H, s), 12.16 (1 H, s). ^{13}C

NMR (125 MHz, DMF-d_7) δ 81.67, 104.23, 109.12, 109.90, 111.30, 113.80, 117.75, 124.23, 125.11, 126.57, 128.58, 130.69, 136.00, 136.98, 150.04, 152.35, 153.05, 155.70, 162.83, 163.01, 163.30, 163.99, 168.99, 193.88. FTIR (KBr, cm^{-1}) 3238 (w br), 3075 (w), 1771 (m), 1726 (s), 1653 (s), 1588 (m), 1512 (w), 1467 (m), 1447 (m), 1429 (m), 1401 (m), 1359 (w), 1311 (m), 1294 (m), 1263 (s), 1249 (m sh), 1226 (s), 1151 (m), 1122 (m), 1097 (m br), 1036 (w), 1000 (w), 892 (w), 878 (m), 841 (w), 784 (w), 772 (m), 762 (w), 727 (w), 703 (m), 646 (w), 625 (w), 543 (w), 532 (w), 486 (m). HRMS (ESI) MH$^+$: Calcd for $C_{21}H_{12}ClO_6$, 395.0322; Found, 395.0308.

N-(3-Amino(*n*-propylamino)-2-(isopropylamino)troponimine (5). Under an atmosphere of argon, finely divided Me_3OBF_4 (2.66 g, 18.0 mmol) was added to a solution of 2-(isopropylamino)tropone (2.00 g, 12.2 mmol) in 30 mL of CH_2Cl_2 and allowed to stir for 2 h. The golden-yellow solution was added dropwise to neat 1,3-diaminopropane (15 mL, 180 mmol) over 45 min and allowed to stir for 2 h. After quenching with 40 mL water, the aqueous layer was extracted with CH_2Cl_2 (3 x 25 mL). The organic extracts were dried over $MgSO_4$, filtered, and the solvent was removed under reduced pressure giving a brown-yellow oil. The crude material was dissolved in dilute aqueous HCl. The solution was first extracted with CH_2Cl_2 to remove unwanted byproducts. The pH of the solution was then raised to 9 with aqueous NaOH and further extraction with CH_2Cl_2 (3 x 75 mL) was performed. The organic extract was dried over $MgSO_4$, filtered, and the solvent was removed under reduced pressure giving **5** (880 mg, 33%) as a yellow oil. ^{1}H NMR (400 MHz, CD_2Cl_2): δ 6.74-6.70 (2H, m), 6.33 (1H, d, J = 11.3 Hz), 6.25 (1H, d, J = 10.9 Hz), 6.13-6.08 (1H, m), 3.82 (1H, septet, J = 6.3 Hz), 3.36 (2H, t, J = 6.8 Hz), 2.82 (2H, t, J = 6.8 Hz), 1.84 (2H, p, J = 6.8 Hz), 1.23 (6H, d, J = 6.3

Hz). ^{13}C NMR (100 MHz, CDCl$_3$): δ 22.72, 34.13, 40.57, 44.99, 107.76, 112.39, 117.42, 132.58, 133.14, 151.08, 153.44. IR (NaCl, cm^{-1}): 3212 (w br), 2964 (m), 2928 (m), 2863 (w), 1589 (m), 1536 (m), 1510 (m), 1463 (m), 1414 (w), 1384 (m), 1326 (w), 1303 (w), 1272 (m), 1232 (w), 1206 (w), 1167 (m), 1121 (m br), 976 (w), 951 (w), 882 (w), 864 (w), 844 (w), 817 (w), 746 (w), 704 (m), 636 (w br). HRMS (ESI) MH$^+$: Calcd. for C$_{13}$H$_{22}$N$_3$, 220.1814; Found, 220.1802.

N-(4-Amino(*n*-butylamino))-2-(isopropylamino)troponimine (6). Under an argon atmosphere, finely divided Me$_3$OBF$_4$ (3.40 g, 23.0 mmol) was added to a solution of 2-(isopropylamino)tropone (3.00 g, 18.4 mmol) in 20 mL CH$_2$Cl$_2$. After stirring for 2 h, the golden solution was added dropwise over 30 min to 1,4-diaminobutane (6 mL, 60 mmol) and allowed to stir for an additional 2.5 h. The reaction was quenched by the addition of 20 of mL H$_2$O and extracted with CH$_2$Cl$_2$ (3 x 50 mL). The solvent was removed under reduced pressure to yield a yellow oil. The crude product was dissolved in water with acidification to pH 3 with HCl. The solution was first extracted with CH$_2$Cl$_2$ to remove unwanted byproducts. The pH of the solution was then raised to 9 with aqueous NaOH followed by extraction with CH$_2$Cl$_2$ (3 x 50 mL). The organic extract was dried over MgSO$_4$, filtered, and the solvent was removed under reduced pressure giving **6** (2.59 g, 60%) as an yellow oil. ^{1}H NMR (400 MHz, DMSO-d_6): δ 6.77-6.72 (2H, m), 6.32 (1H, d, J = 11.1 Hz), 6.26 (1H, d, J = 11.0 Hz), 6.12-6.07 (1H, m), 3.81 (1H, septet, J = 6.3 Hz), 3.25 (2H, t, J = 7.1 Hz), 2.57 (2H, t, J = 6.9 Hz), 1.65 (2H, p, J = 7.1 Hz), 1.44 (2H, p, J = 7.0 Hz), 1.17 (6H, d, J = 6.3 Hz). ^{13}C NMR (100 MHz, DMSO-d_6): δ 152.1, 150.9, 133.0, 132.9, 117.2, 109.8, 45.7, 45.1, 41.5, 31.4, 27.0, 22.8. IR (NaCl, cm^{-1}): 3371 (w), 3217 (w br), 3022 (w), 2965 (m), 2929 (m), 2860 (m), 1609 (w), 1590 (s),

1538 (s), 1514 (s), 1464 (s), 1415 (m), 1384 (m), 1273 (m), 1207 (m), 1168 (m), 1122 (w), 974 (w), 952 (w), 882 (w), 863 (w), 845 (w), 818 (w), 745 (m br), 704 (m), 641 (w). HRMS (ESI) MH^+: Calcd for $C_{14}H_{24}N_3$, 234.1970; Found, 234.1962.

$H_2{}^{iPr}SATI-3$ (7). Salicylaldehyde (157 mg, 1.29 mmol) in 5 mL of pentane was added to a solution of 5 (289 mg, 1.29 mmol) in 15 mL pentane and the reaction was stirred for 30 min. The pentane was decanted from the reaction flask to separate it from a small amount of brown oil that formed during the reaction. Removal of the pentane under reduced pressure afforded 7 as a yellow solid (370 mg, 89%). ^1H NMR (400 MHz, CD_2Cl_2): δ 8.38 (1H, s), 7.32-7.25 (2H, m), 6.93-6.85 (2H, m), 6.76-6.70 (2H, m), 6.40 (1H, d, J = 11.3 Hz), 6.20 (1H, d, J = 10.5 Hz), 6.12 (1H, t, J = 9.3 Hz), 3.86-3.75 (3H, m), 3.41 (2H, t, J = 6.7 Hz), 2.18 (2H, pentet, J = 6.4 Hz), 1.27 (6H, d, J = 6.3 Hz). ^{13}C NMR (100 MHz, CD_2Cl_2): δ 22.97, 32.27, 45.29, 45.62, 58.14, 107.42, 113.88, 117.26, 117.96, 118.89, 119.46, 131.76, 132.48, 133.05, 133.84, 151.43, 154.13, 161.80, 165.65. IR (NaCl, cm^{-1}): 3213 (w br), 3062 (w), 2966 (m), 2927 (m), 2863 (m), 1632 (s), 1609 (m), 1589 (s), 1537 (s), 1510 (s), 1463 (s), 1414 (w), 1384 (m), 1276 (s), 1207 (m), 1167 (m), 1151 (w), 1119 (w), 975 (w), 952 (w), 882 (w), 845 (w), 755 (m), 704 (m), 640 (w). HRMS (ESI) MH^+: Calcd for $C_{20}H_{26}N_3O$, 324.2076; Found, 324.2073.

$H_2{}^{iPr}SATI-4$ (8). To a solution of 6 (150 mg, 0.60 mmol) in 4 mL of CH_2Cl_2 was added salicylaldehyde (73 mg, 0.60 mmol) in 2 mL of CH_2Cl_2. After stirring overnight, the solvent was removed under reduced pressure yielding a golden-yellow oil that crystallized upon standing. The crystalline product was washed with cold hexanes to affording pure 8 (163 mg, 81%). ^1H NMR (400 MHz, DMSO-d_6): δ 8.38 (1H, s), 7.30-7.27 (2H, m), 6.93-6.88 (2H, m), 6.73-6.70 (2H, m), 6.34 (1H, d, J = 11.3 Hz), 6.24 (1H,

d, J = 10.8 Hz), 6.12-6.09 (1H, m), 3.82 (1H, septet, J = 6.3 Hz), 3.67 (2H, t, J = 5.4 Hz),

3.36 (2H, t, J = 6.5 Hz), 1.88-1.82 (4H, m), 1.24 (6H, d, J = 6.3 Hz). ^{13}C NMR (100

MHz, DMSO-d_6): δ 165.4, 161.8, 153.7, 151.6, 133.6, 133.0, 132.5, 131.7, 119.5, 118.9,

117.8, 117.3, 112.4, 108.5, 60.0, 47.4, 45.7, 29.5, 28.5, 23.0. IR (KBr, cm^{-1}): 3446 (w br),

3191 (w br), 3052 (w), 3027 (w), 2967 (w), 2917 (w), 2865 (w), 1629 (m), 1609 (w),

1589 (m), 1534 (m), 1509 (s), 1462 (m), 1383 (m), 1275 (m), 1205 (m), 1161 (w), 1150

(m), 1122 (w), 1083 (w), 1057 (w), 990 (w), 976 (w), 948 (w), 879 (w), 857 (w), 779 (w),

760 (m), 748 (m), 705 (m), 636 (w), 456 (w). HRMS (ESI) MH$^+$: Calcd for $C_{21}H_{28}N_3O$,

338.2232; Found, 338.2213.

$H_2^{iPr}FATI$-3 (9). To a solution of 4 (90 mg, 0.23 mmol) in 100 mL of Et$_2$O was

added 5 (50 mg, 0.23 mmol) in 8 mL of Et$_2$O. An orange precipitate formed immediately

upon addition of 4. After stirring for 30 min, the reaction was filtered, and the orange

precipitate was dried in vacuo giving 9 (96 mg, 70%). ^{1}H NMR (400 MHz, DMSO-d_6): δ

9.10 (1H, s), 8.01 (1H, d, J = 7.5 Hz), 7.77-7.68 (2H, m), 7.27 (1H, d, J = 7.5 Hz), 6.89

(1H, s), 6.81-6.75 (2H, m), 6.69 (1H, s), 6.58 (1H, d, J = 9.2 Hz), 6.45 (1H, d, J = 11.5

Hz), 6.39 (1H, d, J = 9.3 Hz), 6.13 (1H, t, J = 9.2 Hz), 3.91-3.79 (3H, m), 3.42 (2H, t, J =

6.7 Hz), 2.11 (2H, p, J = 6.7 Hz), 1.20 (6H, d, J = 6.3 Hz). IR (KBr, cm^{-1}): 3419 (w br),

3159 (w br), 2970 (w), 2923 (w), 1761 (m), 1644 (s), 1584 (s), 1517 (s), 1482 (s br), 1465

(s sh), 1440 (m sh), 1371 (s), 1343 (m sh), 1322 (m sh), 1277 (m), 1218 (m), 1169 (m),

1157 (m), 1093 (w), 997 (w), 884 (w), 830 (w), 762 (w), 703 (w), 667 (w), 627 (w), 595

(w), 549 (w), 470 (w). ^{13}C NMR (100 MHz, DMSO-d_6): δ 22.06, 30.31, 44.28, 44.48,

51.88, 103.68, 103.89, 104.08, 108.72, 110.56, 114.28, 118.36, 119.13, 124.75, 125.73,

127.98, 130.18, 133.01, 134.08, 134.91, 148.9, 150.41, 150.79, 151.56, 152.91, 158.3,

160.46, 168.58, 173.10. HRMS (ESI) MH$^+$: Calcd. for $C_{34}H_{31}N_3O_5Cl$, 596.1952; found 596.1957.

$H_2^{iPr}FATI-4$ (10). To a solution of 4 (80 mg, 0.20 mmol) in 8 mL of ethyl acetate was added 6 (53 mg, 0.23 mmol) in 2 mL of ethyl acetate. The solution containing a bright orange precipitate that formed was stirred for 30 min and filtered. The solid was washed with ethyl acetate and dried in vacuo, yielding 10 (79 mg, 65%) as a bright orange powder. ^1H NMR (400 MHz, DMSO-d_6): δ 9.12 (1H, s), 8.02 (1H, d, J = 7.5 Hz), 7.80-7.78 (2H, m), 7.29 (1H, d, J = 7.5 Hz), 6.90 (1H, s), 6.86-6.79 (2H, m), 6.70 (1H, s), 6.59 (1H, d, J = 9.3 Hz), 6.43 (1H, d, J = 11.4 Hz), 6.39 (1H, d, J = 9.3 Hz), 6.35 (1H, d, J = 11.0 Hz), 6.21-6.17 (1H, m) (1H, m), 3.85-3.76 (3H, m), 3.34 (2H, d, J = 6.3 Hz), 1.80-1.73 (4H, m), 1.15 (6 H, d, J = 6.2 Hz). ^{13}C NMR (100 MHz DMSO-d_6) δ 21.71, 26.44, 28.00, 44.84, 45.57, 52.71, 103.88, 104.02, 110.05, 110.39, 112.87, 118.88, 119.09, 120.23, 125.19, 126.16, 127.86, 129.0, 130.04, 133.14, 134.15, 134.29, 134.61, 147.3, 150.56, 151.45, 152.13, 152.37, 160.37, 168.66, 173.16. IR (KBr, cm^{-1}): 3443 (w br), 3159 (w br), 3023 (w), 2970 (w), 2931 (w), 2865 (w), 1762 (m), 1643 (s), 1585 (s), 1516 (s), 1483 (s), 1465 (s sh), 1370 (s), 1275 (m), 1219 (m), 1169 (m), 1093 (w), 997 (w), 883 (w), 830 (w), 705 (w), 667 (w), 627 (w), 595 (w), 550 (w), 469 (w). HRMS (ESI) MH$^+$: Calcd. for $C_{35}H_{33}N_3O_5Cl$, 610.2108; found 610.2099.

$[Co(^{iPr}SATI-3)]$ (11). Under an atmosphere of N$_2$, KH (480 mg, 12.0 mmol) was added to a solution of 7 (1.88 g, 5.8 mmol) in 40 mL of CH$_3$CN. An orange solution was obtained after stirring for 1 h. Upon addition of CoCl$_2$ (844 mg, 6.5 mmol) in 15 mL of CH$_3$CN over 15 min, the solution turned dark burgundy in color. After stirring for 3 h, the solvent was removed in vacuo. Crystallization from hot heptane afforded X-ray

quality burgundy crystals of **11** (816 mg, 37%). IR (KBr, cm^{-1}): 2993 (w), 2960 (w), 2925 (w), 2835 (w), 2809 (w), 1602 (m), 1582 (m), 1535 (m), 1504 (m), 1471 (m), 1441 (m), 1405 (m), 1369 (m), 1351 (m), 1327 (m), 1275 (m), 1257 (w), 1228 (m), 1143 (m), 1127 (m), 1060 (m), 954 (w), 901 (w), 886 (w), 842 (w), 806 (w), 761 (w), 752 (m), 727 (m), 716 (m), 625 (w), 576 (w), 550 (w), 529 (w), 488 (w), 459 (w). Anal: Calcd. for $C_{20}H_{23}N_3OCo$: C, 63.16; H, 6.10; N, 11.05. Found: C, 62.98; H, 6.16; N, 11.12.

[Co(NO)(^{iPr}SATI-3)] (12). Under an atmosphere of Ar, **11** (200 mg, 0.52 mmol) was dissolved in 10 mL of CH_2Cl_2 and exposed to excess NO. After stirring for 30 min, the solvent was removed in vacuo, and the resulting brown residue was washed with Et_2O and extracted into hot heptane. X-ray quality crystals of **12** (60 mg, 15%) were grown by slow evaporation of a solution of the crude product from heptane under an atmosphere of N_2. IR (KBr, cm^{-1}): 2950 (w), 2919 (w), 2879 (w), 1639 (s), 1619 (s), 1587 (m), 1538 (w), 1504 (m), 1472 (m), 1455 (m), 1437 (m), 1412 (m), 1400 (m), 1333 (w), 1274 (w), 1230 (w), 1147 (w), 1067 (w), 959 (w), 912 (w), 889 (w), 871 (w), 844 (w), 758 (w), 737 (w), 724 (w), 715 (w), 612 (w), 481 (w), 462 (w), 437 (w). Anal: Calcd. for $C_{20}H_{23}N_4O_2Co$: C, 58.54; H, 5.65; N, 13.65. Found: C, 58.77; H, 5.56; N, 13.92.

[Co$_2$(^{iPr}SATI-4)$_2$] (13). A portion of KH (12 mg, 0.30 mmol) was added to a 5 mL THF solution of **8** (50 mg, 0.15 mmol) under N_2. An orange solution was obtained after stirring for 1 h. Addition of [Co(CH$_3$CN)$_4$](PF$_6$)$_2$ (92 mg, 0.18 mmol) in 10 mL of THF turned the solution dark burgundy. After stirring for 4 h, the solvent was removed in vacuo. The residue was extracted into CH_2Cl_2 and filtered through celite. Pentane diffusion into a CHCl$_3$ solution of the complex gave X-ray quality crystals of **13** (39 mg, 66%). IR (KBr, cm^{-1}): 2958 (w), 2923 (w), 2862 (w), 1624 (m), 1593 (m), 1551 (w),

1510 (s), 1472 (m), 1445 (s), 1426 (m), 1412 (s), 1360 (m), 1331 (w), 1289 (m), 1263

(m), 1226 (m), 1149 (m), 1122 (w), 1011 (w), 987 (w), 853 (w), 886 (w), 857 (w), 817

(w), 783 (w), 758 (m), 719 (m), 669 (w), 588 (w), 568 (w), 463 (w), 443 (w). Anal:

Calcd. for $C_{42}H_{50}N_6O_2Co_2$: C, 63.96; H, 6.39; N, 10.65. Found: C, 63.86; H, 6.31; N,

10.68.

[Co(^{iPr}FATI-3)] (14). To a slurry of 9 (80 mg, 0.134 mmol) under an atmosphere

of N_2 in 10 mL CH_3CN was added KH (11 mg, 0.275 mmol). After stirring for 1 h,

[Co($CH_3CN)_4$]($PF_6)_2$ (72 mg, 0.140 mmol) in 5 mL CH_3CN was added. After stirring

overnight the dark red precipitate was filtered off and dried in vacuo to afford 14 (83 mg,

95%). IR (KBr, cm^{-1}): 3336 (w br), 3052 (w), 2963 (w), 2928 (w), 2870 (w), 1760 (m),

1633 (s sh), 1604 (s sh), 1575 (s), 1538 (s), 1503 (s), 1463 (s), 1397 (m), 1360 (m), 1339

(m), 1274 (w), 1221 (w), 1170 (m br), 1098 (w), 990 (m br), 885 (w), 827 (w), 761 (w),

716 (m), 630 (w), 591 (w), 551 (w), 480 (w), 467 (w). HRMS (ESI) M$^+$: Calcd. for

$C_{34}H_{28}N_3O_5ClCo$, 652.1049; found 652.1046. Because of difficulties in the purification

of 14, it was not possible to obtain a satisfactory elemental analysis.

[Co(^{iPr}FATI-4)] (15). A 2 mL MeOH solution of NaOMe (600 μL, 0.12 mmol of

a 0.2 M solution in MeOH) was added to a 10 mL MeOH slurry of 10 (36.0 mg, 0.057

mmol) under N_2. A clear, dark red-orange solution was obtained after stirring for 45 min.

Upon addition of [Co($CH_3CN)_4$]($PF_6)_2$ (29.0 mg, 0.057 mmol) in 5 mL of MeOH, the

solution darkened. The reaction was allowed to stir for 5 h and the solvent was removed

in vacuo. The residue was extracted with 8 mL of acetone and filtered to leave 15 (29

mg) as a red-brown powder. IR (KBr, cm^{-1}): 3056 (w), 2956 (w), 2924 (w), 2861 (w),

1761 (w), 1709 (w), 1636 (m), 1608 (m), 1575 (s), 1537 (m), 1492 (m), 1465 (s), 1396

(s), 1338 (s), 1267 (m), 1228 (m), 1170 (m), 1096 (w), 1003 (m), 885 (w), 830 (w), 762 (w), 715 (w), 630 (w), 555 (w), 479 (w). HRMS (ESI) M$^+$: Calcd. for $C_{35}H_{30}N_3O_5ClCo$, 666.1206; Found 666.1216. Due to difficulties in the purification of **15**, it was not possible to obtain a satisfactory elemental analysis.

X-Ray Crystallography. Single crystals suitable for data collection were covered in Infineum V8512 oil (formerly called Paratone-N oil), mounted on the tips of glass capillary tubes and transferred to a low-temperature nitrogen cold stream maintained by a Bruker KRYOFLEX BVT-AXS nitrogen cryostat. Data were collected on the Bruker diffractometer (MoK$_\alpha$ λ = 0.71073 Å) controlled by the SMART software package running on a Pentium II PC.[5] The general procedures used for data collection are reported elsewhere.[6] Empirical absorption corrections were calculated with the SADABS program.[7] Structures were solved by direct methods and refined with the SHELXTL and SAINTPLUS software packages on a Pentium II PC running the Windows NT operating system.[8,9] All non-hydrogen atoms, unless otherwise noted, were refined anisotropically. Hydrogen atoms were assigned idealized positions and given a thermal parameter of 1.2 times the thermal parameter of the atom to which it was attached. All structure solutions were checked for higher symmetry with the PLATON program.[10]

Complex **11** was solved in monoclinic P2$_1$/c. The β angle of approximately 90° indicated the possibility of higher symmetry or twinning whereby the unit cell is pseudo-orthorhombic. Attempts to model the twinning were made using the TWIN parameter in SHELXTL, but no suitable solution could be obtained. In addition, it was not possible to solve the structure using the higher symmetry orthorhombic cell by either direct or Patterson methods. The entire complex **11** is disordered over two positions and was

modeled with 73.6 and 26.4% occupancies for the two orientations. It was not possible to refine anisotropically all atoms of the 26.4% occupancy model.

Results and Discussion

Synthesis. The general synthetic route for the $H_2^{iPr}SATI$-n and $H_2^{iPr}FATI$-n ligands is outlined in Scheme 2.2. These molecules are constructed from the N,N'-disubstituted aminotroponimine class of ligands condensed either with salicylaldimine or 7'-chloro-4'-fluoresceincarboxaldehyde (**4**). The isopropyl group on the aminotroponimine ring was chosen for ease of synthesis. A variety of other alkyl groups such as *t*-butyl, benzyl, and methyl were prepared with the related dansyl-aminotroponiminate (H^RDATI) ligands,[1] but there were no major differences among the metal complexes with these alkyl groups.

The preparation of intermediates **5** and **6** is achieved by activation of 2-(isopropylamino)tropone with Me_3OBF_4 under argon followed by slow addition of the activated tropone to an excess of diamine. Intermediates **5** and **6** are then purified by selective precipitation and extraction from a dilute aqueous HCl solution when the pH is raised to 9 with NaOH in 33 and 60% yields, respectively. Compounds **5** and **6** are thermally sensitive yellow oils. On prolonged standing, even at -80° C, **5** decomposes to a yellow solid, **16**, identified by ^1H NMR spectroscopy and comparison to literature data (Scheme 2.3).[11] The condensations of **5** and **6** with salicylaldehyde give the salicylaldimines **7** and **8** in 80-90% yields. Ligands **7** and **8** are soluble in a variety of organic solvents including hexanes, Et_2O, CH_2Cl_2, CH_3CN, and MeOH.

The fluorescein carboxaldehyde is prepared in three steps. Condensation of 2-methylresorcinol with **1** is accomplished by heating the reagents with $ZnCl_2$ to 200° C.

The condensation also proceeds in neat solutions of trifluoroacetic acid or methanesulfonic acid. The product of the condensation reaction contains a mixture of the 7'-chloro-4'-methylfluorescein, 4',5'-dimethylfluorescein, and 2',7'-dichlorofluorescein. Because of the similarity of their structures it was not possible separate the three components in appreciable amounts. Formation of **2**, the dibenzoate protected product, followed by recrystallization provides an alternative purification procedure. Radical bromination of **2** with either 1,3-dibromo-5,5-dimethylhydantoin or N-bromosuccinamide cleanly affords **3** in nearly quantitative yield. The bromomethyl intermediate is then converted into carboxaldehyde **4** by heating to 150° C with NaHCO$_3$ in anhydrous DMSO. Purification of **4** by column chromatography followed by crystallization from hot chlorobenzene results in isolated yields of approximately 20%. Reaction of the appropriate aminotroponimine with **4** in either EtOAc or Et$_2$O cleanly and easily affords **9** or **10** as bright orange powders, which precipitate from the reaction in 65-70% yields.

The metal complexes **11** and **13** are prepared by deprotonation of the ligand with 2 equiv of potassium hydride in THF or CH$_3$CN followed by addition of [Co(CH$_3$CN)$_4$](PF$_6$)$_2$ or CoCl$_2$. Complex **11** is mononuclear whereas **13** is dinuclear. In attempts to prepare mononuclear complexes with ligand **13**, bases such as sodium methoxide and sodium hydride were employed. The metallation reaction was also attempted in alternative solvents such as CH$_2$Cl$_2$, CH$_3$CN, and MeOH; however, in all cases only dinuclear complexes were obtained. Both **11** and **13** are air-stable for several days as solids. The analogous H$_2$^{iPr}SATI-5 ligand, with an n-pentyl linker between the aminotroponimine and salicylaldimine groups, was also prepared, but it was not possible to isolate any metal complexes with this ligand. All metallation reactions with H$_2$^{iPr}SATI-

5 produced intractable solids that had limited or no solubility in all solvents investigated, indicating possible oligomer formation. By admission of excess NO gas to a Schlenk flask containing **11**, the dark brown mononitrosyl **12** was formed. No nitrosyl products were isolated from the reaction of NO with **13**, however.

The fluorescein-containing complexes **14** and **15** were prepared by deprotonation of the ligand with either potassium hydride or sodium methoxide followed by addition of [Co(CH$_3$CN)$_4$](PF$_6$)$_2$. Purification of **14** and **15** was hindered by the inability to crystallize the products.

Structural Studies. The structures of complexes **11**, **12**, and **13** are displayed in Figures 2.1 and 2.2 as ORTEP diagrams, and X-ray crystallographic data for the complexes are given in Table 2.1. Selected bond distances and angles from the single crystal X-ray diffraction data and those of related salicylaldimine[12,13] and aminotroponimine[14] complexes are presented in Table 2.2. Complex **11** has a square planar geometry similar to those of [Co(SALEN)] and [Co(TC-3,3)] (Figure 2.3). The steric constraints imposed by the ethyl and propyl linkers in these ligands enforce square-planar geometry, which is in contrast to the tetrahedral geometry common in many Co^{2+} complexes.[15] The square planar geometry of **11** confers other structural similarities to [Co(SALEN)] and [Co(TC-3,3)].[12,16] The average Co–N distance from the aminotroponiminate moiety of 1.874(6) Å in **11** is similar to the corresponding average of 1.869 Å in [Co(TC-3,3)].[16] The Co–O and Co–N distances of 1.875(5) and 1.887(6) Å, respectively, are only slightly longer than the corresponding average distances of 1.852 and 1.845 Å, respectively, in [Co(SALEN)].[12]

The dihedral angle Θ, measured between the planes of the salicylaldiminate and aminotroponiminate chelate rings, is 9.4° in **11**, indicating slight distortion from an ideal square planar geometry. The dihedral angle in **11** is similar to the corresponding angle of 9.0° observed in [Co(TC-3,3)], but larger than the Θ value of 2.2° in [Co(SALEN)].[12,16] Another related but more flexible complex, [Co(TC-4,4)][16] has a Θ value of 32.0° and displays similar reactivity to **11**, vida infra.

The mononitrosyl **12**, is also structurally similar to the corresponding nitrosyl complexes of [Co(SALEN)] and [Co(TC-3,3)]. The nitrosyl N–O distance in **12** of 1.132(4) Å is intermediate between the 1.118 Å average and 1.137 Å value from [Co(SALEN)NO] and [Co(TC-3,3)NO], respectively.[13,14] The 1.807(4), 1.806, and 1.785 Å Co–NO distances in **12**, [Co(SALEN)(NO)], and [Co(TC-3,3)(NO)], respectively, are also quite similar. The Co–N–O angle of 128.2(4)° is in good agreement with the values reported for [Co(SALEN)(NO)] and [Co(TC-3,3)(NO)].[13,14] Although **11** is structurally similar to [Co(SALEN)] and [Co(TC-3,3)], its reactivity in the presence of excess NO follows more closely that of [Co(TC-4,4)].

Ligand **8** was designed to form mononuclear Co(II) complexes with a distorted tetrahedral geometry as observed previously with [Co(^{iPr}DATI)$_2$] and [Co(DATI-4)]. Instead, only dinuclear complexes were isolated. The two ligands in **13** bridge the Co(II) centers resulting in nearly tetrahedral geometries. The Θ values of 86.8 and 87.2° of the two metal centers in **13** are close to the 90° value for an idealized tetrahedron. These Θ values are very similar to the 89.5° Θ value reported for [Co(i-Pr$_2$ATI)$_2$] but much less constrained than the 63.3° Θ value for the mononuclear [Co(DATI-4)], which also has a n-butyl linker.[1] The average Co–N bond distance of 1.968(3) Å in **13** is only slightly

shorter than the value of 1.980 Å reported for [Co(i-Pr$_2$ATI)$_2$] and quite similar to the 1.971 Å value for [Co(TC-6,6)].[1,16]

Although no X-ray structural data for **14** and **15** are available due to the inability to crystallize these complexes, known structures can be used to postulate their coordination geometry. Complex **14** is expected to have a square-planar geometry analogous to that of **11**. Based on the structural data for **13**, a similar dinuclear structure could be proposed for **15**, although no evidence was observed in the APCI and high resolution ESI mass spectral data to indicate the presence of a dinuclear species with an expected MH$^+$ mass of 1334.3 amu. Given this result, a mononuclear complex with a distorted tetrahedral geometry similar to [Co(DATI-4)] seems more plausible, but the possibility of a dinuclear complex cannot be ruled out.

Reactivity. Figure 2.4 displays the solution IR spectra of a DMSO solution of **11** purged with Ar following admission of excess NO at room temperature. The initial yellow-brown solution quickly turns dark red-brown within 10 min after exposure to NO. The first step in the reaction is formation of the crystallographically characterized mononitrosyl **12**, identified by its NO stretch at 1621 cm^{-1}. Within 40 min, additional IR features at 1598 and 2115 cm^{-1} begin to form. After 2.5 h, no additional spectral changes are observed. The IR band at 2115 cm^{-1} is attributed to formation of a cobalt-dinitrogen species.[17] The related complex, [Co(TC-4,4)] also reacts similarly with formation of an IR band at 2108 cm^{-1}. Isotope labeling experiments using ^{15}NO previously conducted with [Co(TC-4,4)] indicated the presence of a dinitrogen adduct. The additional band that appears at 1598 cm^{-1} in Figure 2.4 is consistent with formation of a Co(NO)(NO$_2$) species, which was also proposed for the reaction of [Co(TC-4,4)] with NO.[14] The

initially formed mononitrosyl band at 1621 cm^{-1} shifts to 1629 cm^{-1} after approximately

30 min. Such a shift to higher energy was also observed in the disproportionation reaction

of [Fe(TC-5,5)] with NO.[18] In that reaction, NO_2 formed during the reaction nitrated the

tropolone rings of the ligand, creating a more electron withdrawing ligand environment,

and thus a higher energy nitrosyl stretch. With 11 there is no evidence for dissociation of

the salicylaldiminate moiety from the cobalt center or for the formation of a $Co(NO)_2$

species, as observed for the reactions of [Co(^{iPr}DATI)$_2$] and [Co(DATI-4)] with NO.

Although 11 shares several structural similarities with [Co(SALEN)] and [Co(TC-

3,3)], it is important to note that their reactivities with NO differ. Neither [Co(SALEN)]

nor [Co(TC-3,3)] display any further reactivity after formation of the mononitrosyl

adducts. In fact, once formed, [Co(TC-3,3)(NO)] is stable enough that it can be

recrystallized in air.[14] The difference in reactivity is interesting, since 11, [Co(SALEN)],

and [Co(TC-3,3)] all have similar Co-ligand bond lengths and Θ values less than 10°,

which indicate nearly planar geometries. In contrast, the observed NO reactivity of

[Co(TC-4,4)], which has a Θ value of 32.0°, is nearly identical to that observed for 11.

Based on these observations, we conclude that the differences reactivity may be more a

function of ligand flexibility than structural similarities at the cobalt center. Both 11 and

[Co(TC-4,4)] should be more flexible than either [Co(SALEN)] or [Co(TC-3,3)]. In the

case of [Co(TC-3,3)], the two n-propyl linkers between the aminotroponiminate rings

severely limit the ability of the cobalt center to adopt new conformations. The n-butyl

linkers in [Co(TC-4,4)] are more flexible and even allow for formation of a trigonal

bipyramidal mononitrosyl complex.[14] In 11, the presence of only one n-propyl linker

instead of the two present in [Co(TC-3,3)] should afford more flexibility.

The time dependent solution IR spectra for the reaction of an Ar purged solution of **13** with excess NO at room temperature in DMSO are presented in Figure 2.5. During the course of the reaction a single nitrosyl band grows in at 1594 cm^{-1}. This feature may correspond to a Co(NO) or a Co(NO)(NO$_2$) species, the latter having been postulated for the reactions of **11** and [Co(TC-4,4)] with excess NO. An additional IR band at 2119 cm^{-1} also begins to form within the first 15 min of the reaction. Its appearance is significantly faster than in the reaction between **11** and NO, where the corresponding band at 2115 cm^{-1} was apparent only after 40 min. As with **11** and [Co(TC-4,4)], the IR band at 2119 cm^{-1} can be ascribed to formation of a cobalt-dinitrogen species. All attempts to isolate and characterize further such a putative dinitrogen adduct proved unsuccessful. If the solvent is removed from the reaction, however, the IR band at 2119 cm^{-1} is stable for several days in air. Although the possibility cannot be ruled out, there is no direct evidence for dissociation of the salicylaldiminate moiety of **13** from the cobalt center to form a dinitrosyl species.

The reaction of **14** with NO was followed by IR spectroscopy. Within five minutes after exposure of a solution of **14** in DMSO to excess NO, a new band that is consistent with a nitrosyl stretch appears at 1630 cm^{-1}(Figure 2.6), a result in good agreement with the nitrosyl band at 1621 cm^{-1} observed in the reaction of **11** with NO. Additionally, a second band begins appear at 2114 cm^{-1} one hour after exposure to NO. Again, this feature is in good agreement with the results from **11**. As with **11**, no evidence for formation of a dinitrosyl species is observed; however, the intense band from the fluorescein carboxylic acid at 1759 cm^{-1} (Figure 2.6) may conceal bands from a dinitrosyl species.

Complex **15** reacts with excess NO in CH₃CN and displays similar IR features as those observed for the reaction of **13** with NO. Following exposure to excess NO, a new band at 2117 cm^{-1} appears. As with **11** and **14**, the 2117 cm^{-1} band corresponds to a possible dinitrogen adduct. An additional new, but very weak, IR band at 1830 cm^{-1} could be a NO stretching band of a cobalt dinitrosyl complex. An intense band at 1760 cm^{-1}, as expected, is consistent with either a lactone or carboxylic acid from the fluorescein.[19]

Fluorescence Spectroscopic Measurements. The reaction of **14** with NO, when followed by fluorescence spectroscopy, does not show a significant increase in fluorescence. Exposure of **14** to excess NO in MeOH results in only a 20% increase in fluorescence emission intensity four hours after exposure to NO (Figure 2.7). If there were complete dissociation of the fluorescein moiety from the cobalt center, as observed with [Co(DATI-4)], a larger fluorescence increase, approaching that of the free ligand, would be expected. The absence of a large fluorescence increase, however, is not surprising because the solution IR data for the reaction do not indicate the formation of a dinitrosyl species, generation of which would indicate dissociation of the fluorescein moiety, as observed in the reaction of NO with [Co(^{iPr}DATI)₂].

A fluorescence study of **15** in MeOH shows a 3-fold increase in fluorescence after 22 hours of exposure to excess NO (Figure 2.8). This fluorescence response is similar to that previously observed for [Co(DATI-4)], but is significantly slower. It is difficult to rationalize the fluorescence response of this system given the complex nature of the NO reactivity in these systems. The IR data reveal chemistry similar to that previously reported for [Co(TC-3,3)] and [Co(TC-4,4)] with NO, where formation of several

different species could be observed by IR spectroscopy. In addition, the spectra revealed mononitrosyl and dinitrogen adducts. Because of the formation of multiple products, it is unclear which species gives rise to the increase in fluorescence, the dinitrogen adduct, a dinitrosyl species, a mononitrosyl species, or some other unidentified species. Based on the small increase in fluorescence emission intensity observed on the reaction of **14** with NO, it seems unlikely that the fluorescence response of **15** results from the formation of the dinitrogen or mononitrosyl adducts, which are both observed by solution IR spectroscopy with **14**. Compound **15** is moderately stable to trace amounts of H_2O, although a 13% increase in fluorescence emission intensity is observed after addition of 10 μL of H_2O to a 10 μM solution of **15** in MeOH. The fluorescence emission intensity rapidly increases when **15** is dissolved pH 7.4 phosphate buffer, however. A 2.5-fold increase in emission intensity is observed between 10 min and 3 h after preparation of the buffer solution (Figure 2.9). The fluorescence increase in aqueous solution is presumably due to dissociation of the metal complex to afford the free ligand. Although **14** and **15** are sufficiently air stable in solution, the complicated slow reactivity with NO and sensitivity to water limits the potential uses of this system for measuring of NO in aqueous environments.

Conclusions

A new series of ligands containing an aminotroponimine moiety linked by an alkyl chain to a salicylaldimine or a fluorescein have been prepared and their coordination chemistry investigated. The Co(II) complexes of the salicylaldimine ligands, **7** and **8** were prepared and characterized. Cobalt complex **11** reacts with NO to form an initial mononitrosyl species, which then undergoes further reactivity in the presence of

excess NO to form a dinitrogen adduct as characterized by solution IR spectroscopy. The reactivity of **11** is similar to that of [Co(TC-4,4)]. Complex **13**, formed by the reaction of $[Co(CH_3CN)_4](PF_6)_2$ with ligand **8,** gives a dinuclear species where the two ligands bridge the two cobalt centers. It also reacts with NO ultimately to form a dinitrogen adduct. Although no X-ray crystallographic characterization of **14** and **15** was possible, mass spectrometry data indicates both complexes to be mononuclear, although in the case of **15** a dinuclear structure similar to **13** cannot be ruled out. As expected, the NO reactivity of **14** and **15** is similar to that observed for the model complexes **11** and **13**. A modest, but slow 3-fold increase in fluorescence emission intensity is observed 22 h after exposure of **15** to excess NO. Because multiple products form during the reaction, none of which could be crystallized, it is unclear what species gives rise to the increase in fluorescence emission intensity. It is unlikely that the increase in emission intensity is from the mononitrosyl or dinitrogen adducts, since only minimal fluorescence response observed following exposure of **14** to NO, where both the dinitrogen and mononitrosyl adducts are also observed.

References

(1) Franz, K. J.; Singh, N.; Spingler, B.; Lippard, S. J. *Inorg. Chem.* **2000**, *39*, 4081.

(2) Pangborn, A. B.; Giardello, M. A.; Grubbs, R. H.; Rosen, R. K.; Timmers, F. J. *Organometallics* **1996**, *15*, 1518.

(3) Dias, H. V. R.; Jin, W.; Ratcliff, R. E. *Inorg. Chem.* **1995**, *34*, 6100.

(4) Lorkovic, I. M.; Ford, P. C. *Inorg. Chem* **2000**, *39*, 632.

(5) *SMART: Software for the CCD Detector System*, version 5.626; Bruker AXS: Madison, WI, 2000.

(6) Kuzelka, J.; Mukhopadhyay, S.; Spingler, B.; Lippard, S. J. *Inorg. Chem* **2004**, *43*, in press.

(7) Sheldrick, G. M. *SADABS: Aera-Detector Absorption Correction*; University of Göttingen, Göttingen Germany, 2001.

(8) *SHELXTL: Program Library for Structure Solution and Molecular Graphics*, version 6.2; Bruker AXS: Madison, WI, 2001.

(9) *SAINTPLUS: Software for the CCD Detector System*, version 5.01; Bruker AXS: Madison, WI, 1998.

(10) Spek, A. L. *PLATON, A Multipurpose Crystallographic Tool*; Utrecht University: Utrecht, The Netherlands, 2000.

(11) Nozoe, T.; Shindo, K.; Wakabayashi, H.; Ishikawa, S. *Heterocycles* **1992**, *34*, 881.

(12) Schaefer, W. P.; Marsh, R. E. *Acta. Crystallogr., Sect. B* **1969**, *B25*, 1675.

(13) Haller, K. J.; Enemark, J. H. *Acta. Crystallogr., Sect. B* **1978**, *B34*, 102.

(14) Franz, K. J.; H., D. L.; Spingler, B.; Lippard, S. J. *Inorg. Chem* **2001**, *40*, 3774.

(15) Cotton, F. A.; Wilkinson, G. *Advanced Inorganic Chemistry*; 5th ed.; Wiley-Interscience: New York, 1998.

(16) Jaynes, B. S.; Doerrer, L. H.; Liu, S.; Lippard, S. J. *Inorg. Chem* **1995**, *34*, 5735.

(17) Chatt, J.; Dilworth, J. R.; Richards, R. L. *Chem. Rev.* **1978**, *78*, 589.

(18) Franz, K. J.; Lippard, S. J. *J. Am. Chem. Soc.* **1999**, *121*, 10504.

(19) Silverstein, R. M.; Webster, F. X. *Spectrometric Identification of Organic Compounds*; 6th ed.; John Wiley and Sons, Inc.: New York, 1998.

Table 2.1. Summary of X-ray Crystallographic Data for **11**, **12**, and **13**.

	11	**12**	**13·CHCl$_3$·C$_5$H$_{12}$**
formula	C$_{20}$H$_{23}$N$_3$OCo	C$_{20}$H$_{23}$N$_4$O$_2$Co	C$_{48}$H$_{65}$N$_6$O$_2$Cl$_3$Co$_2$
fw	380.34	410.35	982.27
space group	P2$_1$/c	P2$_1$/c	P2$_1$/n
a,Å	9.351(1)	13.723(2)	13.8321(2)
b Å	9.252(1)	14.452(2)	24.9517(1)
c Å	20.722(3)	9.803(2)	14.6924(1)
β, deg	90.29(3)	109.674(3)	99.229(1)
V, Å^3	1792.8(4)	1830.6(5)	5005.21(8)
Z	4	4	4
ρ_{calc}, g/cm^3	1.409	1.489	1.304
T, °C	-100	-100	-100
μ(Mo Kα), mm^{-1}	0.970	0.961	0.865
total no. of data	7888	14325	30866
no. of unique data	2586	4271	11459
no. of params	226	336	550
R (%)[a]	6.54	6.18	7.09
wR^2 (%)[b]	16.33	12.57	15.15

[a]$R = \Sigma||F_o|-F_c||/\Sigma|F_o|$, [b]$wR^2 = \{w(F_o^2-F_c^2)^2/\Sigma[w(F_o^2)^2]\}^{1/2}$

Table 2.2. Selected Bond Distances and Angles for **11**, **12**, and **13**.[a]

Compound	Distances	(Å)	Angles	(deg)
[Co(^{iPr}SATI-3)]	Co1-N1	1.898(5)	N1-Co1-N2	83.4(3)
(**11**)	Co1-N2	1.849(5)	N1-Co1-N3	176.9(2)
	Co1-N3	1.887(6)	N1-Co1-O1	90.1(2)
	Co1-O1	1.875(4)	N2-Co1-N3	96.6(3)
			N2-Co1-O1	169.0(2)
			N3-Co1-O1	89.4(3)
[Co(^{iPr}SATI-3)NO]	Co1-N1	1.914(3)	N1-Co1-N2	82.0(1)
(**12**)	Co1-N2	1.904(3)	N1-Co1-N3	157.7(1)
	Co1-N3	1.954(4)	N1-Co1-N4	102.0(2)
	Co1-N4	1.807(4)	N1-Co1-O1	89.5(1)
	Co1-O1	1.903(3)	N2-Co1-N3	93.6(2)
	N4-O2	1.132(5)	N2-Co1-N4	96.7(2)
			N2-Co1-O1	166.5(1)
			N3-Co1-N4	100.3(2)
			N3-Co1-O1	90.4(1)
			N4-Co1-O1	95.2(2)
			Co1-N4-O2	128.2(4)
[Co$_2$(^{iPr}SATI-4)$_2$]	Co1-N3	1.984(3)	N1-Co2-N2	81.6(2)
(**13**)	Co1-N4	1.970(3)	N1-Co2-N6	123.2(1)
	Co1-N5	1.955(3)	N1-Co2-O2	113.3(1)
	Co1-O1	1.904(3)	N2-Co2-N6	121.2(1)
	Co2-N1	1.978(4)	N2-Co2-O2	121.4(1)
	Co2-N2	1.968(3)	N6-Co2-O2	95.8(1)
	Co2-N6	1.993(3)	N3-Co1-N4	120.5(1)
	Co2-O2	1.908(3)	N3-Co1-N5	121.6(1)
			N3-Co1-O1	96.7(1)
			N4-Co1-N5	82.3(1)
			N4-Co1-O1	115.4(1)
			N5-Co1-O1	122.4(1)
[Co(SALEN)][b]	Co-O$_{salen}$	1.852		
	Co-N$_{salen}$	1.845		
[Co(SALEN)(NO)][c]	Co-O$_{salen(avg)}$	1.872	Co-N-O$_{av}$	127.0
	Co-N$_{salen(avg)}$	1.878		
	Co-NO	1.806		
	N-O	1.118		
[Co(TC-3,3)][d]	Co-N$_{av}$	1.896		
[Co(TC-3,3)NO][e]	Co-N$_{TC(avg)}$	1.90	Co-N-O	127.3
	Co-NO	1.785		
	N-O	1.137		

[a]Numbers in parentheses are estimated standard deviations of the last significant figure. Atoms are labeled as indicated in Figures 2.1 and 2.2. [b]Ref. 12. [c]Ref. 13. [d]Ref. 16. [e]Ref. 14.

Table 2.3. Atomic coordinates (x 10^4) and equivalent isotropic displacement parameters ($\text{\AA}^2$x 10^3) for [Co(^{iPr}SATI-3)] **(11)**. U(eq) is defined as one third of the trace of the orthogonalized U^{ij} tensor.

	x	y	z	U(eq)
Co(1)	1844(1)	4702(1)	1886(1)	31(1)
N(1)	3447(12)	3479(16)	2187(3)	33(2)
N(1A)	1760(40)	3470(60)	1105(15)	44(6)
N(2)	2148(8)	5561(7)	2687(3)	67(3)
N(2A)	287(8)	5768(7)	1583(3)	41(7)
N(3)	275(7)	5890(8)	1588(3)	61(4)
N(3A)	2071(7)	5708(8)	2643(3)	27(5)
O(1)	1486(9)	3406(18)	1232(4)	41(2)
O(1A)	3070(30)	3550(30)	2257(12)	50(6)
C(1)	492(7)	3346(8)	800(3)	49(3)
C(1A)	3589(7)	3509(8)	2822(3)	39(8)
C(2)	410(8)	2202(9)	358(3)	50(3)
C(2A)	4442(8)	2470(9)	3136(3)	42(9)
C(3)	-698(9)	2053(10)	-69(4)	63(4)
C(3A)	4761(9)	2341(10)	3791(4)	52(9)
C(4)	-1831(10)	2983(12)	-103(4)	68(4)
C(4A)	4301(10)	3201(12)	4308(4)	56(9)
C(5)	-1852(9)	4188(13)	305(5)	74(4)
C(5A)	3434(9)	4405(13)	4241(5)	54(9)
C(6)	-690(7)	4326(9)	755(4)	43(2)
C(6A)	3053(19)	4540(20)	3452(13)	41(5)
C(7)	-671(6)	5617(8)	1177(3)	43(2)
C(7A)	2214(17)	5820(20)	3231(9)	58(4)
C(8)	-17(11)	7296(9)	1930(5)	56(3)
C(8A)	1190(30)	7430(20)	2626(9)	46(5)
C(9)	1232(10)	7888(8)	2308(5)	50(2)
C(9A)	710(30)	7870(20)	1945(12)	44(5)
C(10)	1606(7)	6958(7)	2873(4)	43(2)
C(10A)	-360(20)	6920(20)	1612(10)	52(5)
C(11)	2851(6)	4739(7)	3113(4)	28(2)
C(11A)	-250(20)	4700(20)	1013(9)	41(4)
C(12)	2815(7)	5078(8)	3767(4)	43(2)
C(12A)	-1380(30)	4910(20)	766(9)	57(5)
C(13)	3457(8)	4346(11)	4260(4)	64(4)
C(13A)	-1983(8)	4237(11)	270(4)	61(8)
C(14)	4329(9)	3189(10)	4308(3)	56(4)
C(14A)	-1872(9)	3040(10)	-115(3)	67(9)
C(15)	4765(8)	2346(8)	3802(4)	51(4)
C(15A)	-723(8)	2099(8)	-77(4)	61(9)
C(16)	4448(7)	2483(8)	3154(3)	42(4)
C(16A)	400(7)	2259(8)	360(3)	54(9)
C(17)	3583(6)	3518(7)	2832(3)	39(3)
C(17A)	465(6)	3432(7)	805(3)	48(7)
C(18)	4173(5)	2426(5)	1756(2)	28(1)
C(18A)	3211(17)	2495(16)	1047(7)	55(4)
C(19)	4602(4)	3115(5)	1113(2)	45(1)

Table 2.3. Continued.

	x	y	z	U(eq)
C(20)	3378(10)	998(11)	1699(4)	36(2)
C(20A)	3030(30)	1030(30)	1453(12)	54(7)

Table 2.4. Atomic coordinates (x 10^4) and equivalent isotropic displacement parameters (Å^2x 10^3) for [Co(NO)(^{iPr}SATI-3)] (**12**). U(eq) is defined as one third of the trace of the orthogonalized U^{ij} tensor.

	x	y	z	U(eq)
Co(1)	3033(1)	5742(1)	4001(1)	27(1)
N(1)	1970(3)	4900(2)	2945(4)	30(1)
N(2)	2453(3)	5505(2)	5480(4)	27(1)
N(3)	4362(3)	6142(2)	5373(4)	31(1)
N(4)	2417(3)	6851(3)	3446(4)	40(1)
O(1)	3619(2)	5671(2)	2501(3)	38(1)
O(2)	1843(3)	7218(3)	3860(5)	72(1)
C(3)	3541(4)	6685(3)	7090(6)	37(1)
C(10)	1553(3)	4407(3)	3748(5)	31(1)
C(11)	5186(3)	6331(3)	5070(5)	32(1)
C(17)	5298(3)	6332(3)	3677(5)	30(1)
C(19)	1750(3)	4828(3)	5196(5)	29(1)
C(21)	6232(3)	6626(3)	3514(5)	34(1)
C(25)	4478(3)	5999(3)	2436(5)	30(1)
C(26)	539(4)	3886(4)	6105(6)	39(1)
C(31)	6378(4)	6605(3)	2205(5)	38(1)
C(33)	1419(4)	5619(4)	495(6)	47(1)
C(38)	1202(4)	4603(3)	6122(5)	36(1)
C(39)	4476(4)	6235(4)	6931(5)	35(1)
C(40)	1014(4)	3559(3)	3304(5)	37(1)
C(41)	5578(4)	6296(3)	1013(5)	39(1)
C(42)	212(4)	3152(4)	5164(6)	42(1)
C(45)	445(4)	3023(4)	3931(6)	43(1)
C(46)	2651(4)	6035(3)	6817(5)	36(1)
C(49)	4656(4)	6001(3)	1107(5)	37(1)
C(52)	2315(5)	4062(5)	909(6)	47(2)
C(54)	1614(4)	4719(4)	1346(5)	39(1)

Table 2.5. Atomic coordinates (x 10^4) and equivalent isotropic displacement parameters ($\mathring{A}^2$x 10^3) for [Co$_2$(^{iPr}SATI-3)$_2$] (**13**). U(eq) is defined as one third of the trace of the orthogonalized U^{ij} tensor.

	x	y	z	U(eq)
Co(1)	5314(1)	1000(1)	6303(1)	31(1)
Co(2)	3958(1)	-947(1)	8669(1)	38(1)
N(3)	4786(2)	1077(1)	7475(2)	34(1)
O(2)	2998(2)	-537(1)	9162(2)	48(1)
N(4)	6404(2)	1454(1)	6049(2)	34(1)
O(1)	4105(2)	1101(1)	5499(2)	42(1)
N(5)	6228(2)	426(1)	6124(2)	32(1)
N(2)	5362(2)	-878(1)	9160(2)	37(1)
N(6)	3442(3)	-789(1)	7351(2)	40(1)
C(13)	5994(3)	552(2)	8569(2)	36(1)
N(1)	4192(3)	-1683(1)	9155(2)	45(1)
C(25)	7158(3)	1187(2)	5808(2)	32(1)
C(14)	5441(3)	1078(2)	8365(3)	40(1)
C(35)	3874(4)	-1044(2)	6604(3)	50(1)
C(32)	6068(3)	-147(2)	6242(3)	35(1)
C(30)	7857(3)	230(2)	5851(3)	43(1)
C(10)	5776(3)	-1314(2)	9574(2)	39(1)
C(21)	3255(3)	1208(2)	5751(3)	35(1)
C(31)	7084(3)	592(2)	5923(2)	32(1)
C(20)	2441(3)	1303(2)	5060(3)	44(1)
C(15)	3867(3)	1176(2)	7475(3)	36(1)
C(12)	5348(3)	87(2)	8774(2)	35(1)
C(26)	7924(3)	1441(2)	5435(3)	38(1)
C(34)	4909(3)	-859(2)	6573(3)	42(1)
C(33)	5012(3)	-277(2)	6292(3)	36(1)
C(16)	3108(3)	1241(2)	6684(3)	36(1)
C(37)	2119(3)	-212(2)	7715(3)	45(1)
C(27)	8779(3)	1250(2)	5189(3)	49(1)
C(29)	8761(3)	295(2)	5569(3)	53(1)
C(4)	5075(4)	-1760(2)	9645(3)	44(1)
C(36)	2693(3)	-485(2)	7119(3)	45(1)
C(9)	6799(3)	-1347(2)	9878(3)	50(1)
C(11)	5962(3)	-403(2)	9074(3)	38(1)
C(17)	2163(3)	1363(2)	6875(3)	47(1)
C(42)	2291(3)	-252(2)	8698(3)	44(1)
C(24)	6322(3)	2043(2)	5976(3)	43(1)
C(41)	1651(3)	30(2)	9186(3)	53(1)
C(40)	897(4)	336(2)	8744(4)	62(1)
C(18)	1381(3)	1448(2)	6189(4)	54(1)
C(7)	7115(5)	-2170(2)	10845(4)	66(2)
C(5)	5316(4)	-2212(2)	10235(3)	59(1)
C(8)	7374(4)	-1719(2)	10419(3)	60(1)
C(38)	1328(4)	104(2)	7291(4)	60(1)
C(23)	5774(4)	2199(2)	5036(3)	54(1)
C(39)	728(4)	371(2)	7776(4)	69(2)
C(19)	1531(3)	1420(2)	5274(3)	51(1)

Table 2.5. Continued.

	x	y	z	U(eq)
C(6)	6176(5)	-2375(2)	10768(3)	70(2)
C(28)	9181(3)	742(2)	5256(4)	54(1)
C(22)	5796(5)	2250(2)	6744(4)	67(2)
C(3)	3417(4)	-2093(2)	9115(3)	60(1)
C(2)	2749(5)	-2053(2)	8189(4)	82(2)
C(1)	2829(5)	-2011(3)	9905(4)	77(2)
Cl(3)	-103(2)	1268(1)	866(2)	144(1)
Cl(2)	56(4)	1293(2)	2803(2)	218(2)
Cl(1)	1429(2)	733(2)	1947(4)	275(3)
C(48)	228(5)	927(3)	1874(4)	87(2)
C(47)	8458(5)	1085(4)	8365(6)	115(3)
C(46)	9106(8)	1508(5)	8147(10)	191(7)
C(45)	8702(8)	1987(5)	7965(6)	145(4)
C(44)	9273(11)	2402(5)	7559(7)	193(7)
C(43)	8703(11)	2930(5)	7507(8)	188(6)
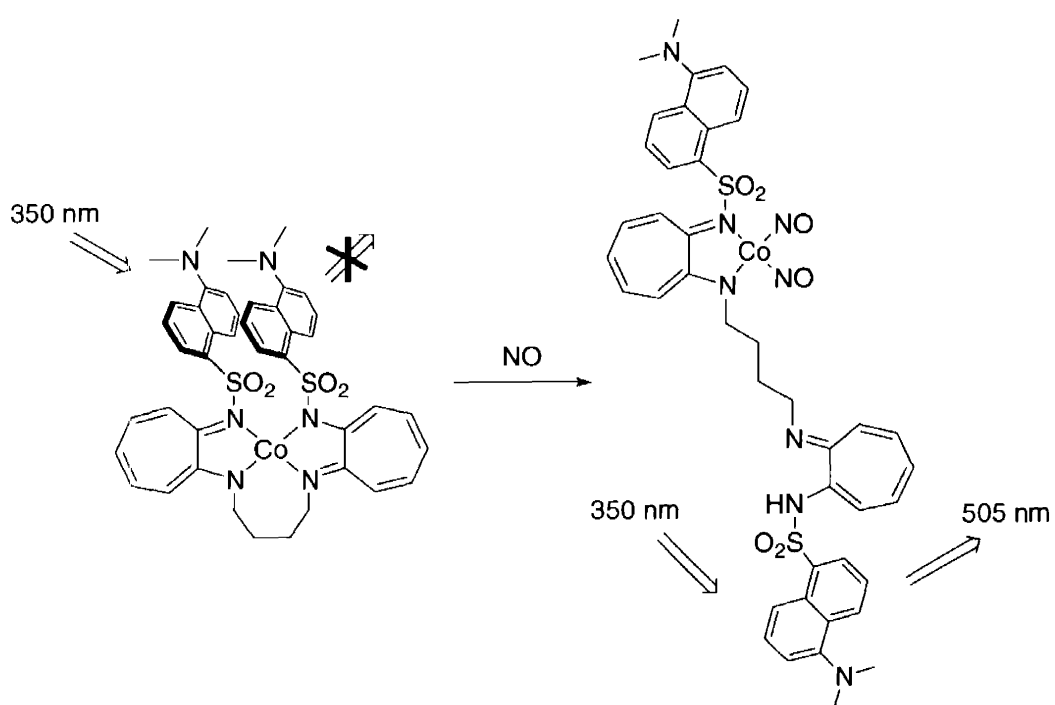
Scheme 2.1. Reaction of [Co(DATI-4)] with NO.
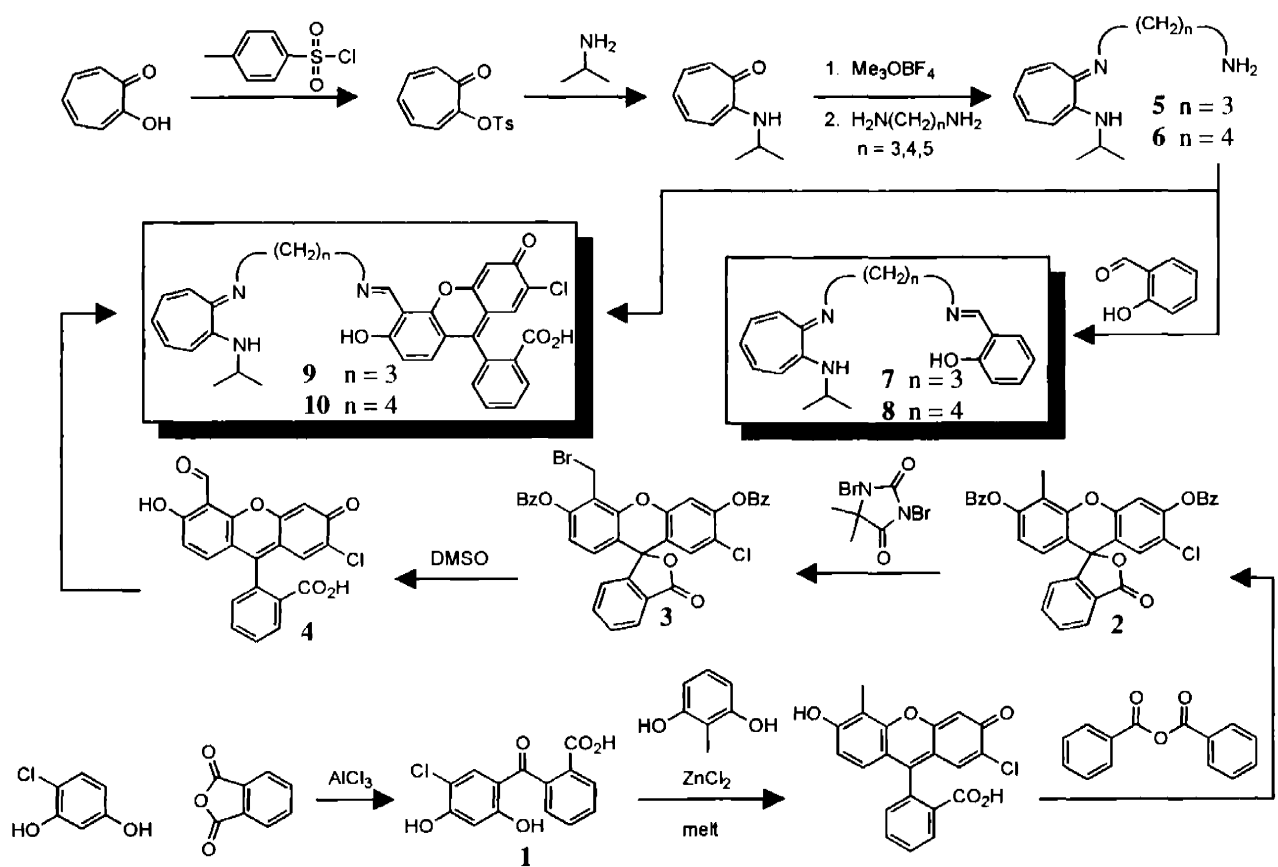
Scheme 2.2. Synthesis of the H_2^{iPr}SATI-n and H_2^{iPr}FATI-n ligands.

5   **16**

Scheme 2.3.

a

b
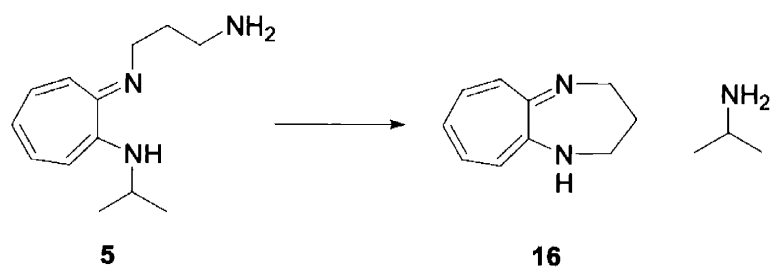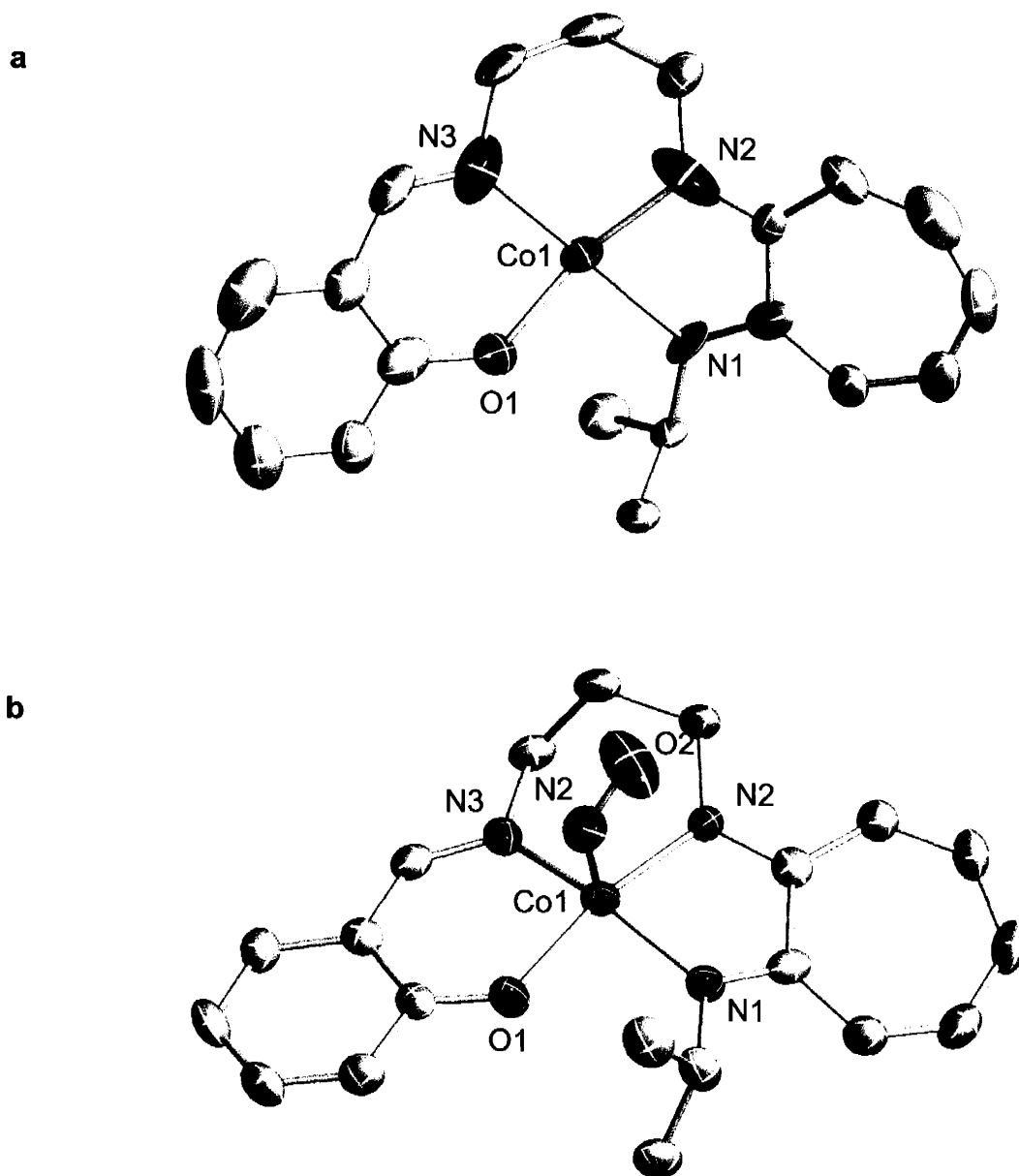
Figure 2.1. ORTEP diagrams of (**a**) [Co(^{iPr}SATI-3)] (**11**) and (**b**) [Co(NO)(^{iPr}SATI-3)] (**12**) showing selected atom labels and 50% probability ellipsoids for all non-hydrogen atoms.
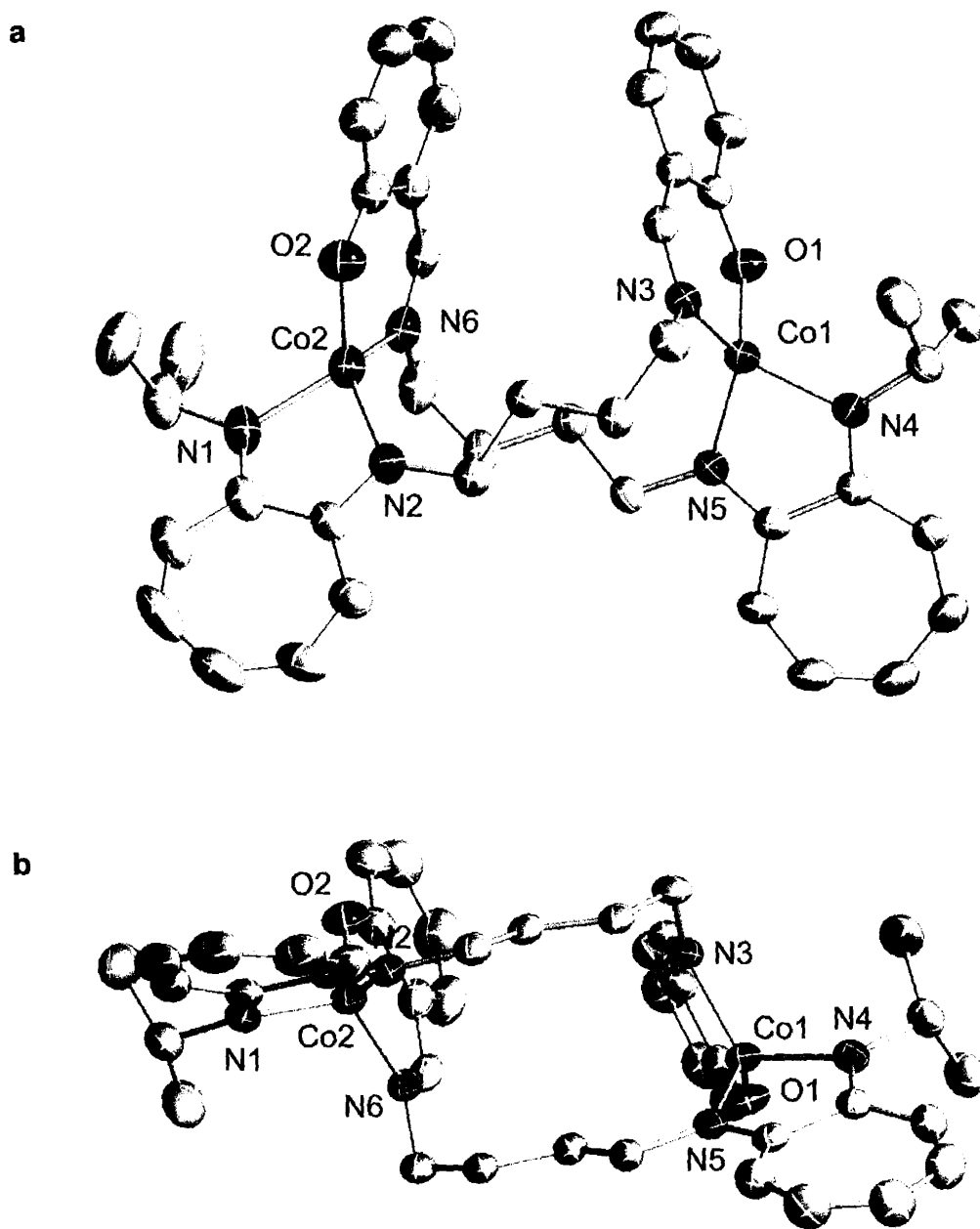
Figure 2.2. ORTEP diagrams from the side (**a**) and top (**b**) of [Co$_2$(^{iPr}SATI-4)$_2$] (**13**) showing selected atom labels and 50% probability ellipsoids for all non-hydrogen atoms.
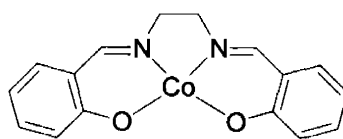
16
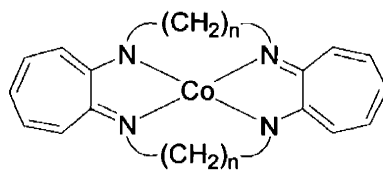
17 n = 3
18 n = 4

Figure 2.3. Structures of [Co(SALEN)] **(16)**, [Co(TC-3,3)] **(17)**, and [Co(TC-4,4)] **(18)**.
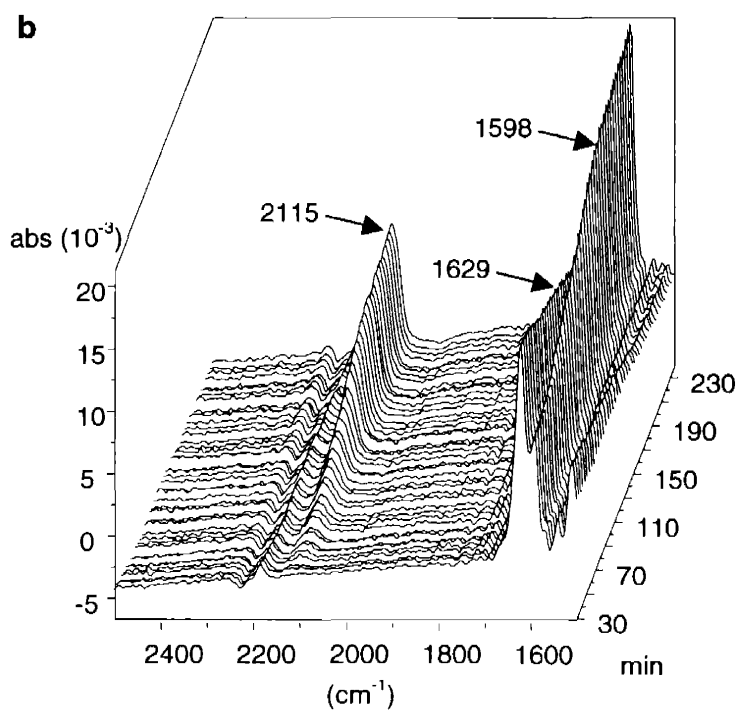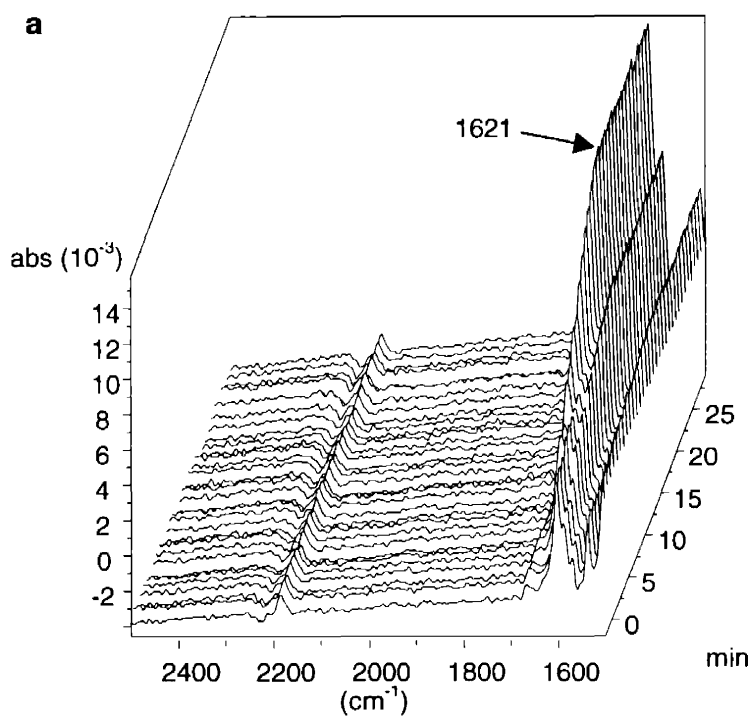
Figure 2.4. Solution IR spectra of [Co(^{iPr}SATI-3)] (**11**) after exposure to excess NO in DMSO at room temperature (**a**) 0 to 30 min exposure to NO and (**b**) 30 to 230 min after the addition of NO.
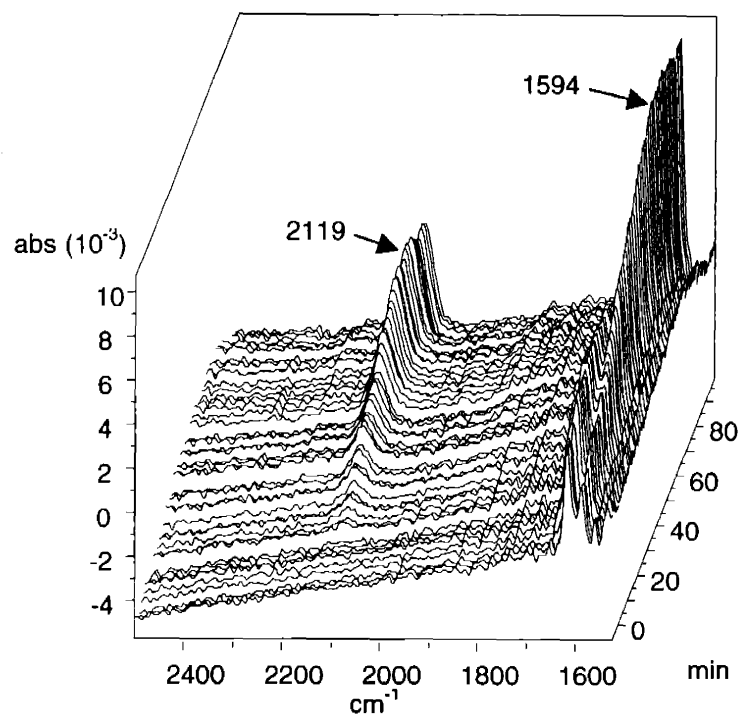
Figure 2.5. Solution IR spectra of [Co$_2$(^{iPr}SATI-4)$_2$] (**13**) after exposure to excess NO in DMSO at room temperature.
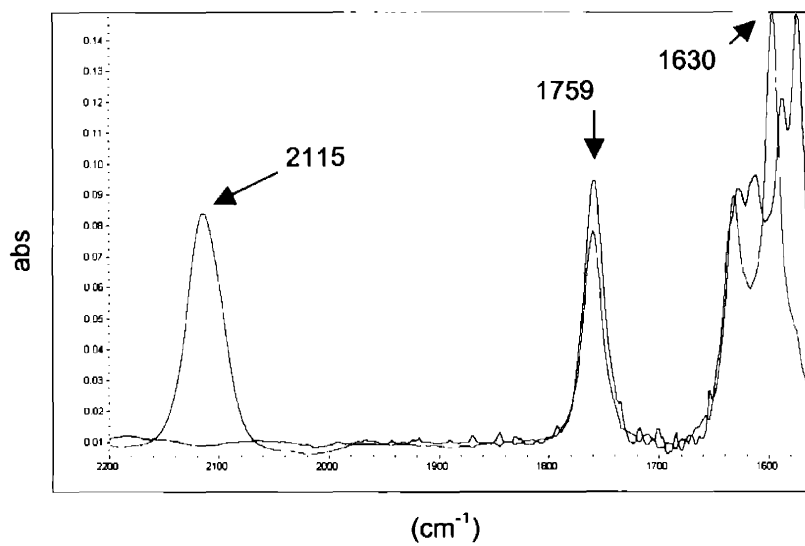
Figure 2.6. Solution IR spectra of [Co(FATI-3)] (**14**) before (blue) and after (red) exposure to excess NO in DMSO at room temperature. The IR band at 1759 cm^{-1} is from the fluorescein carboxylic acid.
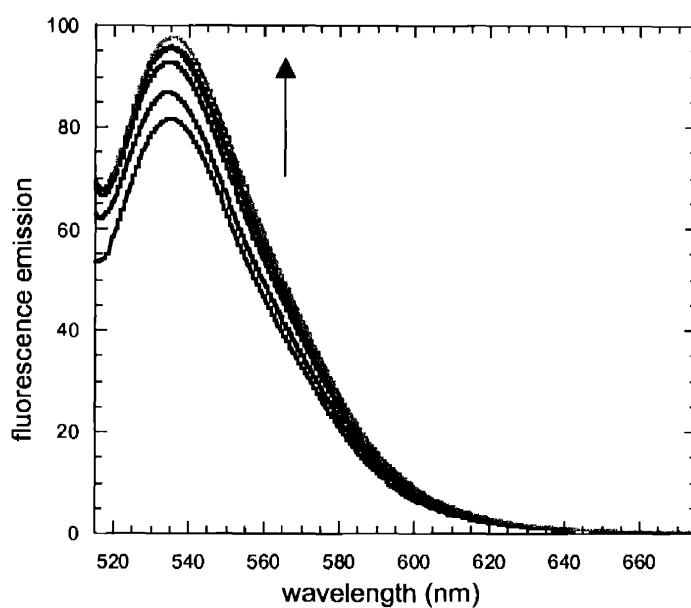
Figure 2.7. Fluorescence emission intensity spectra at 0, 0.5, 1, 1.5, and 4 h following addition of excess NO to a 10 µM solution of [Co(^{iPr}FATI-3)] **(14)** in MeOH showing a 120% increase in fluorescence emission intensity. Excitation is at 509 nm and the emission maximum is at 530 nm.
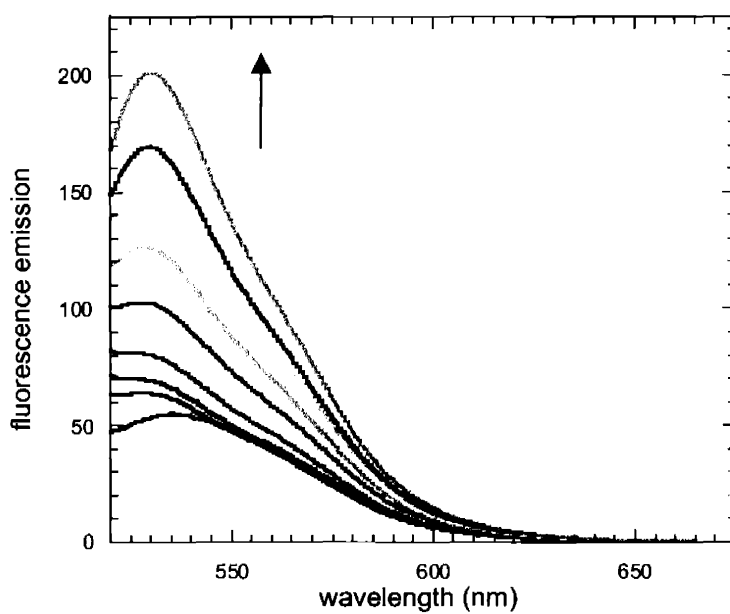
Figure 2.8. Fluorescence emission intensity spectra at 0 min, 5 min 0.5, 1, 2, 4, 6, 8, 11, and 22 h following addition of excess NO to a 10 µM solution of [Co(^{iPr}FATI-4)] (**15**) in MeOH showing a 3-fold increase in fluorescence emission intensity. Excitation is at 503 nm and the emission maximum shifts from 535 nm before addition of NO to 530 nm after 22 h.
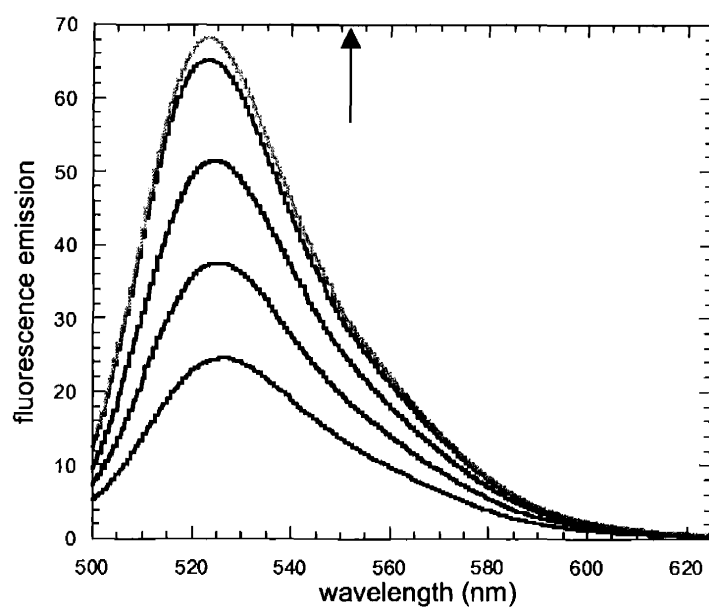
Figure 2.9. Fluorescence emission intensity spectra at 10 min, 0.5, 1, 2, and 3 h of a 10 μM solution of [Co(^{iPr}FATI-4)] (**15**) 0.1 M pH 7.4 phosphate buffer. After 3 h, a 2.5-fold increase in emission intensity is observed. Excitation is at 497 nm and the emission maximum is at 524 nm.

Chapter 3

Carboxylate-Bridged Dimetallic Complexes as Potential Nitric Oxide

Sensors

Introduction

Several factors complicate the ability to detect NO in biological systems. The reaction of NO with O_2 is facile, resulting in formation the of reactive nitrogen oxide species (RNOS) such as NO_2, N_2O_3, and N_2O_4 in aprotic solutions. In aqueous environments, formation of NO_2^- is also possible. NO reacts with superoxide to $ONOO^-$, which is highly toxic[1] as well as with amines, thiols, and transition metals.[2-5] This diverse reactivity of NO complicates efforts to detect NO and decipher its biological functions. In many cases, it is unclear whether NO itself or some more reactive product is involved in cellular signaling.

In the central nervous system, sub-micromolar concentrations of NO are believed to function in neurotransmission. NO may be involved in the process of long-term potentiation (LTP), the basis of learning and memory.[6,7] LTP requires a retrograde neurotransmitter that can diffuse from its point of origin in a post-synaptic nerve cell back to the pre-synaptic neuron. Studies have indirectly identified NO as a candidate for this process.[6-9] Most current research relies on the use of nitric oxide synthase inhibitors or NO releasing compounds rather than direct detection of the gas to investigate its biological functions. These methods do not distinguish between direct actions of NO and those of more reactive products formed by the action of dioxygen-derived species with NO.

To investigate the potential roles of NO in biology, and the central nervous system in particular, methods for the direct detection of NO are highly desirable. One approach to preparing suitable sensors is to couple transition metal-nitrosyl chemistry with fluorescence signaling.

In particular, we are interested in developing sensors that utilize the formation of transition metal nitrosyl complexes to trigger an increase in fluorescence. For applications in biological sensing, an event that results in a positive fluorescence response is preferable to one that results in quenching.[10] Our strategy is based on reversing the fluorescence-quenching properties of transition metals with partially filled d-shells.[11,12] By reaction of NO with a transition metal complex containing a coordinated fluorophore in such a manner as to dissociate the latter from the coordination sphere of the metal, fluorophore emission that was initially quenched by coordination to the metal can be restored.

Previous work in our lab with $[Co(^{iPr}DATI)_2]$, where $^{iPr}DATI$ is an aminotroponiminate ligand containing a dansyl moiety, and related compounds such as $[Co(^{iPr}DATI-4)]$, reveals them to have decreased fluorescence when compared to the free ligands.[12] In the case of $[Co(^{iPr}DATI)_2]$, reaction with NO affords the dinitrosyl $[Co(NO)_2(^{iPr}DATI)]$ and one molecule of $H^{iPr}DATI$. Release of the latter resulted in increased fluorescence emission intensity. The reaction with NO is slow, however; after four days, approximately 75% conversion to the dinitrosyl species occurs, with an 8-fold increase in fluorescence intensity.[12] The slow response time of these systems is a significant impediment to their use for NO detection. We therefore initiated an investigation of other transition metal complexes in an effort to develop improved sensors.

The dioxygen reactivity of carboxylate-bridged non-heme dinuclear complexes is well known in biology and has been a focus of research in our laboratory for several years.[13-16] Non-heme diiron enzymes such as hemerythrin, the hydroxylase component of

soluble methane monooxygenase, and the R2 component of class I ribonucleotide reductase all react with dioxygen.[13,15,17-19] The NO reactivity of these proteins has also been demonstrated.[20-22] A synthetic non-heme carboxylate-bridged diiron complex previously prepared by us also reacts with NO.[23] As a result of this documented NO reactivity, an investigation was undertaken into the use of carboxylate-bridged dinuclear complexes as potential NO sensors. In particular, although the dioxygen reactivity of diiron complexes of the formula $[Fe_2(O_2CAr^{Tol})_4(L)_2]$, where O_2CAr^{Tol} = 2,6-di(p-tolyl)benzoic acid and L = a nitrogen base has been investigated extensively, their NO chemistry has not.[14,16,24] To examine the potential suitability of these systems for use as NO sensors, related diiron and dicobalt complexes were prepared in which the nitrogen bases were modified to carry a dansyl fluorophore. The synthesis and investigation of the NO reactivity of these complexes is the subject of the present report.

Experimental

General Considerations. Pentane, tetrahydrofuran (THF), diethyl ether (Et_2O), acetonitrile (CH_3CN), and methylene chloride (CH_2Cl_2) were purified by passage through alumina columns under a N_2 atmosphere.[25] All other solvents were purchased from Mallinckrodt or EM Science and used without further purification. Silica gel 60 (230-400 mesh, EM Science) was used for column chromatography. The starting materials dansyl-piperazine (Ds-pip), HO_2CAr^{Tol}, and $[Fe_2(\mu-O_2CAr^{Tol})_2(O_2CAr^{Tol})_2(THF)_2]$ were prepared as previously described.[24,26-29] Nitric oxide (Matheson 99%) was purified by a method adapted from the literature.[30] The NO stream was passed through an Ascarite (NaOH fused on silica gel) column and a 6 ft coil filled with silica gel cooled to −78 °C. For fluorescence experiments, NO was introduced into the headspace above the sample

solution in a sealed fluorescence cell via a Schlenk manifold. All other reagents were obtained commercially and used without further purification. IR spectra were recorded on a ThermoNicolet Avatar 360 spectrophotometer. In situ IR spectra were recorded on a ReactIR 1000 instrument from ASI equipped with a 1-in.-diameter, 30-reflection silicon ATR (SiComp) probe. UV-visible spectra were recorded on a Hewlett-Packard 8435 spectrophotometer. Unless otherwise mentioned, fluorescence emission intensity spectra were recorded at 25 ± 0.2 °C on a Hitachi F-3010 fluorescence spectrophotometer. Electrospray ionization (ESI) mass spectrometry was performed on an Agilent 1100 series LC/MSD trap or in the MIT Department of Chemistry Instrumentation Facility. NMR spectra were recorded on a Bruker DPX-400 spectrometer at ambient temperature and referenced to internal ^{1}H and ^{13}C solvent peaks.

[Fe$_2$(μ-O$_2$CAr^{Tol})$_4$(Ds-pip)$_2$] (1). To a solution of [Fe$_2$(μ-O$_2$CAr^{Tol})$_2$(O$_2$CAr^{Tol})$_2$-(THF)$_2$] (100 mg, 0.068 mmol) in 10 mL of CH$_2$Cl$_2$, Ds-pip (44 mg, 0.12 mmol) in 2 mL of CH$_2$Cl$_2$ was added and allowed to stir under a N$_2$ atmosphere for 1 h. X-ray quality crystals of **1** (92 mg, 68%) were isolated by vapor diffusion (Et$_2$O/CH$_2$Cl$_2$). IR (KBr, cm$^-$ ^{1}): 3440 (w br), 3252 (w), 3048 (w), 3018 (w), 2983 (w), 2940 (w), 2918 (w), 2862 (w), 2786 (w), 1605 (s), 1513 (m), 1448 (m), 1403 (s), 1383 (s), 1345 (s), 1330 (m), 1304 (w), 1262 (w), 1229 (w), 1165 (s), 1146 (m), 1063 (w), 933 (m), 842 (w), 813 (m sh), 790 (s), 705 (m), 617 (w), 584 (w), 568 (m), 526 (m), 487 (w), 461 (w). Anal Calcd. for C$_{116}$H$_{110}$N$_6$O$_{12}$S$_2$Fe$_2$: C, 71.23; H, 5.67; N, 4.30. Found: C, 70.98; H, 5.77; N, 4.12.

[Co$_2$(μ-O$_2$CAr^{Tol})$_4$(Ds-pip)$_2$] (2) and [Co$_2$(μ-O$_2$CAr^{Tol})$_2$(O$_2$CAr^{Tol})$_2$(Ds-pip)$_2$] (3). Portions of TEA (460 µL, 3.0 mmol), HO$_2$CAr^{Tol} (905 mg, 3.0 mmol), Co(NO$_3$)$_2$·6(H$_2$O) (455 mg, 1.55 mmol), and Ds-pip (500 mg, 1.55 mmol) were allowed

to stir in 75 mL of dry THF for 2.5 h. After removal of the solvent under reduced pressure, the crude residue was extracted with CH_2Cl_2 and filtered through a glass frit of medium porosity. Using approximately one half of the crude reaction residue, light blue X-ray quality crystals of **2** (400 mg) were prepared by vapor diffusion (Et_2O/CH_2Cl_2) at room temperature. With the remainder of the reaction residue, dark purple X-ray quality crystals of **3** (358 mg) were obtained by vapor diffusion (Et_2O/CH_2Cl_2) at -24° C. The overall yield of **2** and **3** is 50%.

Characterization of Isomer 2. IR (KBr, cm^{-1}): 3247 (w), 3049 (w), 3019 (w), 2985 (w), 2939 (w), 2919 (w), 2862 (w), 2785 (w), 1616 (s), 1585 (m), 1573 (m), 1547 (w sh), 1513 (m), 1449 (m), 1403 (m), 1384 (s), 1344 (m), 1329 (m), 1308 (w), 1261 (w), 1229 (w), 1165 (m), 1147 (m), 1108 (w), 1063 (w), 1023 (w), 937 (m), 844 (w), 813 (m sh), 790 (m), 707 (m), 617 (w), 584 (w), 568 (m), 526 (m), 487 (w), 462 (w). Anal Calcd. for $C_{116}H_{110}N_6O_{12}S_2Co_2$: C, 71.01; H, 5.65; N, 4.28. Found: C, 70.86; H, 5.56; N, 4.30.

Characterization of Isomer 3. IR (KBr cm^{-1}): 3252 (w), 3056 (w), 2978 (w), 2942 (w), 2917 (w), 2866 (w), 2791 (w), 1611 (s), 1587 (m sh), 1574 (m sh), 1514 (m), 1454 (m), 1405 (w), 1384 (m), 1345 (m), 1330 (w), 1308 (w), 1260 (w), 1166 (m), 1146 (w), 1112 (w), 1095 (w), 1066 (w), 1048 (w), 1022 (w), 933 (m), 924 (m sh), 851 (w), 822 (m), 801 (s), 781 (m), 763 (w), 735 (w), 714 (m), 616 (w), 584 (w), 566 (m), 544 (w), 521 (w), 487 (w), 468 (w). Anal Calcd. for $C_{116}H_{110}N_6O_{12}S_2Co_2$: C, 71.01; H, 5.65; N, 4.28. Found: C, 70.90; H, 5.83; N, 4.51.

***N*-Nitroso-dansyl-piperazine (4) and $[Co_2(NO)_2(\mu-O_2CAr^{Tol})_2]$ (5).** Under an atmosphere of Ar, **2** (120 mg, 0.064 mmol) in 25 mL of CH_2Cl_2 was exposed to excess NO. During the reaction the solution changed color from blue-purple to brown. The

solvent was removed in vacuo after stirring under an NO atmosphere for 3 h. The crude residue was washed with 20 mL of Et$_2$O and filtered, leaving pure **4** (37 mg, 84%) as an off-white solid. The brown Et$_2$O solution was concentrated to 4 mL in vacuo. Dark brown crystals of **5** (34 mg, 63 %) were grown from the concentrated Et$_2$O solution at -40° C. It was also possible to isolate the free carboxylic acid, HO$_2$Car^{Tol} (**6**), from the remaining Et$_2$O mother liquor; however, no attempt was made to obtain a yield.

Characterization of 4. ^{1}H NMR (400 MHz, CD$_2$Cl$_2$): δ 8.59 (1 H, d, J = 7.6 Hz), 8.31 (1 H, d, J = 8.7 Hz), 8.20 (1 H, dd, J = 7.4, 1.3 Hz), 7.59-7.54 (2 H, m), 7.20 (1 H, d, J = 7.1 Hz), 4.28 (2 H, t, J = 5.2 Hz), 3.82 (2 H, t, J = 5.4 Hz), 3.43 (2 H, t, J = 5.3 Hz), 3.17 (2 H, t, J = 5.3 Hz), 2.87 (6 H, s). ^{13}C NMR (100 MHz, CD$_2$Cl$_2$): δ 152.61, 132.77, 131.78, 131.33, 130.64, 128.90, 123.72, 119.43, 115.56, 49.66, 46.59, 45.71, 45.12, 39.28. IR (KBr, cm^{-1}): 2980 (w), 2939 (w), 2864 (w), 2786 (w), 1588 (w), 1573 (w), 1502 (w), 1485 (w), 1454 (m), 1429 (m), 1404 (w), 1357 (m), 1336 (s), 1319 (m), 1284 (m), 1227 (m), 1198 (w), 1162 (s), 1109 (m), 1075 (w), 1057 (w), 1045 (w), 987 (m), 924 (s), 810 (w), 793 (s), 773 (w), 713 (s), 682 (w), 622 (m), 602 (m), 570 (m), 538 (w), 485 (w), 474 (m). MS-ESI (m / z): [M + Na]$^+$ Calcd. for NaC$_{16}$H$_{20}$N$_4$O$_3$S, 371.1154; Found 371.1133.

Characterization of 5. IR (KBr, cm^{-1}): 3049 (w), 3023 (w), 2918 (w), 2861 (w), 1861 (m), 1785 (s), 1754 (s), 1588 (s), 1561 (s), 1515 (m), 1447 (m), 1406 (m), 1388 (m), 1109 (w), 847 (w), 815 (m), 790 (m), 762 (w), 728 (w), 715 (w), 703 (w), 586 (w), 540 (w), 525 (m). Anal Calcd. for C$_{42}$H$_{34}$N$_4$O$_8$Co$_2$: C, 60.01; H, 4.08; N, 6.66. Found: C, 60.17; H, 4.27; N, 6.44.

X-Ray Crystallography. Single crystals suitable for data collection were covered in Infineum V8512 (formerly called Paratone N oil) mounted on the tips of quartz capillary tubes and transferred to the -100°C low-temperature nitrogen stream a Bruker KRYOFLEX BVT-AXS cryostat. Data was collected on the Bruker diffractometer (MoK$_\alpha$ λ = 0.71073 Å) controlled by the SMART software package running on a Pentium II PC.[31] The general procedures used for data collection are reported elsewhere.[32] Empirical absorption corrections were calculated with the SADABS program.[33] Structures were solved and refined with the SHELXTL and SAINTPLUS software packages on a Pentium II PC running the Windows NT operating system.[34,35] All non-hydrogen atoms were refined anisotropically by least-squares cycles and Fourier syntheses. Hydrogen atoms were assigned idealized positions and given thermal parameters of 1.2 times the thermal parameter of the carbon or nitrogen atom to which each was attached. All structure solutions were checked for higher symmetry with the PLATON program.[36]

Two of the CH_2Cl_2 molecules in the structure of **1** are disordered. In the first disordered CH_2Cl_2, one of the chlorine atoms resides in two positions and was refined with 50% occupancy for each atom. The second CH_2Cl_2 molecule also has a disordered chlorine atom that was modeled with 75 and 25% occupancies. In the structure of **2** three of the CH_2Cl_2 solvent molecules are disordered. The first has a chlorine atom disordered over two positions with 60 and 40% occupancies. The remaining two disordered CH_2Cl_2 atoms in **2** are each disordered over two positions, both with 100% occupancy of the central carbon atom. The chlorine atoms are disordered over two sites modeled with 60 and 40% occupancies for the first solvent molecule and 75 and 25% for the second. The

oxygen atom of nitrosyl in **4** is disordered over two positions and was refined with occupancies of 55 and 45%.

Results and Discussion

Synthesis. A range of iron terphenylcarboxylate complexes having a variety of N-donor ligands have been prepared and reported in the literature (Figure 3.1).[24] Complex **1** was synthesized in a similar manner. The reaction of two equivalents of dansyl-piperazine with $[Fe_2(\mu-O_2CAr^{Tol})_2(O_2CAr^{Tol})_2(THF)_2]$ under an inert atmosphere in CH_2Cl_2 followed by crystallization from vapor diffusion of Et_2O into CH_2Cl_2 afforded **1** in 68% yield as light yellow-green crystals. The reaction is complete in less than 1 h. The fluorescence emission intensity of crystalline **1** is significantly diminished by comparison to a solid sample of dansyl-piperazine when illuminated with long-wavelength UV light from a hand held lamp. The quenched fluorescence in **1** suggests coordination of the piperazine N-atoms to the iron centers. All previously prepared tetra(carboxylato)diiron(II) complexes obtained in our laboratory are sensitive to O_2 and have been used to investigate structural and mechanistic aspects of O_2 binding and activation parallel to that occurring in carboxylate-bridged diiron containing proteins.[24] Given the similarity of **1** to these previously reported diiron complexes, it is not surprising that **1** is sensitive to O_2, both when dissolved in halogenated solvents and in the solid state.

In an effort to circumvent the O_2 sensitivity of the tetracarboxylate complexes, the chemistry of the dicobalt(II) analogue was examined. The known dicobalt(II) complex, $[Co_2(\mu-O_2CAr^{Tol})_2(O_2CAr^{Tol})_2(C_5H_5N)_2]$, which contains two pyridine ligands, is air stable.[37] There are a few examples of air-stable cobalt(II) complexes, such as

[Co(^{iPr}DATI)$_2$], that react with NO via a reductive nitrosylation mechanism. The synthesis of the dicobalt(II) analogue of **1** was therefore undertaken in order to prepare an air-stable complex capable of reductive nitrosylation to form a dicobalt tetranitrosyl species with concomitant fluorophore release. Complex **2** was synthesized by the reaction of Co(NO$_3$)$_2$·(H$_2$O)$_6$ with dansyl-piperazine, HO$_2$CAr^{Tol}, and triethylamine in a 1:1:2:2 ratio with THF as solvent. Blue rods of **2** were isolated by crystallization from vapor diffusion of Et$_2$O into a blue-purple solution of the dicobalt complex in CH$_2$Cl$_2$ at room temperature. When the crystallization setup is cooled to -24° C or below, **3** was isolated as purple plates. The overall yield for isolation of **2** and **3** from the same reaction, but under different crystallization conditions, optimized for each, is 50%. As with [Co$_2$(μ-O$_2$CAr^{Tol})$_2$(O$_2$CAr^{Tol})$_2$(C$_5$H$_5$N)$_2$], both **2** and **3** are air stable for an extended period both as a solids and in solution, and both can be synthesized on the benchtop. The interconversion of the dicobalt complex between the paddlewheel- and windmill-core structures (Scheme 3.1) is temperature dependent and is discussed in more detail below.

Structural Characterization of the Diiron(II) and Dicobalt(II) Complexes. Crystallographic data and selected geometric information for **1-3** are given in Table 3.1 and Table 3.2, respectively. The ORTEP diagram of **1** is presented in Figure 3.2, and the ORTEP diagrams of **2** and **3** are given in Figure 3.3. Complex **1** adopts a paddlewheel geometry with four 1,3-bridging carboxylate ligands and two Ds-pip fluorophores occupying apical positions on the Fe–Fe vector. This core of **1** is structurally similar to that in several other tetra(μ-carboxylato)diiron(II) complexes previously synthesized in our laboratory. The Fe–Fe distance of 2.725(1) Å in **2** is significantly shorter than the reported 4.282 Å Fe-Fe distance in [Fe$_2$(μ-O$_2$CAr^{Tol})$_2$(O$_2$CAr^{Tol})$_2$(THF)$_2$], which adopts

the more open windmill geometry.[24] The Fe-Fe distance in **1** is nearly identical to the

2.728 Å distance reported for the paddlewheel isomer of $[Fe_2(\mu\text{-}O_2CAr^{4\text{-}FPh})_4(THF)_2]$,

which contains two THF molecules in the axial coordination sites of the diiron core. The

reported Fe–Fe distances of other paddlewheel complexes with nitrogenous bases,

however, such as 1-methylimidazole, pyridine, and 4-*t*-butylpyridine, coordinated in the

axial sites range between 2.823 and 2.848 Å. The origin of the shortened Fe–Fe distance

in **1** by comparison to these other nitrogen base adducts is unclear. Although rather bulky,

the Ds-pip ligands in **1** are oriented away from the diiron core and therefore minimize

any potential issues with respect to steric crowding at the diiron core. The average Fe–N

bond in **1** of 2.130(3) Å is somewhat longer than the 2.041-2.098 Å range reported for the

other structurally characterized complexes with imidazole and pyridine ligands. The

longer Fe–N distances in **1** are consistent with expectations based on the diminished π-

acceptor ability of the piperazine in comparison to imidazole and pyridine.

A carboxylate shift must occur during the reaction of $[Fe_2(\mu\text{-}O_2CAr^{Tol})_2(O_2CAr^{Tol})_2(THF)_2]$ with dansyl-piperazine to form **2**, since the former has a

windmill configuration with only two bridging carboxylate ligands. Interconversion

between the windmill and paddlewheel geometries can occur by carboxylate shifts of two

of the bridging carboxylate ligands in the tetra-bridged paddlewheel structure to give the

doubly bridged paddlewheel geometry. The temperature dependence of these carboxylate

shifts was previously investigated by ^{19}F NMR spectroscopic analysis of

tetra(carboxylato)diiron(II) complexes carrying the fluoro-substituted 2,6-di(4-

fluorophenyl)benzoate analog of the HO_2CAr^{Tol} ligand.[24] Variable temperature ^{19}F NMR

spectra of $[Fe_2(\mu\text{-}O_2CAr^{4\text{-}FPh})_2(O_2CAr^{4\text{-}FPh})_2(THF)_2]$ displayed three fluorine resonances

that can be attributed to the bridging and terminal carboxylate ligands in the windmill structure, $[Fe_2(\mu\text{-}O_2CAr^{4\text{-}FPh})_2(O_2CAr^{4\text{-}FPh})_2(THF)_2]$. Cooling of the sample to below -60 °C gave a single fluorine signal, which can be accounted for by invoking a paddlewheel structure, $[Fe_2(\mu\text{-}O_2CAr^{4\text{-}FPh})_4(THF)_2]$, where the fluorine substituents of the four bridging carboxylate ligands are in identical magnetic environments.[24]

In an attempt to isolate the corresponding windmill structure of **1**, several vapor diffusion crystallization chambers were set-up at multiple temperatures down to -40° C. Under all conditions investigated, only the paddlewheel complex was isolated. These results are not surprising, however, in view of the variable temperature ^{19}F NMR results for $[Fe_2(\mu\text{-}O_2CAr^{4\text{-}FPh})_4(4\text{-}^tBuC_5H_4N)_2]$. Unlike the THF complex, which shows a distinctive temperature dependence of its ^{19}F NMR signals, only a single sharp fluorine signal is observed with $[Fe_2(\mu\text{-}O_2CAr^{4\text{-}FPh})_4(4\text{-}^tBuC_5H_4N)_2]$ between 20 and -70 °C, indicating that the paddlewheel structure is favored over the windmill geometry.[24] Therefore, assuming that the stability of **1** is similar to that of $[Fe_2(\mu\text{-}O_2CAr^{4\text{-}FPh})_4(4\text{-}^tBuC_5H_4N)_2]$, it is unlikely that the windmill structure could be isolated, even if the diffusion crystallization setup temperature was lowered to -70° C.

As with the previously reported $[Fe_2(\mu\text{-}O_2CAr^{4\text{-}FPh})_2(O_2CAr^{4\text{-}FPh})_2(THF)_2]$ system, the geometry of the dicobalt(II) Ds-pip complexes is temperature dependent. X-ray diffraction studies of **2** and **3** demonstrate conclusively that **2** adopts a paddlewheel geometry whereas **3** has the windmill structure. This is the first example where windmill and paddlewheel structures of dicobalt terphenyl carboxylate complexes of the same stoichiometry have been isolated. The carboxylate shift involved in the transition from structure **2** to **3** results in an increase of the Co–Co distance from 2.720(2) to 3.898(1) Å.

The latter distance is in good agreement with the previously reported 3.9168(7) Å distance in $[Co_2(\mu-O_2CAr^{Tol})_2(O_2CAr^{4-Tol})_2(C_5H_4N)_2]$. The Co–N distance in **3** of 2.079(3) Å is essentially identical to the 2.072(4) Å Co–N distance in **2**. It is surprising that the IR spectra (KBr) of **2** and **3** are very similar given the shift in coordination environment at the two cobalt centers. The carboxylate stretch of 1616 cm^{-1} in **5** shifts to 1611 cm^{-1} in **6**. No additional carboxylate stretching bands are observed in **6**, even though the carboxylate ligands have two different coordination modes. The diiron(II) paddlewheel complex **1** is isomorphous with the corresponding dicobalt(II) complex, with both crystallizing in the P$\bar{1}$ space group. The distances between the two metal centers are essentially identical at 2.725(1) and 2.720(2) Å in **1** and **2**, respectively. As with the distance between the two metals, the average Co–N distance of 2.121(3) Å in **2** is nearly identical to the average Fe–N bond of 2.130(3) Å in **1**.

Reactivity of $[Fe_2(\mu-O_2CAr^{Tol})_4(Ds-pip)_2]$ (1). Addition of NO to a solution of **1** in CH_2Cl_2 results in an immediate color change from light yellow-green to brown. Complex **1** is also sensitive towards O_2 When CH_2Cl_2 solutions of **1** are exposed to air at room temperature, a light yellow solution is obtained. Although the O_2 reactivity of **1** was not studied in detail, the O_2 reactivity of similar diiron(II) tetracarboxylate complexes have been investigated extensively previously.[14,16,24]

The reaction of **1** with NO was also monitored by solution IR spectroscopy. When 10 equiv of NO were admitted to a sealed flask containing a 0.5 mM solution of **1** in CH_2Cl_2, new IR bands at 1797 and 1726 cm^{-1} appear (Figure 3.4). These features are consistent with formation of a $Fe(NO)_2$ unit. The distinct carboxylate stretching band of the starting complex at 1605 cm^{-1}, which is indicative of the paddlewheel and windmill

structures, also disappears. These IR data indicate that the core of the diiron complex has been disrupted. The potential exists for the formation of a diiron tetranitrosyl complex with two bridging carboxylate ligands. The diiron tetranitrosyl complex, if formed, may have a structure similar to that of $[Co_2(\mu-O_2CAr^{Tol})_2(NO)_4]$, vida infra, although no structural information for the iron nitrosyl species is available. All attempts to isolate and characterize structurally iron nitrosyl products from the reaction of 1 with NO proved to be unsuccessful. Several reactions with different amounts of NO from 1 to 200 equiv were investigated. The reaction of 1 with 200 equiv of NO gave a few brown crystals when recrystallized over an atmosphere of excess NO. The brown crystals formed together with a light tan precipitate and did not diffract. No further characterization of the crystals was attempted.

Reactivity of the Dicobalt Complexes 2 and 3 with Nitric Oxide. All NO experiments with the dicobalt terphenyl carboxylate complexes were performed at room temperature, where 2 is expected to be the predominant species in solution. When the reaction of 2 with excess NO in CH_2Cl_2 was followed by IR spectroscopy in situ several new features appeared in the IR spectra (Figure 3.5) as the solutions color changed from blue-purple to brown. The most noticeable change is the appearance of peaks at 1864 and 1783 cm^{-1}, which first begin to form six minutes after exposure to NO. The IR bands are consistent with the formation of a cobalt dinitrosyl species.[12] In addition to the formation of dinitrosyl bands, the carboxylate stretching mode at 1610 cm^{-1} in 2 disappears as the reaction progresses, indicating a significant change in the structure, confirmed by X-ray crystallography, vida infra. A final IR feature at 1745 cm^{-1} appears as the reaction

progresses. This band is consistent with the presence of free carboxylic acid, but may also be due to an additional nitrosyl species.

Three products from the reaction of **2** with NO in CH_2Cl_2 have been isolated and structurally characterized. X-ray crystallographic parameters, selected bond lengths, and an ORTEP diagrams of **4** and **5** are given in Tables 3.2 and 3.4 and Figure 3.5, respectively. After removal of the solvent from the NO reaction, the residue was washed with Et_2O, leaving behind impure **4**. Light yellow rods of **4**, which fluoresce under UV illumination, were prepared by vapor diffusion of Et_2O into a CH_2Cl_2 solution of the impure compound in 84% yield. X-ray crystallographic analysis of **4** indicated that the Ds-pip ligands in **2** underwent *N*-nitrosation. The ^1H NMR spectrum of **4** indicates that the methylene protons of the piperazine ring in **4** are no longer equivalent, as expected after functionalization of the secondary amine to form the *N*-nitroso species. The *N*-nitroso product **4** is moderately air-stable, decomposing only after several days of standing in air.

Concentration of the brown Et_2O filtrate from the nitrosylation reaction followed by crystallization at -40° C gave **5** in 64% yield as dark brown blocks. With further manipulation of the remaining mother liquor, it was possible to isolate HO_2CAr^{Tol}. X-ray diffraction studies on the dark brown plates revealed that **5** is a dicobalt tetranitrosyl complex where two of the carboxylate ligands and both of the dansyl-piperazine moieties from **5** have been replaced by nitrosyl ligands. Complex **2** thus undergoes reductive nitrosylation to form **5**, which is composed of two $\{Co(NO)_2\}^{10}$ centers. The average N–O bond length in **5** is 1.152 Å and the average NO–Co angle is 163.5°. These values are consistent with those previously reported in the literature for $\{Co(NO)_2\}^{10}$ species.[38-40] In

some examples, $\{Co(NO)_2\}^{10}$ units are formed from Co^{2+} starting complexes, with the metal center providing the needed electron to form the dinitrosyl species by disproportionation of $[Co^{2+}L_2]$ to give $[Co(NO)_2L]$ and $[Co^{3+}L_3]$.[41-43] In this system, however, no Co^{3+} species were isolated. It appears that NO acts as the electron source for reduction of Co^{2+}. The NO^+ equivalent generated by initial reduction of the Co^{2+} is then free to attack the aliphatic nitrogen in Ds-pip, forming **4** with concomitant abstraction of the NH proton by a molecule of the carboxylate. NO has previously been proposed to be a source of reducing equivalents for the reduction of Fe^{3+} dithiocarbamates to produce Fe^{2+} dithiocarbamates and S-nitrosated dithiocarbamate.[44] A similar mechanism may occur with the present dicobalt system.

From the X-ray analysis of the products and the solution IR data on the reaction, a possible mechanism can be proposed (Scheme 3.2). Reaction of NO with **2** may result in formation of an initial mononitrosyl cobalt complex, where the nitrosyl has a significant δ^+ charge. Because no mononitrosyl is observed in the solution IR reactions, even when conducted at -78° C, such a species, if present, must be transient and highly reactive. The transient cobalt mononitrosyl could then act as an NO^+ source by reducing the cobalt center to Co(I). The secondary nitrogen of the Ds-pip, which may be in close proximity to the putative NO^+ equivalent, would be able to undergo N-nitrosation. The presence of a base, the m-tolyl terphenyl carboxylate, also present at the dicobalt core, could assist by abstracting the amine proton, facilitating attack of cobalt mononitrosyl species to give **4** and **6**. The formation of **4** and **6** would result in their dissociation from the dicobalt core. The resulting electron rich Co(I) species would then quickly react with additional NO present in the reaction solution to give the observed double dinitrosyl **5**.

Fluorescence Studies. The reactivity of **1** with NO was investigated by fluorescence spectroscopy. Exposure of **1** to one equivalent of NO in CH_2Cl_2 results in a 4-fold increase in fluorescence emission intensity within five minutes when excited at 350 nm (Figure 3.7). The fluorescence response, coupled with the solution IR data, indicate significant changes in the diiron core, such as dissociation of Ds-pip. The free ligand, effectively removed from the influence of the iron centers, is the probable source of the increase in fluorescence emission intensity. In addition to an NO-induced fluorescence response, **1** also reacts with O_2 to afford an increase in fluorescence emission intensity. When **1** is exposed to one equivalent of O_2 in CH_2Cl_2 the fluorescence increases slowly by 2.6-fold after 5 min and maximizes at 5-fold after standing overnight (Figure 3.7). Although this system shows a fluorescence response to O_2, its response to NO is significantly faster than for the previously investigated aminotroponiminate compounds.[12] Even though the reaction of **1** with NO is faster than its reaction with O_2, a common property of iron(II) aminocarboxylate complexes,[45] the dioxygen sensitivity is a significant impediment for the use of the diiron complex **1** as an in vivo NO sensor.

From the X-ray crystallographic results showing dissociation of the dansyl moiety from the cobalt centers when **2** is exposed to excess NO, it is not surprising, an increase in fluorescence is also observed. When **5** is allowed to react with 150 equivalents of NO in CH_2Cl_2, a 9.6-fold increase in fluorescence is observed after 60 minutes (Figure 3.8). During this period, the emission maximum also shifts from 503 to 513 nm. This shift in emission wavelength is due to the N-nitrosation of the dansyl-piperazine ligand. When the fluorescence experiment is repeated with 1 or 20 equivalents of NO, only 1.2- and 1.4-fold increases in fluorescence intensity, respectively, are observed. The lack of a

major fluorescence response with these amounts of NO is consistent with the observed solution IR reactivity, where the nitrosyl bands and concomitant formation of a brown solution only occurred when a large excess of NO was employed. This lack of response to small amounts of NO indicates that formation of the proposed initial mononitrosyl intermediate is the rate-limiting step in the reaction and that its formation is only favored in presence of a large excess of NO. Although air-stable, the lack of sensitivity and water solubility of this system make it less than ideal for use as a biological NO sensor. If the water solubility of this system could be improved, however, it would be a potential candidate for future development.

Conclusions

New carboxylate-bridged dimetallic complexes with fluorophore-containing ligands coordinated to the metal core have been prepared. Design of the complexes was based on previous research indicating that the reaction of NO with the hydroxylase component of soluble methane monooxygenase and synthetic analogues thereof may result in ligand displacement from the diiron core. Both the diiron and dicobalt complexes react with NO to elicit an increase in fluorescence emission intensity caused by dissociation of the fluorophores from the transition metal centers. Such decomplexation removes them from the non-radiative decay pathways that quench the emission from the parent complexes. In the case of the dicobalt system, the reaction with NO proceeds by reductive nitrosylation, where the cobalt atoms are formally reduced to Co(I) dinitrosyl units. Isolation and characterization of the nitrosylation reaction products provides insight into a possible mechanism for this reaction. Formation of *N*-nitroso

dansyl-piperazine indicates generation of NO^+ or an NO^+ donor during the course of the reaction. Thus, it appears that NO is the ultimate source of the electron used to reduce the dicobalt(II) core in the reaction, forming $[Co_2(\mu-O_2CAr^{Tol})_2(NO)_4]$. These complexes demonstrate the potential use of the ligand dissociation strategy to prepare fluorescence-based sensors for NO that evoke an increase in fluorescence emission intensity.

References

(1) Squadrito, G. L.; Pryor, W. A. *Free Radical Biol. Med.* **1998**, *25*, 392.

(2) Kelm, M. *Biochim. Biophys. Acta* **1999**, *1411*, 273.

(3) Cooper, C. E. *Biochim. Biophys. Acta* **1999**, *1411*, 290.

(4) Denninger, J. W.; Marletta, M. A. *Biochim. Biophys. Acta* **1999**, *1411*, 335.

(5) Butler, A. R.; Megson, I. L. *Chem. Rev.* **2002**, *102*, 1155.

(6) Grassi, S.; Pettorossi, V. E. *Neuroscience* **2000**, *101*, 157.

(7) Hölscher, C. *Eur. J. Pharmacol.* **2002**, *457*, 99.

(8) Boehme, G. A.; Bon, C.; Lemaire, M.; Reibaud, M.; Piot, O.; Stutzmann, J.-M.; Doble, A.; Blanchard, J.-C. *Proc. Natl. Acad. Sci. USA* **1993**, *90*, 9191.

(9) Schuman, E. M.; Madison, D. V. *A. Rev. Neurosci.* **1994**, *17*, 153.

(10) de Silva, A. P.; Gunaratne, H. Q. N.; Gunnlaugsson, T.; Huxley, A. J.; McCoy, J. T.; Rademacher, C. P.; Rice, T. E. *Chem. Rev.* **1997**, *97*, 1515.

(11) Franz, K. J.; Singh, N.; Lippard, S. J. *Angew. Chem., Int. Ed. Engl.* **2000**, *39*, 2120.

(12) Franz, K. J.; Singh, N.; Spingler, B.; Lippard, S. J. *Inorg. Chem.* **2000**, *39*, 4081.

(13) Valentine, A. M.; Lippard, S. J. *J. Chem. Soc., Dalton Trans.* **1997**, 3925.

(14) Yoon, S.; Lippard, S. J. *Inorg. Chem.* **2003**, *46*, 8606.

(15) Merkx, M.; Kopp, D. A.; Sazinsky, M. H.; Blazyk, J. L.; Müller, J.; J., L. S. *Angew. Chem., Int. Ed.* **2001**, *40*, 2782.

(16) Lee, D.; Lippard, S. J. *J. Am. Chem. Soc.* **2001**, *123*, 4611.

(17) Stubbe, J.; van der Donk, W. A. *Chem. Rev.* **1998**, *98*, 705.

(18) Stenkamp, R. E. *Chem. Rev.* **1994**, *94*, 715.

(19) Logan, D. T.; Su, X.-D.; Åberg, A.; Regnström, K.; Hajdu, J.; Eklund, H.; Nordlund, P. *Structure* **1996**, *4*, 1053.

(20) Coufal, D. E.; Tavares, P.; Pereira, A. S.; Hyunh, B. H.; Lippard, S. J. *Biochemistry* **1999**, *38*, 4504.

(21) Haskin, C. J.; Ravi, N.; Lynch, J. B.; Münck, E.; Que, L., Jr. *Biochemistry* **1995**, *34*, 11090.

(22) Nocek, J. M.; Kurtz, D. M., Jr.; Sage, J. T.; Xia, Y.-M.; Debrunner, P.; Shiemke, A. K.; Sanders-Loehr, J.; Loehr, T. M. *Biochemistry* **1988**, *27*, 1014.

(23) Feig, A. L.; Bautista, M. T.; Lippard, S. J. *Inorg. Chem.* **1996**, *35*, 6892.

(24) Lee, D.; Lippard, S. J. *Inorg. Chem.* **2002**, *41*, 2704.

(25) Pangborn, A. B.; Giardello, M. A.; Grubbs, R. H.; Rosen, R. K.; Timmers, F. J. *Organometallics* **1996**, *15*, 1518.

(26) Saavedra, J. E.; Booth, M. N.; Hrabie, J. A.; Davies, K. M.; Keefer, L. K. *J. Org. Chem.* **1999**, *64*, 5124.

(27) Du, C.-J. F.; Hart, H.; Ng, K.-K. D. *J. Org. Chem.* **1986**, *51*, 3162.

(28) Saednya, A.; Hart, H. *Synthesis* **1996**, 1455.

(29) Chen, C.-T.; Siegel, J. S. *J. Am. Chem. Soc.* **1994**, *116*, 5959.

(30) Lorkovic, I. M.; Ford, P. C. *Inorg. Chem* **2000**, *39*, 632.

(31) *SMART: Software for the CCD Detector System*, version 5.626; Bruker AXS: Madison, WI, 2000.

(32) Kuzelka, J.; Mukhopadhyay, S.; Spingler, B.; Lippard, S. J. *Inorg. Chem* **2004**, *43*, in press.

(33) Sheldrick, G. M. *SADABS: Aera-Detector Absorption Correction*; University of Göttingen, Göttingen Germany, 2001.

(34) *SHELXTL: Program Library for Structure Solution and Molecular Graphics*, version 6.2; Bruker AXS: Madison, WI, 2001.

(35) *SAINTPLUS: Software for the CCD Detector System*, version 5.01; Bruker AXS: Madison, WI, 1998.

(36) Spek, A. L. *PLATON, A Multipurpose Crystallographic Tool*; Utrecht University: Utrecht, The Netherlands, 2000.

(37) Lee, D.; Hung, P.-L.; Spingler, B.; Lippard, S. J. *Inorg. Chem.* **2002**, *41*, 521.

(38) Aresta, M.; Balliver-Tkatchenko, D.; Bonnet, M. C.; Faure, R.; Loiseleur, J. *J. Am. Chem. Soc.* **1985**, *107*, 2994.

(39) Kaduk, J. A.; Ibers, J. A. *Inorg. Chem* **1977**, *16*.

(40) Roustan, J.-L.; Ansari, N.; Le Page, Y.; Charland, J.-P. *Can. J. Chem.* **1992**, *70*, 1650.

(41) Del Zotto, A.; Mezzetti, A.; Rigo, P. *Inorg. Chim. Acta* **1990**, *171*, 61.

(42) Hendrickson, A. R.; Y., H. R. K.; L., M. R. *Inorg. Chem.* **1974**, *13*, 1279.

(43) Martin, R. L.; Taylor, D. *Inorg. Chem.* **1976**, *15*, 2970.

(44) Fujii, S.; Yoshimura, T.; Kamada, H. *Chem. Lett.* **1996**, 785.

(45) Schneppensieper, T.; Finkler, S.; Czap, A.; van Eldik, R.; Heus, M.; Nieuwenhuizen, P.; Wreesmann, C.; Abma, W. *Eur. J. Inorg. Chem.* **2001**, 491.

Table 3.1. Summary of X-ray Crystallographic Data for **1**, **2**, and **3**.

	1·4CH₂Cl₂	2·4CH₂Cl₂	3·Et₂O
formula	$C_{120}H_{118}O_{12}N_6S_2Cl_8Fe_2$	$C_{120}H_{118}O_{12}N_6S_2Cl_8Co_2$	$C_{120}H_{120}O_{13}N_6S_2Co_2$
fw	2295.70	2301.79	2036.27
space group	P$\bar{1}$	P$\bar{1}$	P$\bar{1}$
a,Å	15.219(3)	15.191(7)	12.582(3)
b Å	19.752(4)	19.660(9)	13.760(4)
c Å	21.337(4)	21.30(1)	16.521(3)
α, deg	116.18(3)	115.974(7)	100.98(1)
β, deg	105.44(3)	105.37(1)	106.60(1)
γ, deg	90.63(3)	90.353(8)	103.58(2)
V, Å³	5486(1)	5459(5)	2560(1)
Z	2	2	1
ρ_{calc}, g/cm³	1.387	1.379	1.311
T, °C	-100	-100	-100
μ(Mo Kα), mm⁻¹	0.562	0.603	0.431
total no. of data	47931	48323	22865
no. of unique data	24367	24669	11629
no. of params	1369	1409	658
R (%)[a]	7.43	6.96	7.54
wR² (%)[b]	16.43	17.91	19.81

[a]$R = \Sigma||F_o|-F_c||/\Sigma|F_o|$, [b]$wR^2 = \{w(F_o^2-F_c^2)^2/\Sigma[w(F_o^2)^2]\}^{1/2}$

Table 3.2. Selected bond distances and angles for **1**, **2**, and **3**.[a]

Compound	Distances	(Å)	Angles	(deg)
[Fe$_2$(μ-O$_2$CAr^{Tol})$_4$(Ds pip)$_2$]	Fe1-Fe2	2.725(1)	N1-Fe1-Fe2	159.55(9)
(**1**)	Fe1-N1	2.138(3)	N1-Fe1-O1	95.6(1)
	Fe1-O1	2.084(3)	N1-Fe1-O3	113.2(2)
	Fe1-O3	2.074(3)	N1-Fe1-O5	97.2(1)
	Fe1-O5	2.066(2)	N1-Fe1-O7	83.8(1)
	Fe1-O7	2.162(3)	N4-Fe2-Fe1	159.54(9)
	Fe2-N4	2.122(3)	N4-Fe2-O2	100.6(1)
	Fe2-O2	2.052(2)	N4-Fe2-O4	87.5(1)
	Fe2-O4	2.126(3)	N4-Fe2-O6	95.8(1)
	Fe2-O6	2.064(3)	N4-Fe2-O8	110.9(1)
	Fe2-O8	2.042(3)		
[Co$_2$(μ-O$_2$CAr^{Tol})$_4$(Ds pip)$_2$]	Co1-Co2	2.720(2)	N1-Co1-Co2	163.95(8)
(**2**)	Co1-N1	2.114(3)	N1-Co1-O1	96.2(1)
	Co1-O1	2.039(2)	N1-Co1-O3	108.2(1)
	Co1-O3	1.993(2)	N1-Co1-O5	98.9(1)
	Co1-O5	2.033(2)	N1-Co1-O7	84.7(1)
	Co1-O7	2.031(2)	N4-Co2-Co1	164.38(8)
	Co2-N4	2.128(3)	N4-Co2-O2	96.7(1)
	Co2-O2	2.051(2)	N4-Co2-O4	86.5(1)
	Co2-O4	2.038(2)	N4-Co2-O6	96.0(1)
	Co2-O6	2.066(2)	N4-Co2-O8	109.9(1)
	Co2-O8	2.024(3)		
[Co$_2$(μ-O$_2$CAr^{Tol})$_2$ (O$_2$CAr^{Tol})$_2$(Ds pip)$_2$]	Co1-Co1A	3.898(1)	O1-Co1-N1	101.0(1)
(**3**)	Co-N1	2.079(3)	O1-Co1-O3	118.0(1)
	Co-O1	1.938(2)	O3-Co1-N1	93.8(1)
	Co-O3	1.951(3)		

[a]Numbers in parentheses are estimated standard deviations of the last significant figure. Atoms are labeled as indicated in Figures 3.2 and 3.3.

Table 3.3. Summary of X-ray Crystallographic Data for **4** and **5**.

	4	**5·CH₂Cl₂**
formula	$C_{16}H_{20}O_3N_4S$	$C_{43}H_{36}O_8N_4Cl_2Co_2$
fw	348.42	925.54
space group	C2/c	P1̄
a,Å	28.32(1)	11.983(2)
b Å	6.594(3)	12.907(2)
c Å	19.966(9)	14.474(2)
α, deg		71.121(2)
β, deg	117.454	76.355(2)
γ, deg		77.119(2)
V, Å³	3309(3)	2032.2(5)
Z	8	2
ρ_{calc}, g/cm³	1.399	1.432
T, °C	-100	-100
μ(Mo Kα), mm⁻¹	0.219	0.939
total no. of data	14013	17868
no. of unique data	3918	9120
no. of params	306	532
R (%)[a]	6.00	4.02
wR₂ (%)[b]	12.12	10.42

[a]$R = R = \Sigma||F_o|-F_c||/\Sigma|F_o|$, [b]$\omega R^2 = \{\omega(F_o^2-F_c^2)^2/\Sigma[\omega(F_o^2)^2]\}^{1/2}$

Table 3.4. Selected bond distances and angles for **4** and **5**.[a]

Compound	Distances	(Å)	Angles	(deg)
N-Nitroso-dansyl-piperazine	N4-O3$_{(avg)}$	1.055(6)	N1-N4-O3$_{avg}$	125.7(7)
(**4**)	N1-N4	1.322(3)	N4-N1-C13	121.4(2)
			N4-N1-C14	121.3(2)
[Co$_2$(NO)$_4$(O$_2$CAr^{Tol})$_2$]	Co-NO$_{(avg)}$	1.662(2)	Co-N-O$_{(avg)}$	163.5(2)
(**5**)	N-O$_{(avg)}$	1.152(3)	N3-Co1-O1	114.71(8)
	Co1-O1	1.982(1)	N3-Co1-O3	120.16(8)
	Co1-O3	1.983(1)	N3-Co1-N4	109.8(1)
	Co2-O2	1.974(1)	N4-Co1-O1	106.53(8)
	Co2-O4	1.978(1)	N4-Co1-O3	110.04(8)
			O1-Co1-O3	94.16(5)
			N1-Co2-O2	110.73(8)
			N1-Co2-O4	106.94(8)
			N1-Co2-N2	110.4(1)
			N2-Co2-O2	116.08(8)
			N2-Co2-O4	117.41(8)
			O2-Co2-O4	94.12(5)

[a]Numbers in parentheses are estimated standard deviations of the last significant figure. Atoms are labeled as indicated in Figure 3.6.

Table 3.5. Atomic coordinates ($\times 10^4$) and equivalent isotropic displacement parameters ($\text{Å}^2\times 10^3$) for [Fe$_2$(μ-O$_2$CAr$^{\text{Tol}}$)$_4$(Ds-pip)$_2$] (**1**). U(eq) is defined as one third of the trace of the orthogonalized U^{ij} tensor.

	x	y	z	U(eq)
Fe(2)	2387(1)	2794(1)	5767(1)	19(1)
Fe(1)	2283(1)	2376(1)	4347(1)	20(1)
O(1)	3711(2)	2505(1)	4768(1)	24(1)
O(2)	3749(2)	3129(1)	5943(1)	23(1)
O(3)	2187(2)	1256(1)	4176(1)	27(1)
O(4)	2652(2)	1648(1)	5381(1)	24(1)
O(5)	883(2)	2350(1)	4197(1)	25(1)
O(6)	1004(2)	2362(1)	5265(1)	23(1)
O(7)	2374(2)	3605(1)	4841(1)	24(1)
O(8)	2098(2)	3846(1)	5892(1)	24(1)
O(9)	3256(2)	1137(2)	1054(2)	50(1)
O(10)	1570(2)	1007(2)	576(2)	47(1)
O(11)	1614(3)	3973(2)	9124(2)	65(1)
O(12)	3310(3)	4139(2)	9553(2)	63(1)
N(3)	1711(3)	4684(2)	1000(2)	47(1)
N(2)	2357(2)	1747(2)	1900(2)	30(1)
N(1)	2290(2)	2479(2)	3391(2)	27(1)
N(6)	3401(3)	513(3)	9195(2)	55(1)
N(5)	2485(2)	3403(2)	8238(2)	34(1)
N(4)	2472(2)	2697(2)	6732(2)	26(1)
S(1)	2424(1)	1466(1)	1068(1)	38(1)
S(2)	2455(1)	3664(1)	9078(1)	49(1)
C(1)	2364(3)	-689(2)	4902(3)	42(1)
C(2)	4227(4)	5172(3)	8174(2)	46(1)
C(3)	516(3)	3606(3)	575(3)	48(1)
C(4)	2887(3)	-1103(3)	4468(3)	48(1)
C(5)	3458(4)	5533(3)	8204(3)	54(1)
C(6)	4044(4)	2741(3)	9490(3)	54(1)
C(7)	594(4)	4909(3)	7963(2)	52(1)
C(8)	3119(3)	143(3)	3101(3)	46(1)
C(9)	4509(4)	669(3)	3043(3)	51(1)
C(10)	1190(3)	687(3)	6561(3)	43(1)
C(11)	3596(4)	369(3)	2738(3)	54(1)
C(12)	910(3)	2438(3)	591(2)	43(1)
C(105)	1029(4)	5033(3)	664(3)	59(1)
C(13)	-93(3)	367(2)	1845(2)	40(1)
C(14)	3624(4)	1266(3)	9309(3)	51(1)
C(15)	269(3)	2860(3)	439(2)	46(1)
C(16)	2914(3)	5597(3)	7600(2)	45(1)
C(17)	1772(3)	400(3)	6139(3)	41(1)
C(18)	3255(3)	-800(2)	4107(3)	42(1)
C(19)	4739(3)	1835(2)	6129(2)	33(1)
C(20)	4468(3)	1404(3)	6428(3)	42(1)
C(21)	6656(3)	3186(2)	6493(2)	34(1)
C(22)	3730(3)	3305(3)	1191(2)	43(1)
C(23)	3820(3)	4424(3)	3193(2)	44(1)

Table 3.5. Continued.

	x	y	z	U(eq)
C(24)	1423(3)	3924(3)	831(2)	41(1)
C(25)	1640(3)	2928(3)	6961(2)	40(1)
C(26)	3495(3)	2607(3)	1161(2)	40(1)
C(27)	872(3)	756(2)	5263(2)	30(1)
C(28)	4785(3)	1626(3)	7170(3)	44(1)
C(29)	5672(3)	2737(3)	7312(2)	40(1)
C(30)	-681(3)	898(3)	1860(2)	41(1)
C(31)	5392(3)	2301(3)	7606(3)	48(1)
C(32)	296(3)	1040(2)	5690(2)	35(1)
C(33)	894(3)	4067(2)	2985(2)	36(1)
C(34)	190(3)	4272(2)	7187(2)	36(1)
C(35)	136(3)	3563(2)	2839(2)	34(1)
C(36)	3060(3)	3726(3)	1088(2)	41(1)
C(37)	4444(3)	4887(3)	7527(3)	42(1)
C(38)	-952(3)	1309(3)	2475(2)	37(1)
C(39)	1507(3)	2014(3)	2057(2)	34(1)
C(40)	3559(3)	209(2)	3782(2)	34(1)
C(41)	3310(3)	3132(3)	8045(2)	45(1)
C(42)	233(3)	274(2)	2469(2)	38(1)
C(43)	481(3)	4012(2)	4144(2)	32(1)
C(44)	1446(3)	2481(3)	8971(2)	49(1)
C(45)	5349(3)	2506(2)	6561(2)	29(1)
C(46)	-30(3)	691(2)	3087(2)	34(1)
C(47)	-700(3)	3034(2)	6340(2)	31(1)
C(48)	-59(3)	3545(3)	3431(2)	37(1)
C(49)	430(3)	1001(3)	6342(3)	42(1)
C(50)	3091(3)	2410(3)	9264(2)	41(1)
C(51)	2193(3)	33(2)	4984(2)	31(1)
C(52)	6538(3)	3670(2)	5635(2)	32(1)
C(53)	2342(3)	2802(3)	9140(2)	46(1)
C(54)	-356(3)	3626(3)	7043(2)	36(1)
C(55)	2902(3)	1679(3)	9198(2)	45(1)
C(56)	5003(3)	3749(2)	3685(2)	35(1)
C(57)	2145(3)	6402(2)	5944(2)	36(1)
C(58)	1620(3)	421(2)	5472(2)	31(1)
C(59)	1432(3)	4536(2)	3697(2)	32(1)
C(60)	3916(3)	4953(2)	6928(2)	34(1)
C(61)	3292(3)	3153(3)	7339(2)	40(1)
C(62)	2557(3)	6201(2)	6482(2)	33(1)
C(63)	3149(3)	2258(2)	3205(2)	32(1)
C(64)	-1904(3)	2279(2)	4788(2)	28(1)
C(65)	5712(3)	2944(2)	6241(2)	28(1)
C(66)	5085(2)	3660(2)	4791(2)	25(1)
C(67)	45(3)	3720(2)	5903(2)	26(1)
C(68)	1652(3)	2920(3)	7662(2)	44(1)
C(69)	2118(3)	3468(3)	941(2)	37(1)
C(70)	7070(3)	3554(2)	6203(2)	36(1)
C(71)	1480(3)	2015(3)	2763(2)	33(1)
C(72)	1867(3)	2728(3)	853(2)	36(1)
C(73)	5412(3)	3505(2)	4194(2)	33(1)
C(74)	-2416(3)	1774(2)	4081(2)	34(1)

Table 3.5. Continued.

	x	y	z	U(eq)
C(75)	1765(3)	5839(2)	5236(2)	30(1)
C(76)	381(3)	4314(2)	6606(2)	32(1)
C(77)	3086(3)	-84(2)	4161(2)	31(1)
C(78)	-1967(3)	1451(2)	3559(2)	31(1)
C(79)	2607(3)	5446(2)	6334(2)	26(1)
C(80)	1240(3)	4514(2)	4287(2)	27(1)
C(81)	2590(3)	2314(3)	993(2)	36(1)
C(82)	2561(3)	337(2)	4610(2)	28(1)
C(83)	3941(3)	4300(2)	4339(2)	30(1)
C(84)	3140(3)	5307(2)	6953(2)	28(1)
C(85)	-1019(3)	1622(2)	3725(2)	27(1)
C(86)	4260(3)	4153(2)	3743(2)	31(1)
C(87)	4348(2)	4059(2)	4855(2)	26(1)
C(88)	3169(3)	2247(3)	2496(2)	37(1)
C(89)	4525(3)	1608(3)	9540(3)	54(1)
C(90)	4720(4)	2345(4)	9633(3)	58(2)
C(91)	5585(2)	3450(2)	5368(2)	26(1)
C(92)	-632(3)	1215(2)	3101(2)	28(1)
C(93)	1957(3)	1373(3)	9032(2)	49(1)
C(94)	1271(3)	1762(3)	8928(3)	49(1)
C(95)	2457(2)	1143(2)	4734(2)	24(1)
C(96)	-504(2)	3073(2)	5753(2)	24(1)
C(97)	1764(3)	5073(2)	5057(2)	26(1)
C(98)	-499(2)	2126(2)	4445(2)	23(1)
C(99)	5165(2)	3092(2)	5681(2)	24(1)
C(100)	4129(2)	2890(2)	5440(2)	23(1)
C(101)	2199(2)	4867(2)	5605(2)	23(1)
C(102)	2227(2)	4039(2)	5428(2)	22(1)
C(103)	-949(2)	2465(2)	4986(2)	22(1)
C(104)	538(2)	2296(2)	4652(2)	22(1)
C(115)	212(4)	-89(3)	1173(3)	58(2)
C(114)	4805(4)	5095(3)	8832(3)	72(2)
C(113)	4479(4)	1160(3)	7496(3)	66(2)
C(112)	4483(3)	498(3)	4086(3)	52(1)
C(111)	-229(4)	1282(3)	6796(3)	54(1)
C(110)	2143(4)	5198(3)	1785(3)	62(2)
C(109)	4941(4)	726(4)	3717(3)	65(2)
C(108)	-476(3)	3069(3)	2070(3)	49(1)
C(107)	3051(4)	-25(3)	8425(3)	78(2)
C(106)	4092(4)	224(4)	9577(3)	77(2)
C(116)	5027(4)	932(4)	2657(4)	89(2)
C(120)	2636(6)	5776(4)	-71(4)	99(2)
C(121)	5987(4)	2420(4)	1447(3)	78(2)
C(122)	7874(5)	1988(4)	7970(5)	111(3)
C(123)	7636(5)	662(4)	9592(5)	142(4)
Cl(1)	3341(5)	6103(3)	720(3)	126(2)
Cl(1A)	3853(3)	6136(3)	444(3)	101(1)
Cl(2)	2156(2)	6515(2)	-208(2)	191(2)
Cl(3)	6991(2)	2228(1)	1234(1)	123(1)
Cl(4)	5769(1)	2002(1)	1966(1)	97(1)
Cl(5)	6712(2)	1006(2)	9239(1)	173(1)

Table 3.5. Continued.

	x	y	z	U(eq)
Cl(6)	8435(2)	2760(1)	7997(2)	129(1)
Cl(7)	8595(2)	1606(2)	8472(2)	81(1)
Cl(7A)	8206(17)	1816(9)	8593(9)	209(10)
Cl(8)	8566(1)	1355(1)	10198(1)	79(1)

Table 3.6. Atomic coordinates (x 10^4) and equivalent isotropic displacement parameters (Å^2x 10^3) for [Co$_2$(μ-O$_2$CAr$^{\text{Tol}}$)$_4$(Ds-pip)$_2$] (**2**). U(eq) is defined as one third of the trace of the orthogonalized U^{ij} tensor.

	x	y	z	U(eq)
C(1)	2218(2)	774(2)	634(2)	25(1)
C(2)	4117(2)	2556(2)	450(2)	23(1)
C(3)	561(2)	2347(2)	-355(2)	22(1)
C(4)	2236(2)	1422(2)	457(2)	23(1)
C(5)	5159(2)	2599(2)	693(2)	26(1)
C(6)	-942(2)	2513(2)	-21(2)	25(1)
C(7)	1783(2)	12(2)	84(2)	27(1)
C(8)	-481(2)	2320(2)	-559(2)	23(1)
C(9)	2462(2)	3534(2)	-307(2)	27(1)
C(10)	1488(2)	798(2)	-2222(2)	34(1)
C(11)	4249(3)	-406(2)	-1263(2)	32(1)
C(12)	1255(2)	-201(2)	-682(2)	28(1)
C(13)	-609(2)	1898(2)	-1902(2)	31(1)
C(14)	4339(2)	789(2)	-139(2)	27(1)
C(15)	3939(2)	37(2)	-657(2)	31(1)
C(16)	-997(2)	2115(2)	-1275(2)	28(1)
C(17)	2572(2)	4219(2)	-432(2)	34(1)
C(18)	5577(2)	1930(2)	378(2)	29(1)
C(19)	367(2)	2254(2)	1581(2)	33(1)
C(20)	-1947(2)	2124(2)	-1444(2)	35(1)
C(21)	-503(2)	2666(2)	741(2)	27(1)
C(22)	5402(2)	704(2)	-802(2)	34(1)
C(23)	1632(3)	4707(2)	2631(2)	39(1)
C(24)	2632(2)	915(2)	1352(2)	29(1)
C(25)	3157(2)	995(2)	-1778(2)	33(1)
C(26)	3275(3)	4117(2)	2318(2)	39(1)
C(27)	3175(3)	294(2)	-2493(2)	38(1)
C(28)	3172(3)	1673(2)	1968(2)	30(1)
C(29)	1866(3)	-1833(2)	-4140(2)	38(1)
C(30)	-2396(2)	2329(2)	-917(2)	36(1)
C(31)	1786(2)	-577(2)	264(2)	33(1)
C(32)	5083(2)	1142(2)	-204(2)	27(1)
C(33)	39(2)	2157(2)	882(2)	29(1)
C(34)	3301(3)	4847(3)	3028(2)	42(1)
C(35)	2596(3)	-1275(2)	-4001(2)	36(1)
C(36)	7061(2)	2665(2)	1216(2)	38(1)
C(37)	2118(3)	-2496(2)	-4063(2)	39(1)
C(38)	250(3)	2221(2)	-2532(2)	42(1)
C(39)	1451(2)	-808(2)	-1277(2)	33(1)
C(40)	5703(2)	3311(2)	1259(2)	31(1)
C(41)	-1898(2)	2519(2)	-213(2)	31(1)
C(42)	175(3)	2879(2)	2166(2)	36(1)
C(43)	-700(2)	3289(2)	1331(2)	31(1)
C(44)	-369(3)	3393(2)	2031(2)	37(1)
C(45)	5336(2)	4072(2)	1579(2)	33(1)
C(46)	2593(3)	306(2)	1509(2)	37(1)
C(47)	-7(3)	2415(2)	-1908(2)	34(1)
C(48)	3077(3)	6794(3)	4252(2)	41(1)

Table 3.6. Continued.

	x	y	z	U(eq)
C(49)	1618(2)	3988(2)	1923(2)	37(1)
C(50)	3097(3)	4193(3)	-880(2)	42(1)
C(51)	1508(2)	88(2)	-2929(2)	34(1)
C(52)	-49(3)	-96(2)	-1534(2)	39(1)
C(53)	466(3)	5331(2)	1326(2)	46(1)
C(54)	4995(3)	-55(2)	-1321(2)	38(1)
C(55)	3057(3)	-2610(3)	-3922(2)	42(1)
C(56)	1636(3)	5020(2)	440(2)	39(1)
C(57)	2181(3)	-433(2)	970(2)	39(1)
C(58)	-938(3)	1175(2)	-2530(2)	41(1)
C(59)	1428(3)	6441(3)	3969(2)	48(1)
C(60)	2209(3)	4908(2)	-55(2)	39(1)
C(61)	489(3)	148(2)	-825(2)	36(1)
C(62)	6649(2)	3327(2)	1511(2)	37(1)
C(63)	2886(3)	7475(3)	4202(2)	45(1)
C(64)	3500(3)	-1402(3)	-3845(2)	42(1)
C(65)	3957(3)	2000(2)	1946(2)	35(1)
C(66)	5649(3)	4591(2)	2329(2)	43(1)
C(67)	153(3)	-695(2)	-2127(2)	37(1)
C(68)	921(3)	-1046(2)	-1985(2)	39(1)
C(69)	4501(3)	2655(2)	2542(2)	42(1)
C(70)	4727(3)	4311(2)	1146(2)	35(1)
C(71)	2315(3)	6278(3)	4123(2)	42(1)
C(72)	4749(3)	5552(2)	2184(3)	46(1)
C(73)	3727(3)	-2084(3)	-3825(2)	42(1)
C(74)	914(3)	-1795(3)	-4386(2)	44(1)
C(75)	6531(2)	1979(2)	649(2)	35(1)
C(76)	881(3)	4483(2)	231(2)	36(1)
C(77)	4438(3)	5032(2)	1445(2)	43(1)
C(78)	5359(3)	5323(3)	2627(2)	48(1)
C(79)	313(3)	4637(2)	668(2)	40(1)
C(80)	3808(3)	-1221(2)	-1822(2)	45(1)
C(81)	-671(3)	982(3)	-3147(2)	45(1)
C(82)	-80(3)	1499(3)	-3163(2)	44(1)
C(83)	512(3)	-2999(3)	-4418(2)	50(1)
C(84)	1419(3)	-3064(3)	-4165(2)	45(1)
C(85)	4281(3)	3025(2)	3196(2)	47(1)
C(86)	1802(3)	5711(2)	1109(3)	48(1)
C(87)	3619(3)	8007(3)	4312(2)	52(1)
C(88)	-444(3)	-964(3)	-2894(2)	50(1)
C(89)	3559(3)	3517(3)	-1263(2)	42(1)
C(90)	4021(3)	6691(3)	4469(2)	51(1)
C(91)	276(3)	-2381(3)	-4538(2)	48(1)
C(92)	2949(3)	2039(3)	2624(2)	48(1)
C(93)	4431(4)	6346(3)	2510(3)	66(1)
C(94)	220(4)	1288(3)	-3834(2)	61(1)
C(95)	3255(3)	4860(3)	-946(3)	57(1)
C(96)	569(3)	3006(3)	2941(2)	54(1)
C(97)	1954(3)	7631(3)	4047(2)	49(1)
C(98)	1258(3)	7127(3)	3939(2)	51(1)
C(99)	1031(4)	-4352(3)	-4346(3)	63(1)

Table 3.6. Continued.

	x	y	z	U(eq)
C(100)	3497(4)	2706(3)	3220(2)	56(1)
C(101)	1231(3)	5857(3)	1537(3)	51(1)
C(102)	2894(3)	5526(3)	-579(3)	60(1)
C(103)	4090(4)	9329(3)	4585(3)	78(2)
C(104)	4697(3)	7240(3)	4617(2)	59(1)
C(105)	4871(4)	3749(3)	3852(3)	67(2)
C(106)	3015(4)	8424(4)	3430(3)	78(2)
C(107)	4457(4)	3506(4)	-936(3)	78(2)
C(108)	4509(3)	7887(3)	4531(2)	56(1)
C(109)	2144(4)	-3404(3)	-3238(3)	67(1)
C(110)	3164(4)	2935(3)	-1951(3)	63(1)
C(111)	2374(3)	5552(3)	-143(3)	53(1)
C(112)	-190(4)	5507(3)	1786(3)	59(1)
C(113)	3657(4)	2355(3)	-2313(3)	70(2)
C(114)	4549(4)	2333(3)	-1987(3)	66(2)
C(115)	5085(5)	1688(4)	-2368(4)	102(2)
C(116)	4949(4)	2931(4)	-1291(4)	92(2)
C(117)	2370(5)	1093(6)	5392(6)	122(4)
C(118)	6028(5)	9017(4)	6432(3)	99(2)
C(119)	2099(5)	4073(4)	7024(5)	121(3)
C(120)	2545(6)	4055(4)	4894(4)	120(3)
Cl(1)	7052(2)	9020(2)	6269(2)	161(1)
Cl(2)	5779(2)	9941(1)	6938(1)	112(1)
Cl(3)	1410(2)	3151(2)	6514(2)	95(1)
Cl(4)	1416(1)	1147(1)	4793(1)	90(1)
Cl(5)	1517(3)	4810(2)	7024(2)	109(1)
Cl(6)	3284(4)	4550(3)	5695(2)	139(2)
Cl(7)	2229(4)	3071(3)	4646(3)	119(2)
Cl(8)	3342(5)	1714(5)	5663(6)	134(3)
Cl(3A)	1815(14)	3211(6)	6348(6)	167(7)
Cl(5A)	1350(20)	4568(10)	6694(10)	259(14)
Cl(6A)	3802(4)	4271(4)	5428(3)	106(2)
Cl(7A)	2000(8)	3328(8)	4873(8)	236(8)
Cl(8A)	3147(8)	1913(8)	5790(10)	156(6)
Co(1)	2382(1)	2975(1)	749(1)	21(1)
Co(2)	2291(1)	1953(1)	-642(1)	23(1)
N(1)	2461(2)	3988(2)	1711(1)	25(1)
N(2)	2453(2)	4777(2)	3210(2)	35(1)
N(3)	3392(3)	8656(3)	4205(2)	58(1)
N(4)	2295(2)	949(2)	-1598(1)	26(1)
N(5)	2364(2)	205(2)	-3085(2)	32(1)
N(6)	1706(3)	-3663(2)	-4011(2)	52(1)
O(1)	1014(2)	2903(1)	252(1)	24(1)
O(2)	895(2)	1826(1)	-805(1)	26(1)
O(3)	2117(2)	2086(1)	921(1)	24(1)
O(4)	2374(2)	1270(1)	-139(1)	25(1)
O(5)	3741(2)	2850(1)	955(1)	25(1)
O(6)	3707(2)	2239(1)	-219(1)	26(1)
O(7)	2637(2)	3694(1)	346(1)	26(1)
O(8)	2217(2)	2862(1)	-854(1)	31(1)
O(9)	3269(3)	5342(2)	4523(2)	66(1)

Table 3.6. Continued.

	x	y	z	U(eq)
O(10)	1575(3)	5079(2)	4086(2)	66(1)
O(11)	1579(2)	-380(2)	-4411(1)	49(1)
O(12)	3256(2)	-32(2)	-3937(2)	50(1)
S(1)	2420(1)	5347(1)	4048(1)	49(1)
S(2)	2432(1)	-348(1)	-3918(1)	39(1)

Table 3.7. Atomic coordinates (x 10^4) and equivalent isotropic displacement parameters (Å^2x 10^3) for [Co$_2$(μ-O$_2$CAr$^{\text{Tol}}$)$_2$(O$_2$CAr$^{\text{Tol}}$)$_2$(Ds-pip)$_2$] (**3**). U(eq) is defined as one third of the trace of the orthogonalized U^{ij} tensor.

	x	y	z	U(eq)
Co(1)	1651(1)	724(1)	641(1)	28(1)
O(1)	1300(2)	-771(2)	253(1)	36(1)
O(3)	3187(2)	1405(2)	619(1)	40(1)
O(4)	1984(2)	1083(2)	-722(1)	41(1)
O(5)	5769(2)	3199(2)	4800(2)	46(1)
O(6)	5756(2)	1390(2)	4702(2)	46(1)
N(1)	2241(2)	992(2)	1996(2)	33(1)
N(2)	4218(2)	1754(2)	3615(2)	34(1)
N(3)	2017(2)	3127(2)	7069(2)	43(1)
S(1)	5132(1)	2132(1)	4631(1)	36(1)
C(1)	3806(3)	2805(2)	5631(2)	34(1)
C(2)	3980(3)	2071(2)	-359(2)	35(1)
C(3)	3028(3)	376(2)	2270(2)	36(1)
C(4)	3576(3)	629(2)	3255(2)	39(1)
C(5)	4269(3)	2009(2)	5316(2)	36(1)
C(6)	3091(3)	2578(2)	6140(2)	36(1)
C(7)	2959(3)	1460(2)	-167(2)	33(1)
C(8)	2780(3)	1559(2)	6244(2)	40(1)
C(9)	3978(3)	1048(2)	5459(2)	42(1)
C(10)	2880(3)	2120(2)	2398(2)	41(1)
C(11)	3205(3)	814(2)	5903(2)	45(1)
C(12)	3446(3)	2399(2)	3386(2)	40(1)
C(50)	295(3)	-2548(2)	-2041(2)	38(1)
C(51)	4070(3)	422(3)	-1301(2)	39(1)
C(52)	3994(3)	3795(2)	5445(2)	39(1)
C(53)	935(2)	-3040(2)	232(2)	34(1)
C(54)	2027(3)	-2220(3)	2720(2)	44(1)
C(55)	2634(3)	3354(2)	6501(2)	38(1)
C(56)	658(2)	-2563(2)	-452(2)	31(1)
C(57)	808(3)	-1494(3)	-1927(2)	39(1)
C(58)	3456(3)	4475(2)	5730(2)	44(1)
C(59)	1042(3)	-2561(2)	1155(2)	34(1)
C(60)	1085(3)	-4019(3)	24(2)	44(1)
C(61)	268(3)	-2065(2)	1354(2)	36(1)
C(62)	602(3)	-1061(3)	-2632(2)	46(1)
C(63)	450(2)	-1533(2)	-252(2)	30(1)
C(64)	2434(3)	4119(2)	1092(2)	42(1)
C(65)	1929(3)	-2626(2)	1853(2)	39(1)
C(66)	2781(3)	4258(2)	6251(2)	43(1)
C(67)	3842(3)	-278(3)	-817(2)	41(1)
C(68)	4453(3)	3151(2)	54(2)	38(1)
C(69)	712(3)	-4022(3)	-1481(2)	46(1)
C(70)	5848(3)	3238(3)	-683(3)	57(1)
C(71)	1327(4)	3805(3)	7229(3)	61(1)
C(72)	1246(3)	-1742(2)	2918(2)	41(1)
C(73)	5411(3)	2171(3)	-1067(3)	52(1)
C(74)	970(3)	-4506(3)	-825(3)	51(1)
C(75)	3205(3)	4750(2)	1912(2)	43(1)
C(76)	2822(3)	3623(2)	483(2)	38(1)

Table 3.7. Continued.

	x	y	z	U(eq)
C(77)	545(3)	-3049(2)	-1314(2)	37(1)
C(78)	4467(3)	1566(3)	-914(2)	39(1)
C(79)	3997(3)	3706(2)	679(2)	38(1)
C(80)	5401(3)	3721(3)	-126(3)	50(1)
C(81)	4371(3)	4861(3)	2087(2)	49(1)
C(82)	4770(3)	4355(3)	1492(2)	47(1)
C(83)	2719(3)	3017(3)	7907(2)	52(1)
O(2)	-565(2)	-1516(2)	-607(1)	36(1)
C(85)	375(3)	-1658(2)	2218(2)	40(1)
C(86)	3567(3)	-1336(3)	-1175(2)	50(1)
C(87)	-634(4)	-2705(3)	-3583(2)	57(1)
C(88)	2802(4)	5273(3)	2603(3)	61(1)
C(89)	3991(3)	8(3)	-2158(2)	49(1)
C(90)	3712(3)	-1047(3)	-2509(3)	55(1)
C(91)	1324(4)	-1344(3)	3860(2)	57(1)
C(92)	-444(3)	-3142(3)	-2890(2)	50(1)
C(93)	-103(3)	-1658(3)	-3468(2)	51(1)
C(94)	3503(3)	-1745(3)	-2033(3)	56(1)
C(95)	-294(5)	-1205(4)	-4237(3)	78(1)
C(96)	3168(5)	-2902(3)	-2436(4)	86(2)
O(50)	9968(16)	4981(11)	5289(7)	154(5)
C(98)	9086(13)	3845(14)	4888(8)	261(7)
C(99)	8628(8)	4051(8)	5610(11)	263(9)

Table 3.8. Atomic coordinates (x 10^4) and equivalent isotropic displacement parameters ($\mathring{A}^2$x 10^3) for N-nitroso-dansyl-piperazine (**4**). U(eq) is defined as one third of the trace of the orthogonalized U^{ij} tensor.

	x	y	z	U(eq)
S(1)	878(1)	6169(1)	1278(1)	32(1)
N(3)	2901(1)	3994(3)	4539(1)	37(1)
O(1)	694(1)	8212(3)	1076(1)	43(1)
O(2)	1089(1)	5128(3)	849(1)	39(1)
C(1)	2529(1)	3556(4)	3775(1)	31(1)
C(2)	1351(1)	6233(4)	2253(1)	31(1)
N(2)	356(1)	4864(3)	1187(1)	33(1)
C(3)	1742(1)	4694(3)	2613(1)	28(1)
C(4)	2110(1)	4979(4)	3393(1)	30(1)
C(5)	1791(1)	2889(4)	2255(1)	31(1)
C(6)	1656(1)	8065(4)	3421(1)	38(1)
C(7)	2046(1)	6687(4)	3778(1)	36(1)
C(8)	2177(1)	1518(4)	2645(1)	34(1)
C(9)	398(1)	2645(4)	1227(2)	40(1)
N(1)	-460(1)	2626(4)	1220(1)	46(1)
C(10)	2553(1)	1844(4)	3405(1)	35(1)
C(11)	3147(1)	2217(5)	5002(2)	43(1)
C(12)	1311(1)	7868(4)	2647(1)	37(1)
C(13)	-161(1)	1761(5)	866(2)	46(1)
C(14)	-493(1)	4813(5)	1215(2)	46(1)
C(15)	71(1)	5677(5)	1586(2)	40(1)
C(16)	3302(1)	5486(5)	4605(2)	48(1)
N(4)	-608(1)	1514(9)	1643(2)	76(1)
O(3A)	-528(2)	-88(9)	1769(3)	73(2)
O(3)	-803(3)	2055(9)	1928(3)	69(2)

Table 3.9. Atomic coordinates (x 10^4) and equivalent isotropic displacement parameters (Å^2x 10^3) for [Co$_2$(NO)$_2$(μ-O$_2$CAr$^{\text{Tol}}$)$_2$] (**5**). U(eq) is defined as one third of the trace of the orthogonalized U^{ij} tensor.

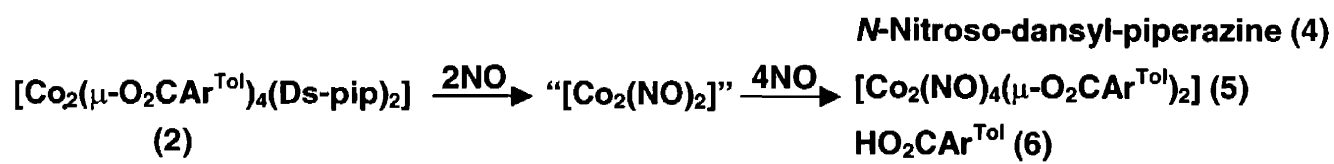|	x	y	z	U(eq)
Co(1)	1240(1)	577(1)	10438(1)	30(1)
Co(2)	3132(1)	1716(1)	8108(1)	29(1)
O(4)	1740(1)	2782(1)	8429(1)	28(1)
O(1)	2202(1)	1609(1)	10503(1)	28(1)
O(2)	3764(1)	1569(1)	9294(1)	29(1)
O(3)	442(1)	1692(1)	9393(1)	31(1)
C(1)	728(2)	2598(2)	8829(1)	26(1)
C(36)	4378(2)	3745(2)	9119(2)	30(1)
C(4)	-976(2)	3375(2)	10414(1)	28(1)
C(2)	-246(2)	3553(2)	8585(1)	25(1)
C(23)	3875(2)	2161(2)	10652(1)	27(1)
C(15)	515(2)	3774(2)	6757(1)	28(1)
C(3)	-1079(2)	3866(2)	9349(1)	27(1)
N(1)	3943(2)	2401(2)	7081(1)	42(1)
C(24)	3919(2)	1593(2)	11652(1)	29(1)
C(11)	-1998(2)	4718(2)	9098(2)	32(1)
C(35)	4438(2)	3088(2)	10168(2)	29(1)
C(25)	3428(2)	546(2)	12165(1)	31(1)
C(13)	-1244(2)	4972(2)	7366(2)	34(1)
C(14)	-323(2)	4109(2)	7588(1)	28(1)
C(16)	676(2)	2696(2)	6698(2)	35(1)
O(8)	-140(2)	-144(2)	12293(2)	68(1)
N(3)	1987(2)	-604(2)	10244(2)	45(1)
C(34)	5035(2)	3432(2)	10704(2)	35(1)
C(22)	3225(2)	1749(2)	10101(1)	25(1)
C(26)	3818(2)	-369(2)	11805(2)	35(1)
C(9)	-1786(2)	2464(2)	12101(2)	40(1)
O(6)	4469(2)	2667(2)	6285(1)	68(1)
N(4)	319(2)	314(2)	11510(2)	42(1)
C(40)	3257(2)	4772(2)	7831(2)	40(1)
C(21)	1139(2)	4523(2)	6012(2)	35(1)
C(32)	4513(2)	1977(2)	12164(2)	35(1)
C(12)	-2081(2)	5265(2)	8116(2)	35(1)
N(2)	2916(2)	550(2)	7980(2)	44(1)
C(17)	1447(2)	2380(2)	5921(2)	40(1)
C(41)	3311(2)	4138(2)	8796(2)	33(1)
C(20)	1915(2)	4198(2)	5241(2)	39(1)
C(33)	5063(2)	2891(2)	11694(2)	37(1)
C(27)	3417(2)	-1364(2)	12312(2)	42(1)
C(18)	2082(2)	3121(2)	5184(2)	36(1)
C(31)	2614(2)	439(2)	13035(2)	43(1)
C(6)	55(2)	3041(2)	11749(2)	43(1)
C(39)	4252(2)	5033(2)	7152(2)	43(1)
C(5)	-13(2)	3451(2)	10750(2)	35(1)
C(38)	5314(2)	4645(2)	7470(2)	43(1)
C(30)	2212(2)	-555(2)	13534(2)	49(1)
C(10)	-1863(2)	2873(2)	11105(2)	34(1)
O(7)	2407(2)	-1511(2)	10341(2)	79(1)
C(7)	-824(2)	2542(2)	12440(2)	40(1)

Table 3.9. Continued.

	x	y	z	U(eq)
C(37)	5378(2)	4015(2)	8443(2)	38(1)
C(28)	2614(2)	-1477(2)	13182(2)	43(1)
O(5)	2881(2)	-163(2)	7688(2)	87(1)
C(19)	2930(2)	2767(2)	4348(2)	53(1)
C(8)	-739(3)	2081(3)	13528(2)	62(1)
C(29)	2208(3)	-2578(2)	13745(2)	64(1)
C(200)	5110(8)	477(6)	5463(5)	78(2)
Cl(2)	6211(3)	886(3)	4444(2)	134(1)
C(42)	4180(3)	5727(3)	6095(2)	65(1)
Cl(1)	4328(2)	-369(2)	5277(2)	101(1)

windmill   paddlewheel

Scheme 3.1.

N-Nitroso-dansyl-piperazine (4)

$[Co_2(\mu-O_2CAr^{Tol})_4(Ds\text{-}pip)_2]$ $\xrightarrow{\text{2NO}}$ "$[Co_2(NO)_2]$" $\xrightarrow{\text{4NO}}$ $[Co_2(NO)_4(\mu-O_2CAr^{Tol})_2]$ (5)
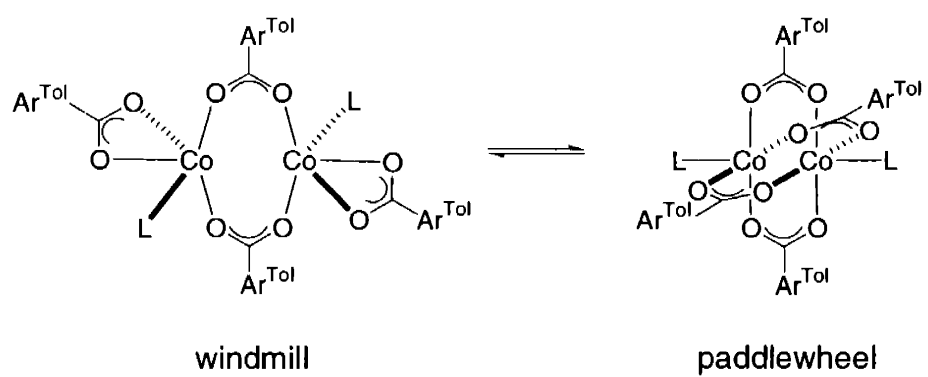
(2) $\qquad\qquad\qquad\qquad\qquad\qquad\qquad\qquad$ HO_2CAr^{Tol} (6)

Scheme 3.2.
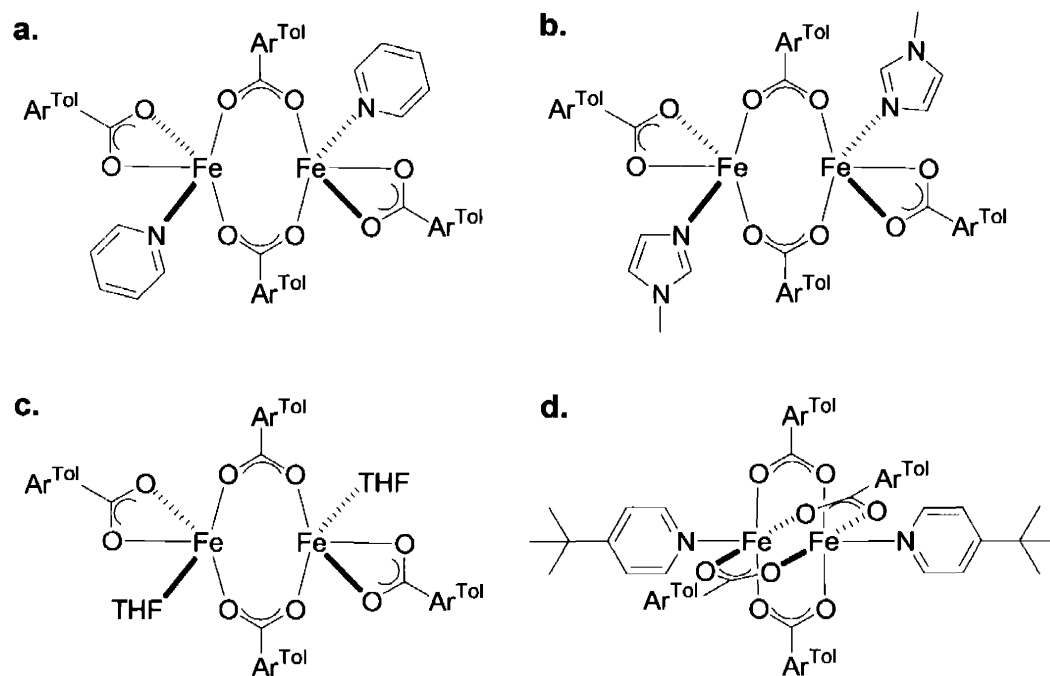
Figure 3.1. Structures of previously characterized tetra(carboxylato)diiron(II) complexes **(a)** [Fe$_2$(μ-O$_2$CAr^{Tol})$_2$(O$_2$CAr^{Tol})$_2$(C$_5$H$_5$N)$_2$], **(b)** [Fe$_2$(μ-O$_2$CAr^{Tol})$_2$(O$_2$CAr^{Tol})$_2$(1-MeIm)$_2$], **(c)** [Fe$_2$(μ-O$_2$CAr^{Tol})$_2$(O$_2$CAr^{Tol})$_2$(THF)$_2$], and **(d)** [Fe$_2$(μ-O$_2$CAr^{Tol})$_4$(4-^{t}BuC$_5$H$_5$N)$_2$].
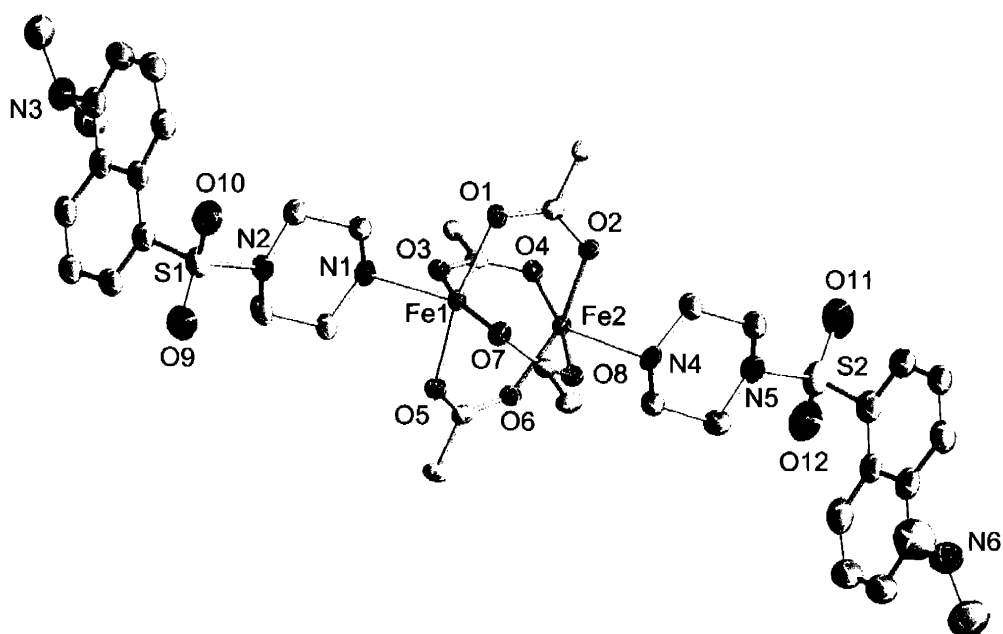
Figure 3.2. ORTEP diagram of [Fe₂(μ-O₂CAr^Tol)₄(Ds-pip)₂] (1) showing 50% probability thermal ellipsoids. The *m*-tolyl terphenyl carboxylate ligands have been truncated and the solvent molecule has been omitted for clarity.
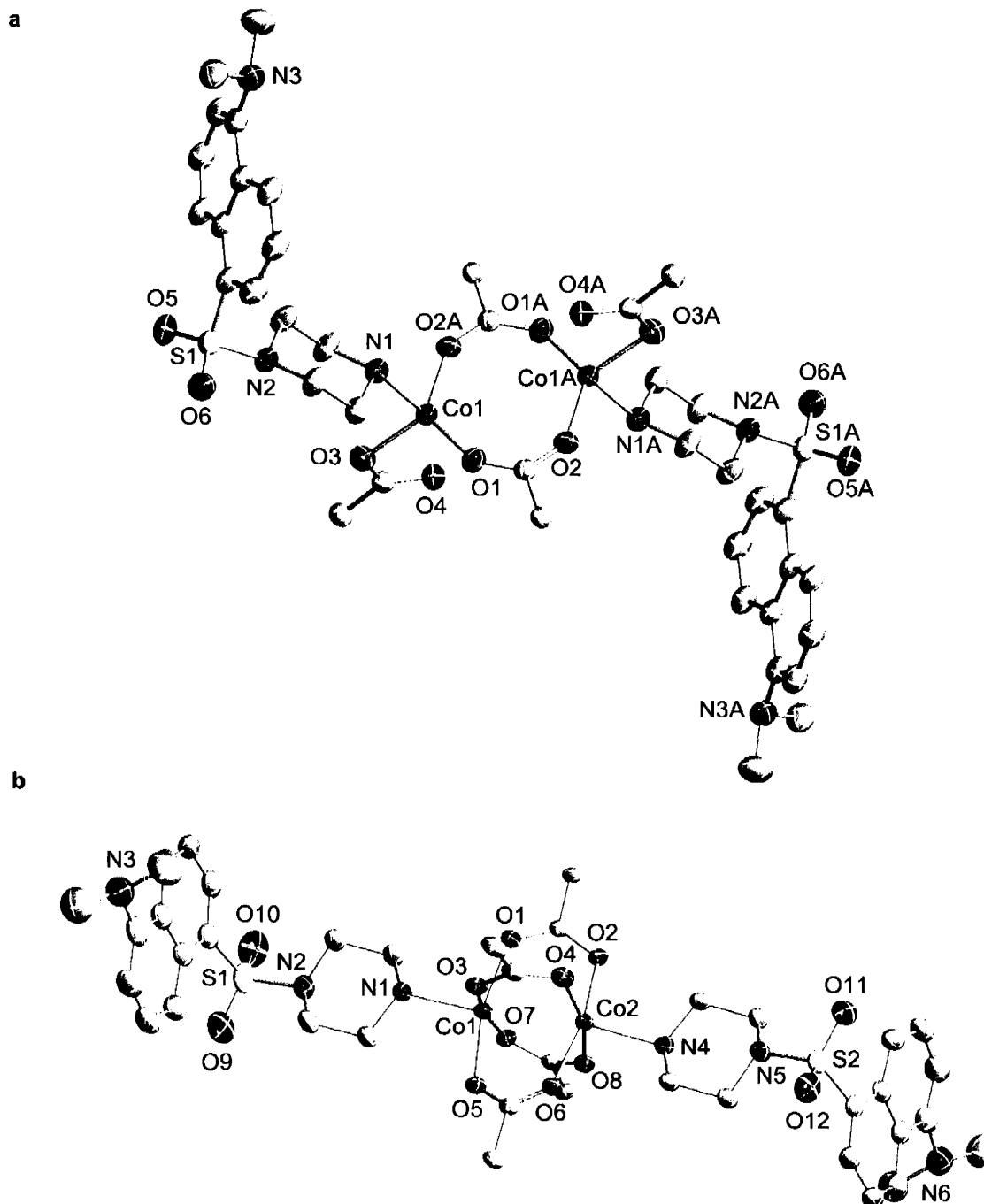
Figure 3.3. ORTEP diagrams of **(a)** [Co₂(μ-O₂CAr^Tol)₄(Ds-pip)₂] (**2**) and **(b)** [Co₂(μ-O₂CAr^Tol)₂(O₂CAr^Tol)₂(Ds-pip)₂] (**3**) showing 50% probability thermal ellipsoids. The *m*-tolyl terphenyl carboxylate ligands have been truncated and the solvent molecule has been omitted for clarity.
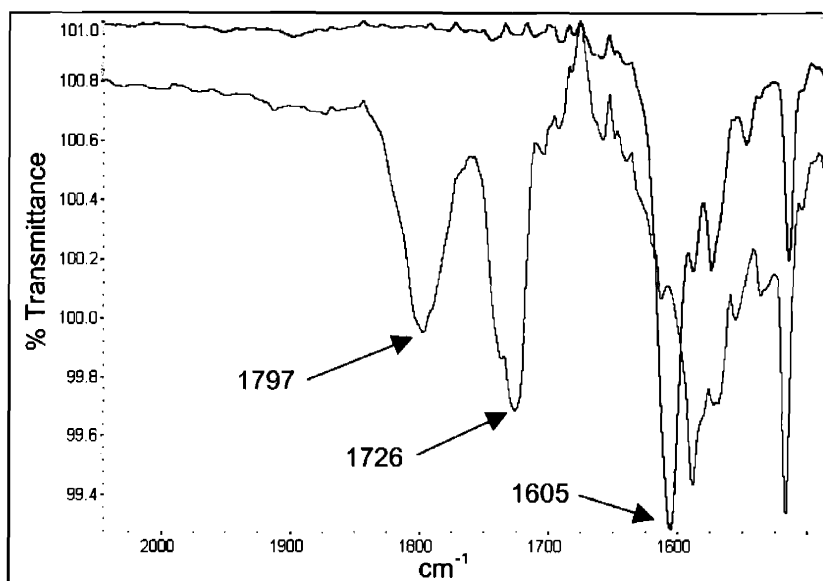
Figure 3.4. Solution IR traces of [Fe$_2$(μ-O$_2$CAr$^{\text{Tol}}$)$_4$(Ds-pip)$_2$] (**1**) in CH$_2$Cl$_2$ before (blue) and 90 min after (red) addition of 10 equiv of NO.

Figure 3.5. Solution IR traces of $[Co_2(\mu-O_2CAr^{Tol})_4(Ds-pip)_2]$ (2) in CH_2Cl_2 after exposure to excess NO over a period of 1 h.

Figure 3.6. ORTEP diagrams of (a) *N*-nitroso-dansyl-piperazine (4) and (b) [Co₂(NO)₂(μ-O₂CAr^Tol)₂] (5) showing 50% probability thermal ellipsoids. The *m*-tolyl terphenyl carboxylate ligands of 5 have been truncated and the solvent molecule has been omitted for clarity.
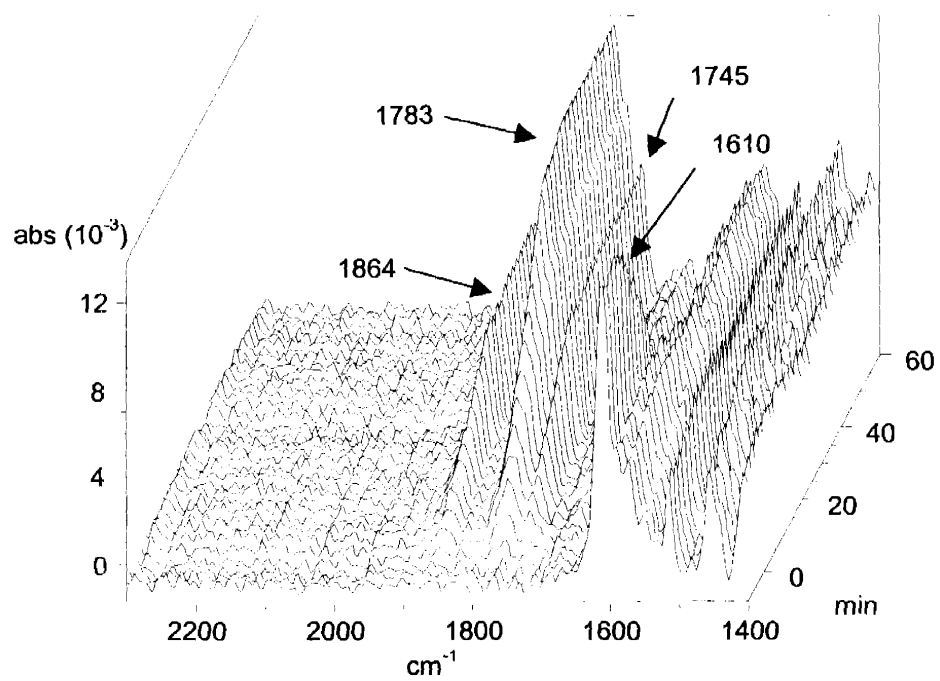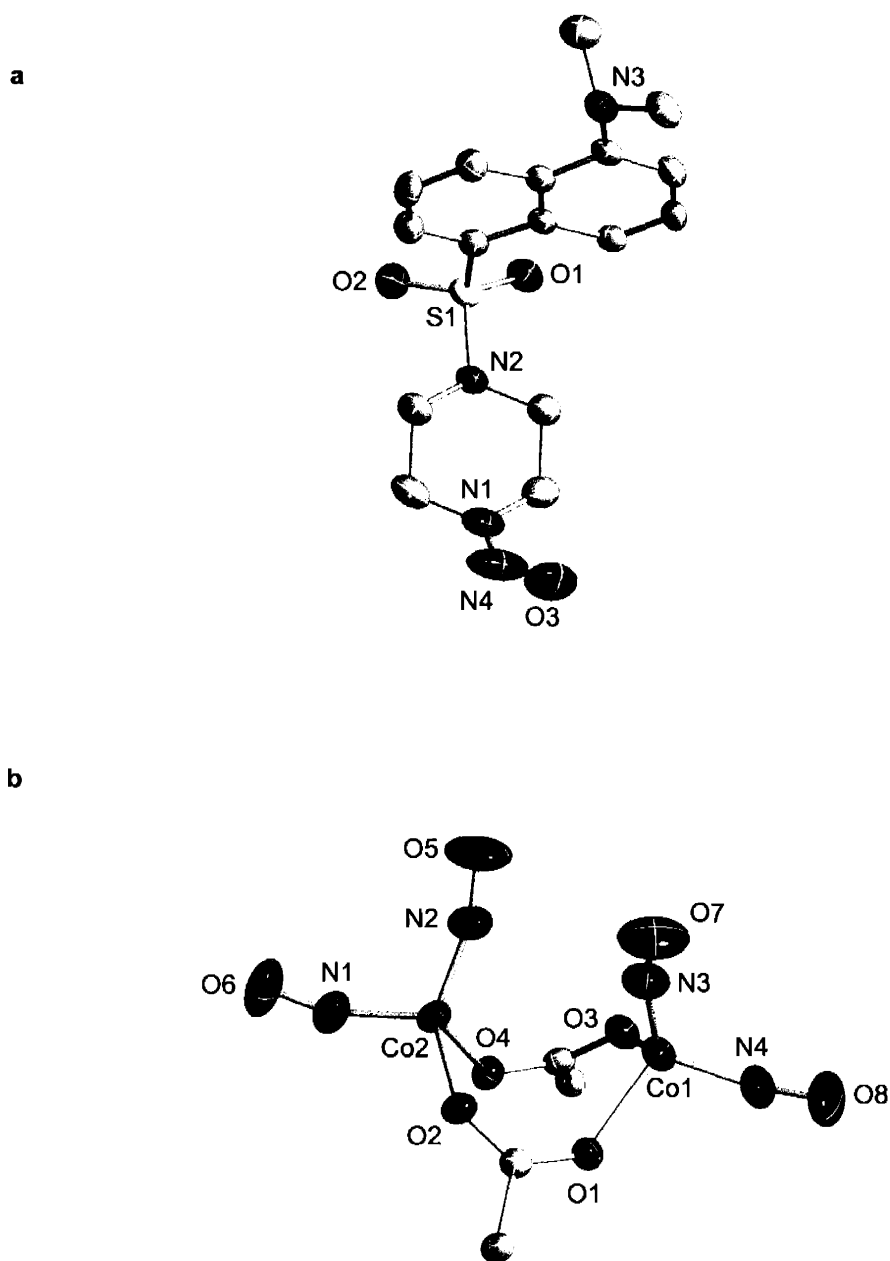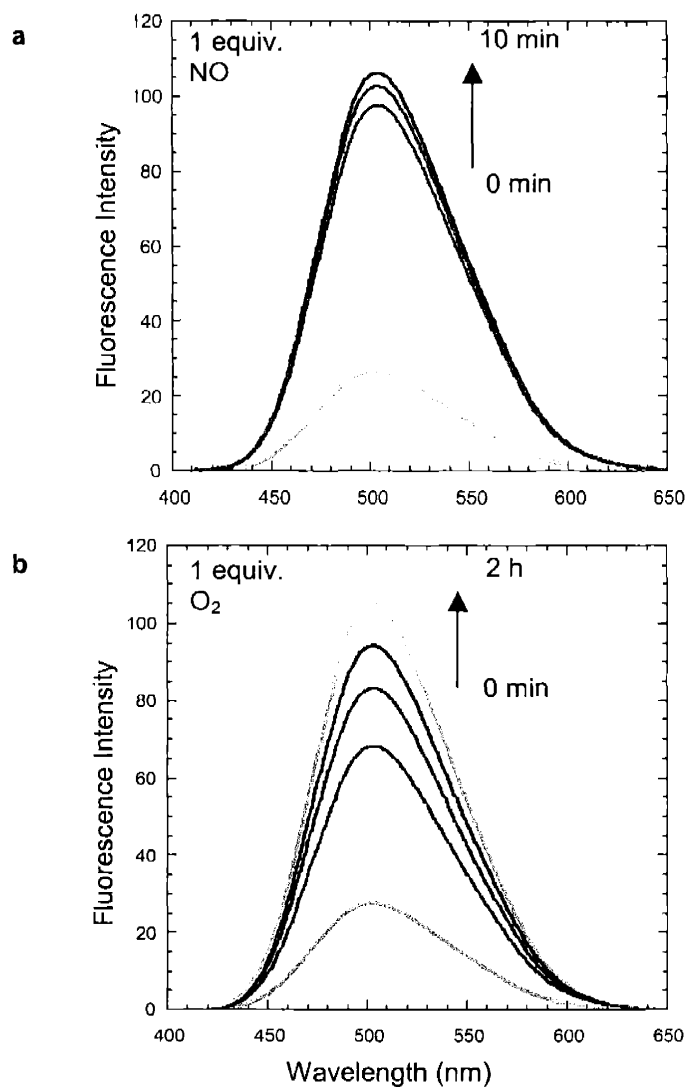
Figure 3.7. The fluorescence response of a 1 x 10^{-4} M solution of **1** (**a**) after addition of 1 equiv of NO and (**b**) after addition of 1 equiv of O_2. Excitation is at 356 nm.
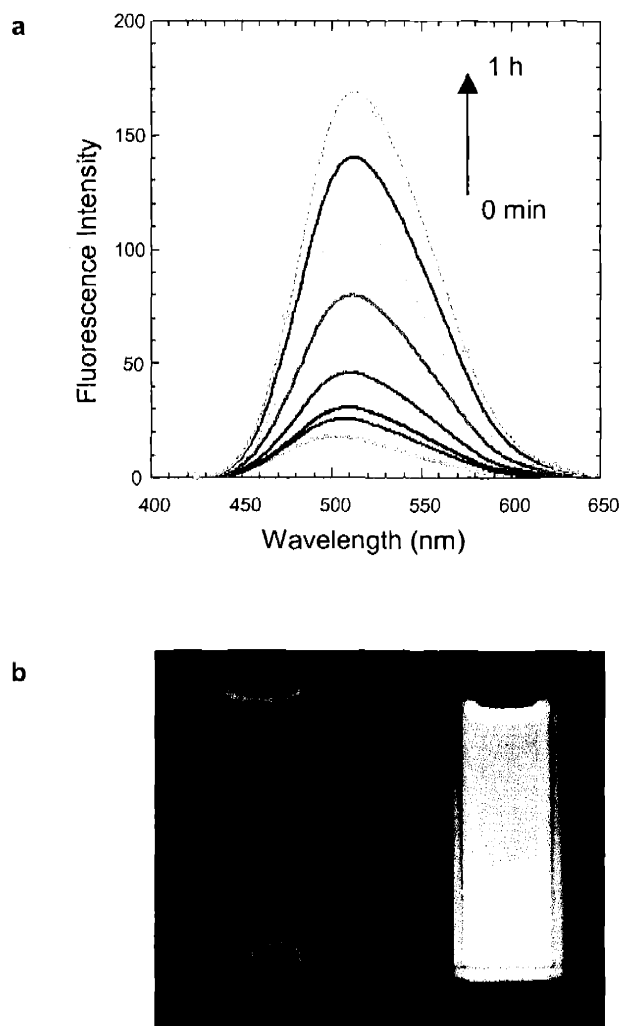
Figure 3.8. The fluorescence response of a 1 x 10^{-4} M solution of **2** after admission of excess NO. Trace **a** shows the time dependence of the fluorescence response with excitation at 350 nm. Picture **b** depicts the visual contrast between the starting complex, **2**, before (left) and after (right) addition of excess NO when illuminated with long-wavelength UV light from a hand held UV lamp.

Chapter 4

Dirhodium Tetracarboxylate Scaffolds as Reversible Fluorescence-

Based Nitric Oxide Sensors

Introduction

Nitric oxide (NO), a neutral inorganic molecule with one unpaired electron, has received considerable attention since its identification as a signaling agent in biological systems.[1] Recent research implicates involvement of NO in physiological processes such as vasodilation,[2] carcinogenesis,[3,4] neurodegenerative disorders,[5] and neurotransmission.[6] Current work focuses on the use of NO donor compounds and nitric oxide synthase inhibitors to elucidate additional biological functions.[7,8] A sensor capable of direct, reversible detection of NO would be invaluable to advance our understanding of its roles in biology.

NO detection methodologies include electrochemical,[9] EPR,[10] chemiluminescent,[11] and fluorescence-based techniques.[12-14] Of these options, those based on fluorescence signaling have the greatest potential for investigating how NO facilitates neurotransmission, an area of focus in our laboratory.[13] Current fluorescence-based NO sensors, however, are not ideal, requiring either dioxygen[15] or an external reductant[16] to form a fluorescent species. Fiber-optic NO biosensors containing a fluorescent dye-labeled heme domain of cytochrome c' or soluble guanylate cyclase (sGC) have been fabricated.[17-19] These fiber-optic detectors are based on attenuation of fluorescence emission intensity in response to NO, instead of the more desirable analyte induced increase in emission intensity. Recently we described an approach that utilizes transition-metal nitrosyl-forming reactions to monitor NO directly by ejection of a fluorescent ligand that had been quenched by coordination.[12] Related sensors using N-oxide-fluorophore conjugates have been described, but display a decrease in fluorescence after reaction with NO or react slowly with NO and are air-sensitive.[14] None of the current

small-molecule based NO sensors is reversible and thus none is capable of providing temporal data about fluctuating NO concentrations.

Our interest in developing sensors that utilize the formation of transition metal nitrosyl complexes to trigger an increase in fluorescence is based on a strategy that takes advantage of the well-known fluorescence-quenching properties of transition metals with partially filled d-shells.[12,20,21] In particular, we have been exploring systems in which reaction of NO with a transition metal complex containing a coordinated fluorophore results in removal of the fluorophore from the coordination sphere of the metal with concomitant fluorescence turn-on. In the present paper we describe the reversible fluorescence-based detection of NO with the use of dirhodium tetracarboxylate scaffolds containing bound fluorophore conjugates.

Dirhodium tetracarboxylates are air-stable compounds that coordinate a variety of ligands at the axial positions of the tetra-bridged dimetallic core.[22] The reaction of NO with solid $[Rh_2(\mu-O_2CMe)_4]$, first reported in 1963, affords a nitrosyl adduct that can be reversed upon heating to 120 °C, although the products were not fully characterized.[23] The only crystallographically defined dirhodium nitrosyl complex is $[Rh_2(\mu-O_2CMe)_4(NO)(NO_2)]$, which was prepared by the reaction of $[Rh_2(\mu-O_2CMe)_4]$ with excess NO in CH_2Cl_2.[24] We find that, if care is taken avoid the reaction of O_2 with NO to form NO_2, the complexes $[Rh_2(\mu-O_2CR)_4(NO)_2]$ (R = Me, Et, Pr) can be isolated in pure form. Here we provide a more complete description of the reactivity of dirhodium tetracarboxylate complexes with NO. We also report that NO can reversibly displace a bound fluorophore axial ligand in solution with concomitant light emission upon excitation at the proper wavelength. The observed reversible fluorescence response of

these dirhodium-fluorophore conjugates in response to NO may ultimately allow their use for imaging biological NO.

Experimental

General Considerations. All reagents, including [Rh$_2$(O$_2$CMe)$_4$] (**1**), were purchased from Aldrich or Alfa Aesar and used without further purification. Dansyl-piperazine (**4**) was prepared according to a literature procedure.[25] The rhodium complexes, [Rh$_2$(μ-O$_2$CEt)$_4$][26] (**2**) and [Rh$_2$(μ-O$_2$CPr)$_4$][27] (**3**), were prepared according to published procedures. Methylene chloride (CH$_2$Cl$_2$) was purified by passage through alumina columns under a N$_2$ atmosphere.[28] 1,2-Dichloroethane (DCE) was purified by distillation under an N$_2$ atmosphere over calcium hydride. Other solvents were used as received. Nitric oxide (Matheson 99%) was purified by a method adapted from the literature.[29] The NO stream was passed through an Ascarite (NaOH fused on silica gel) column and a 6 ft coil filled with silica gel cooled to −78 °C. For fluorescence experiments, NO was transferred to an anaerobic fluorescence cuvette with a gastight syringe. To eliminate the possibility of O$_2$ contamination, the syringe transfer was performed in an MBraun inert atmosphere glove box. Fluorescence emission intensity spectra were recorded at 25.0 ± 0.2 °C on a Hitachi F-3010 or Photon Technology International fluorescence spectrophotometer. NMR spectra were recorded on a Bruker DPX-400 spectrometer at ambient temperature and referenced to internal ^{1}H and ^{13}C solvent peaks.

Dansyl-imidazole (5). To a solution of dansyl chloride (500 mg, 1.85 mmol) in 5 mL of THF were added imidazole (126 mg, 1.85 mmol) and Cs$_2$CO$_3$ (1.3 g, 4.0 mmol). The reaction was allowed to stir overnight, filtered, and the solvent was removed by

rotary evaporation. Crystallization of the crude product from hot EtOAc and hexanes gave yellow-green needles of **5** (520 mg, 93%): mp 100-101 °C. ^{1}H NMR (400 MHz, CD$_2$Cl$_2$): δ 8.67 (1 H, d, J = 9.5 Hz), 8.38 (1 H, dd, J = 7.5, 1.2 Hz), 8.26 (1 H, d, J = 8.6 Hz), 8.10 (1 H, s), 7.63-7.59 (2 H, m), 7.32 (1 H, t, J = 1.4 Hz), 7.21 (1 H, d, J = 7.2 Hz), 7.01 (1 H, s), 2.86 (6 H, s). ^{13}C NMR (100 MHz, CD$_2$Cl$_2$): δ 153.0, 137.3, 133.8, 133.3, 131.3, 131.1, 130.4, 130.1, 129.9, 123.8, 118.4, 117.6, 116.3, 45.7.

[Rh$_2$(μ-O$_2$CMe)$_4$(Ds-im)$_2$] (6). To a solution of [Rh$_2$(μ-O$_2$CMe)$_4$] (50 mg, 0.11 mmol) in 5 mL of CH$_3$CN was added **5** (69 mg, 0.23 mmol). Over 30 min, a red-orange precipitate formed. X-ray quality crystals of [Rh$_2$(μ-O$_2$CMe)$_4$(Ds-im)$_2$] (79 mg, 69 %) were prepared by recrystallization of the crude solid by vapor diffusion (Et$_2$O/CHCl$_3$). ^{1}H NMR (400 MHz, CD$_2$Cl$_2$): δ 8.84 (2 H, t, J = 1.1 Hz), 8.74 (2 H, dd, J = 8.5, 0.9 Hz), 8.59 (2 H, dd, J = 7.5, 1.2 Hz), 8.48 (2 H, d, J = 8.7 Hz), 7.73 (4 H, d, J = 1.1 Hz), 7.70-7.66 (4 H, m), 7.25 (2 H, d, J = 7.4 Hz), 2.89 (12 H, s), 1.78 (12 H, s). ^{13}C NMR (100 MHz, CD$_2$Cl$_2$): δ 191.8, 153.3, 138.6, 134.3, 132.7, 131.9, 131.1, 130.7, 130.3, 130.1, 123.9, 119.3, 117.6, 116.5, 45.7, 23.9. IR (KBr, cm^{-1}): 3135 (w), 2940 (w), 2835 (w), 2791 (w), 1595 (s), 1457 (m sh), 1430 (s), 1410 (s sh), 1367 (s), 1343 (m), 1311 (w), 1233 (w), 1202 (w), 1174 (s), 1157 (s), 1101 (w), 1052 (s), 942 (w), 919 (w), 787 (m), 736 (w), 694 (m), 679 (m sh), 635 (s), 594 (s), 559 (m), 536 (w), 491 (w). Anal. Calcd. for C$_{38}$H$_{42}$N$_6$O$_{12}$S$_2$Rh$_2$: C, 43.69; H, 4.05; N, 8.04. Found: C, 43.58; H, 3.85; N, 8.01.

[Rh$_2$(μ-O$_2$CMe)$_4$(Ds-pip)$_2$]·CHCl$_3$ (7·CHCl$_3$). To a solution of [Rh$_2$(μ-O$_2$CMe)$_4$] (50 mg, 0.11 mmol) in 3 mL of CH$_3$CN was added **4** (70 mg, 0.22 mmol) in 1 mL of CH$_3$CN. The dark burgundy solution was allowed to stir for 4 h and the solvent was removed by rotary evaporation. Burgundy crystals of 7·CHCl$_3$ (102 mg, 77%) were

grown by vapor diffusion (Et$_2$O/CHCl$_3$). Solvent free X-ray quality crystals were prepared by vapor diffusion (pentane/toluene). ^{1}H NMR (400 MHz, CD$_2$Cl$_2$): δ 8.56 (2 H, d, J = 8.5 Hz), 8.45 (2 H, d, J = 8.7 Hz), 8.22 (2 H, dd, J = 7.3, 1.2 Hz), 7.58-7.52 (4 H, m), 7.19 (2 H, d, J = 8.2 Hz), 3.57 (16 H, bs), 2.86 (12 H, s), 1.52 (12 H, s). ^{13}C NMR (100 MHz, CD$_2$Cl$_2$): δ 190.8, 152.3, 134.0, 131.1, 131.0, 130.9, 130.6, 128.4, 123.7, 120.2, 115.7, 47.8, 45.9, 45.7, 23.6. IR (KBr, cm^{-1}): 3294 (w), 3025 (w), 2982 (w), 2924 (w br), 2865 (w br), 1662 (m), 1593 (s), 1490 (w), 1446 (m), 1406 (m), 1358 (m), 1346 (m), 1307 (s), 1246 (m), 1204 (m), 1185 (m), 1158 (m sh), 1127 (s), 1096 (w), 1080 (w), 1050 (w), 965 (w), 941 (s), 883 (w), 801 (w), 776 (m), 752 (s), 696 (s), 666 (w), 651 (w), 621 (w), 564 (w), 541 (w), 532 (w), 498 (w), 478 (w), 444 (w). Anal. Calcd. for C$_{41}$H$_{55}$Cl$_3$N$_6$O$_{12}$S$_2$Rh$_2$: C, 41.03; H, 4.62; N, 7.00. Found: C, 41.14; H, 4.32; N, 6.62.

[Rh$_2$(μ-O$_2$CMe)$_4$(NO)$_2$] (8). To a septum-capped vial containing a slurry of [Rh$_2$(μ-O$_2$CMe)$_4$] (50 mg, 0.11 mmol) in 2 mL of chlorobenzene under an N$_2$ atmosphere was added NO (8.2 mL, 0.34 mmol) by means of a gastight syringe. Upon addition of the NO, the solution turned dark burgundy and the solid [Rh$_2$(μ-O$_2$CMe)$_4$] slowly dissolved. After stirring for 2 h, the burgundy solution was filtered quickly through celite and recrystallized by vapor diffusion (chlorobenzene/pentane) under a N$_2$ atmosphere containing 2 equiv of NO. After 1 week, dark burgundy blocks of **8** (28.2 mg, 49%) suitable for X-ray analysis were harvested. IR (KBr, cm^{-1}): 3418 (w), 1729 (s sh), 1694 (s), 1580 (m), 1427 (m br), 1348 (w), 1047 (w), 696 (m), 628 (w). Anal. Calcd. for C$_8$H$_{12}$N$_2$O$_{10}$Rh$_2$: C, 19.14; H, 2.41; N, 5.58. Found: C, 19.02; H, 2.23; N, 5.71.

[Rh$_2$(μ-O$_2$CEt)$_4$(NO)$_2$] (9). To a septum-capped vial containing a suspension of [Rh$_2$(μ-O$_2$CEt)$_4$] (50 mg, 0.10 mmol) in 10 mL of pentane under an N$_2$ atmosphere, was

added NO (8.0 mL, 0.30 mmol) by means of a gastight syringe. On stirring, the solid green [Rh₂(μ-O₂CEt)₄] complex slowly dissolved as the solution turned dark burgundy. After stirring overnight, the burgundy solution was filtered through celite, concentrated to a volume of 5 mL in vacuo, and placed in a sealed vial under a N_2 atmosphere containing 2 equiv of NO. X-ray quality burgundy blocks of **9** (42 mg, 75%) were prepared by crystallization from the pentane solution at -40° C. IR (KBr, cm⁻¹): 3393 (w), 2984 (w), 2943 (w), 2881 (w), 1698 (s br), 1672 (s), 1581 (s), 1464 (m), 1418 (m), 1375 (m), 1300 (m), 1076 (w), 1012 (w), 886 (w), 810 (w), 705 (w), 650 (w). Anal. Calcd. for $C_{12}H_{20}N_2O_{10}Rh_2$: C, 25.83; H, 3.61; N, 5.02. Found: C, 26.02; H, 3.63; N, 5.04.

[Rh₂(μ-O₂CPr)₄(NO)₂] (10). To a septum-capped vial containing a suspension of [Rh₂(μ-O₂CPr)₄] (50 mg, 0.09 mmol) in 3 mL of pentane under an N_2 atmosphere, NO (5.4 mL, 0.23 mmol) was added using a gastight syringe. On stirring, the green solid slowly dissolved as the solution turned dark burgundy. After stirring overnight, the burgundy solution was filtered through celite, concentrated to a volume of 1.5 mL in vacuo, and placed in a sealed vial under a N_2 atmosphere containing 2 equiv of NO. X-ray quality burgundy blocks of **10** (33.6 mg, 61%) were prepared by crystallization from the pentane solution at -40° C. IR (KBr, cm⁻¹): 3405 (w), 2961 (w), 2930 (w), 2874 (w), 1687 (s), 1579 (s), 1412 (m), 1348 (w), 1314 (w), 1266 (w), 1101 (w), 799 (w), 735 (w), 667 (w). Anal. Calcd. for $C_{16}H_{28}N_2O_{10}Rh_2$: C, 31.29; H, 4.59; N, 4.56. Found: C, 31.45; H, 4.57; N, 4.48.

Aqueous Solution Fluorescence Experiments. The experimental apparatus consisted of a 20 mL vessel containing a smaller 2 mL vial. The internal small vial was filled with a CH_2Cl_2 solution of [Rh₂(μ-O₂CMe)₄] (40 μM) and Ds-pip (20 μM). This vial

was sealed with a screw cap fitted with 2-3 mm thick septum made from Silastic® Q7-4656 biomedical grade ETR elastomer, an NO permeable polymer, which was purchased from Dow-Corning. The external 20 mL vessel containing the 1.5 mL vial was capped and placed under an N_2 atmosphere, after which a saturated aqueous NO solution (15 mL) was transferred into it by a gastight syringe. An aqueous solution saturated with NO was prepared by bubbling a stream of NO gas into deionized water for 30 min at 25 °C. All procedures were performed under an anaerobic atmosphere. The fluorescence response was monitored by digital photography of the experimental apparatus with long-wavelength UV illumination from a hand-held UV lamp model UVGL-25 purchased from VWR International.

X-ray Crystallography. Single crystals suitable for data collection were covered in Infineum V8512 oil (formerly called Paratone N oil), mounted on the tips of quartz capillary tubes and transferred to the -100 °C N_2 stream of a Bruker KRYOFLEX BVT-AXS nitrogen cryostat. Data were collected on Bruker APEX CCD X-ray diffractometer (MoK$_\alpha$ λ = 0.71073 Å) controlled by the SMART software package running on a Pentium III PC.[30] The general procedures used for data collection are reported elsewhere.[31] Empirical absorption corrections were calculated with the SADABS program.[32] Structures were solved and refined with the SHELXTL and SAINTPLUS software packages on a Pentium III PC running the Windows NT operating system.[33,34] All non-hydrogen atoms were refined anisotropically by least-squares cycles and Fourier syntheses. Hydrogen atoms were assigned idealized positions and given thermal parameters of 1.2 times the thermal parameter of the carbon or nitrogen atom to which

each was attached. All structure solutions were checked for higher symmetry with the PLATON program.[35]

Results and Discussion

Synthesis of Fluorophore-Derivatized and Nitrosyl Dirhodium Complexes. Dirhodium tetraacetate complexes of dansyl imidazole or dansyl piperazine[25] were prepared by reaction of **1** with 2 equiv of the fluorophore in acetonitrile in 69 or 77% yield after crystallization, respectively (Scheme 4.1). Synthesis of the dinitrosyl complexes **8, 9,** and **10** was accomplished by exposure of the appropriate dirhodium tetracarboxylate to 2.5 or 3 equiv of NO in chlorobenzene for **8** or in pentane for **9** and **10** (Scheme 4.2). Inadvertent leakage of dioxygen into the reaction vessels containing excess NO altered the characteristic burgundy color indicative of the dinitrosyl complexes to brown, indicating formation of $[Rh_2(\mu\text{-}O_2CR)_4(NO)(NO_2)]$.[24] Crystallization of the dinitrosyl complexes required the presence of excess NO gas in the crystallization chambers to prevent NO loss and recovery of only free dirhodium tetracarboxylate. Complex **8** was isolated in 49% yield by allowing pentane vapor to diffuse into a burgundy-colored chlorobenzene solution of the crude product. Dinitrosyl complexes **9** and **10** were isolated in up to 75% yields by crystallization from saturated pentane solutions cooled to -40° C. In contrast to the synthesis of nitrosyl complexes **8, 9,** and **10,** it was not possible to prepare the analogous dinitrosyl complex of $[Rh_2(\mu\text{-}O_2CCF_3)_4]$. Attempts to isolate 1:1 complexes of $[Rh_2(\mu\text{-}O_2CR)_4]$ with the dansyl-containing ligands or NO were unsuccessful. This result is consistent with literature data. Of the approximately 200 dirhodium tetracarboxylate structures in the Cambridge Structural

Database,[36] only three complexes are reported that contain a monodentate ligand bound in a 1:1 stoichiometry.

Structural Studies. The molecular structures of **6** and **7** are shown in Figure 4.1. Single crystal X-ray diffraction results are given in Table 4.1 and selected bond distances and angles are presented in Table 4.2. The X-ray studies revealed fluorophore coordination at the axial sites of the dirhodium cores in **6** and **7** through the imidazole and piperazine N-atoms, respectively. The Rh-ligand and Rh-Rh distances in both structures are unremarkable and consistent with those of similar complexes reported in the literature (Table 2).[37]

Complexes **8**, **9**, and **10** are the first structurally characterized dinitrosyl adducts of any dirhodium tetracarboxylate and are depicted in Figures 4.2 and 4.3. A summary of the X-ray diffraction results is presented in Table 4.3 and selected bond lengths and angles are given in Table 4.4. Structurally, all three dinitrosyl species are very similar. The observed Rh–axial ligand distances of 1.945(3) – 1.958(3) Å are some of the shortest known for dirhodium tetracarboxylate complexes.[37] The only complex having a shorter Rh–axial ligand bond length is the related [Rh$_2$(μ-O$_2$CMe)$_4$(NO)(NO$_2$)] compound, in which the Rh-NO bond is 1.927(4) Å.[24] The Rh–Rh bond distances for the three dinitrosyl complexes are also quite remarkable. These distances 2.512(1) and 2.5191(9) Å for **9** and **10**, are the longest yet observed for dirhodium tetracarboxylate complexes having N-donor axial ligands. The lengthening of the Rh–Rh bond is consistent with a previous analysis of metal-metal bonding in dirhodium tetracarboxylate complexes, which is discussed in detail elsewhere.[38] Again, the only similar reported Rh–Rh distance is the 2.4537(4) Å value in [Rh$_2$(μ-O$_2$CMe)$_4$(NO)(NO$_2$)].[24] The N–O bond lengths in **8**, **9**, and
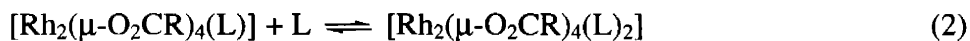
10, which are between 1.131(4) and 1.150(3) Å, are also quite similar. Although still small, the largest geometric variation among the complexes occurs in the Rh–N–O bond angles. One of the two crystallographically independent molecules of 10 has an angle of 122.7(3)°, which is 1.9° larger than the corresponding value from 9. As with [Rh$_2$(μ-O$_2$CMe)$_4$(NO)(NO$_2$)], the bent nitrosyl ligands in 8, 9, and 10 are positioned in between the two planes defined by the bridging carboxylate ligands to minimize the intramolecular non-bonding contacts with their oxygen atoms.

There is no discernable trend in any of the relevant geometric parameters when comparing the three dinitrosyl complexes. This result is not surprising considering the similarity of the carboxylate ligands. The observed variations in bond lengths and angles are more likely a result of crystal packing effects than any electronic differences between the complexes. This conclusion is supported by the observed differences in bond angles and distances between the two crystallographically unique molecules of 10, which are of similar magnitude to the corresponding variations between the three complexes.

The dinitrosyl complexes can be viewed as two separate octahedral {MNO}^{8} units in the standard notation, where the superscript represents the sum of metal d electrons and unpaired π^* electron from the nitrosyl.[39] The nearly idealized bent geometries of the nitrosyl ligands in the three complexes, the average Rh–N–O angle being 121.4°, are consistent with the expected structure of an octahedral {MNO}^{8} complex, which results from population of the antibonding molecular orbital formed by the metal d_{xy} and d_{yz} orbitals and the NO π^* orbital. The related [Ru$_2$(μ-O$_2$CEt)$_4$(NO)$_2$] complex, which can be viewed as two adjacent {MNO}^{7} centers, overall has two fewer d electrons than the dirhodium dinitrosyls, and an Ru–N–O angle of 152.4° that is intermediate between the

idealized bent and linear geometries.[40] If an analogous group 7 transition metal tetracarboxylate complex were to exist, it would consist of two $\{MNO\}^6$ metal centers. As with other $\{MNO\}^6$ complexes, one would predict it to have linear nitrosyl ligands owing to the lack of electrons to populate the antibonding molecular orbital formed by the metal d_{xy} and d_{yz} orbitals and the NO π^* orbital.

Chemical Reactivity Studies. The interactions of the dirhodium complexes **1**, **2**, and **3** with the dansyl-containing ligands **4** and **5** are similar to those observed for other ligands that coordinate to the axial sites of the dirhodium tetraacetate core.[22] In solution, both 1:1 and 1:2 adducts with these bases are apparent, as revealed by absorption spectral titrations that exhibit clear isosbestic points for the equilibria given by eqs 1 and 2 respectively (Figure 4.4).

$$[Rh_2(\mu\text{-}O_2CR)_4] + L \rightleftharpoons [Rh_2(\mu\text{-}O_2CR)_4(L)] \tag{1}$$

$$[Rh_2(\mu\text{-}O_2CR)_4(L)] + L \rightleftharpoons [Rh_2(\mu\text{-}O_2CR)_4(L)_2] \tag{2}$$

The reactions of **1**, **2**, and **3** with NO are extremely fast. Preliminary stopped-flow studies of the reaction of **3** with excess NO shows complete formation of the dinitrosyl species within the 2-ms mixing time of the instrument at -80° C. This result corresponds to an approximate on-rate of at least 4×10^6 s^{-1} at 40° C. This indicates potential of the dirhodium tetracarboxylate scaffold for real-time imaging of NO changes in biological fluids.

By analogy to previously characterized systems, NO should sequentially form mono- and dinitrosyl complexes with dirhodium tetracarboxylates. We were unable, however, to distinguish the mono- and dinitrosyl adducts by IR spectroscopy in solution. Titration experiments revealed the formation of a single nitrosyl band at 1698 cm^{-1} for the

reaction of **3** with NO in DCE at room temperature (Figure 4.5). As with the fluorophore

adducts of **1**, it was not possible to isolate and characterize structurally the 1:1 complexes

of NO with **1**, **2**, and **3**.

Unlike **1**, **2**, and **3**, which form isolable dinitrosyl complexes, it was not possible

to detect the formation of any nitrosyl adducts of $[Rh_2(\mu-O_2CCF_3)_4]$. Exposure of even

sub-stoichoimetric amounts of NO to solutions of $[Rh_2(\mu-O_2CCF_3)_4]$ in halogenated

solvents resulted in precipitation of a yellow-brown solid, indicating decomposition of

the dirhodium core. This result is consistent with previous reactivity studies of $[Rh_2(\mu-O_2CCF_3)_4]$. Addition of piperidine or *N*-methylimidazole to $[Rh_2(\mu-O_2CCF_3)_4]$ in toluene

gave an initial red color, consistent with nitrogen coordination to Rh.[41] After a few hours,

however, the solutions turned yellow and ultimately yielded an intractable yellow tar

indicating dimer cleavage.[26,41] The decomposition is facilitated by the electron-

withdrawing properties of the trifluoroacetate ligands, which enhance the Lewis acidity

of the metal dimer and facilitate displacement of a carboxylate oxygen atom by base,

leading to decomposition.[41]

All three dinitrosyl complexes display similar v_{NO} bands in the solid state. IR

spectra of single crystals of **8** and **9** each show one broad and one sharp v_{NO} band,

respectively, at 1729 and 1694 cm^{-1} for **8** and 1698 and 1672 cm^{-1} for **9**. In solution the

1729 and 1694 cm^{-1} bands from **8** convert to a single nitrosyl band at 1702 cm^{-1}. Similar

behavior was previously observed with $[Ru_2(\mu-O_2CEt)_4(NO)_2]$. In the case of **10**, only a

single broad v_{NO} band at 1687 cm^{-1} is observed in the solid state, which shifts to 1698 cm^{-1} in DCE solution. Figure 4.6 shows an overlay of the solid IR spectra of **1** and **8**, the only

significant difference between the two being the presence of the nitrosyl stretching bands

in **8**. The absence of a large shift in the carboxylate C–O stretching band upon formation of the dinitrosyl adduct indicates that the dirhodium core remains intact and undergoes very little change.

Like the parent dirhodium complexes, **8**, **9**, and **10** are air-stable and their spectroscopic properties revealed no evidence for decomposition of the dirhodium core. Although the core is stable, in solution the dinitrosyl complexes lose NO and reform the corresponding parent complex. At room temperature, solids **8**, **9**, and **10** also slowly lose NO over a period of several days, but the adducts are stable for several months when stored at -80° C. The observed reversible binding of NO with these dirhodium compounds opens the possibility for their application as reversible NO sensors in biological systems.

Fluorescence Spectroscopic Studies. Solutions of **6** and **7** in DCE emit only weakly when excited at 365 nm for Ds-im or at 345 nm for Ds-pip. Neither complex is fluorescent in the solid state. Titrations with [Rh$_2$(μ-O$_2$CMe)$_4$] indicate maximal fluorescence quenching upon addition of four and two equivalents of [Rh$_2$(μ-O$_2$CMe)$_4$] with Ds-im and Ds-pip, respectively. Based on the previous absorption spectroscopy titrations, vida supra, these ligand to [Rh$_2$(μ-O$_2$CMe)$_4$] ratios correspond to formation of the 1:1 adducts.

Exposure of a solution of 10 μM Ds-im and 40 μM [Rh$_2$(μ-O$_2$CMe)$_4$] in DCE to 100 equiv of NO results in an immediate 16-fold increase in the integrated fluorescence intensity. A similar 26-fold increase in integrated fluorescence intensity is observed after introduction of 100 equiv of NO to a DCE solution containing 10 μM Ds-pip and 20 μM [Rh$_2$(μ-O$_2$CMe)$_4$]. In both systems, the fluorescence response is reversible. A 30 min Ar

purge to remove the excess NO restores the fluorescence and this cycle can be repeated at least three times (Figure 4.7).

The reaction of 1 equiv of NO with the [Rh$_2$(μ-O$_2$CMe)$_4$(Ds-im)] complex gives a 27% increase in integrated fluorescence (Figure 4.8). Thus, only one equivalent of the neurotransmitter is necessary to displace the coordinated fluorophore (Scheme 4.3), although we do not know at present whether this reaction occurs by an associative or dissociative mechanism.

To determine the sensitivity of the Ds-im complex for nitric oxide, sequentially decreasing volumes of NO gas were added to aliquots of 2 μM Ds-im and 4 μM [Rh$_2$(μ-O$_2$CMe)$_4$] in DCE. From this experiment we estimate a detection limit of 4-8 μM NO. Greater sensitivity should be possible in the absence of excess, non-fluorophore-bound [Rh$_2$(μ-O$_2$CMe)$_4$].

Although dirhodium tetraacetate is water-soluble and air-stable, the current fluorophore adducts do not function as NO sensors in an aqueous environment. Water effectively competes with the fluorophore for coordination to the dirhodium core. One strategy to achieve aqueous solution compatibility is to isolate the sensor solution behind a NO-permeable membrane that is impervious to water. A Silastic® polymer based membrane was chosen to test this possibility. Silastic® tubing has demonstrable NO permeability and has previously been used for admission of NO to aqueous solutions.[42] The fluorescence response of a 40 μM [Rh$_2$(μ-O$_2$CMe)$_4$] and 20 μM Ds-pip solution, sequestered from a saturated aqueous NO solution by the Silastic® membrane and the experimental set-up are shown in Figure 4.9. The emission of fluorescence was observed immediately after admission of the NO containing aqueous solution into the outer vial.

Titration experiments with sequentially decreasing amounts of NO demonstrated a fluorescence response visible by the naked eye at NO concentrations as low as 100 μM. This experiment illustrates one potential approach for developing sensors capable of imaging biological NO based on the dirhodium tetracarboxylate platform.

Conclusions

Dirhodium tetracarboxylate complexes containing bound fluorophores react directly, rapidly, and reversibly with NO. The resulting completely characterized dinitrosyl adducts lose NO upon standing in air. The reactivity of the fluorophore conjugated dirhodium complexes with NO is fast with on-rates indicating nearly instantaneous binding of the gas at 40° C. These properties indicate them to be suitable for biological imaging of NO. Fluorescence detection methodologies based on the dirhodium platform hold promise for development into viable sensors for NO in biological systems. One potential route for preparation of NO sensors based on this system is to sequester the nonpolar dirhodium fluorophore solution from the surrounding aqueous environment by use of an NO-permeable polymer. Initial experiments demonstrate the potential utility of this strategy for detection of aqueous NO.

References

(1) Furchgott, R. F. *Angew. Chem. Int. Ed.* **1999**, *38*, 1870.

(2) Ignarro, L. J. *Angew. Chem. Int. Ed.* **1999**, *38*, 1882.

(3) Lala, P. K. *Cancer and Metastasis Reviews* **1998**, *17*, 1.

(4) Wink, D. A.; Vodovotz, Y.; Laval, J.; Laval, F.; Dewhirst, M. W.; Mitchell, J. B. *Carcinogenesis* **1998**, *19*, 711.

(5) Calabrese, V.; Bates, T. E.; Stella, A. M. G. *Neurochem. Res.* **2000**, *25*, 1315.

(6) Prast, H.; Philippu, A. *Prog. Neurobiol.* **2001**, *64*, 51.

(7) Hölscher, C. *Eur. J. Pharmacol.* **2002**, *457*, 99.

(8) Grassi, S.; Pettorossi, V. E. *Neurosci.* **2000**, *101*, 157.

(9) Bedioui, F.; Villeneuve, N. *Electroanalysis* **2003**, *15*, 5.

(10) Fujii, S.; Yoshimura, T. *Coord. Chem. Rev.* **2000**, *198*, 89.

(11) Brien, J. F.; McLaughlin, B. E.; Nakatsu, K.; Marks, G. S. *Methods Enzymol.* **1996**, *268*, 83.

(12) Franz, K. J.; Singh, N.; Lippard, S. J. *Angew. Chem., Int. Ed. Engl.* **2000**, *39*, 2120.

(13) Burdette, S. C.; Lippard, S. J. *Coord. Chem. Rev.* **2001**, *216*, 333.

(14) Katayama, Y.; Soh, N.; Maeda, M. *Bull. Chem. Soc. Jpn.* **2002**, *75*, 1681.

(15) Kojima, H.; Nakatsubo, N.; Kikuchi, K.; Kawahara, S.; Kirno, Y.; Nagoshi, H.; Hirata, Y.; Nagano, T. *Anal. Chem.* **1998**, *70*, 2446.

(16) Meineke, P.; Rauen, U.; Groot, H. d.; Korth, H.-G.; Sustmann, R. *Chem. Eur. J.* **1999**, *5*, 1738.

(17) Barker, S. L. R.; Zhao, Y.; Marletta, M. A.; Kopelman, R. *Anal. Chem.* **1999**, *71*, 2071.

(18) Barker, S. L. R.; Kopelman, R.; Meyer, T. E.; Cusanovich, M. A. *Anal. Chem.* **1998**, *70*, 971.

(19) Barker, S. L. R.; Clark, H. A.; Swallen, S. F.; Kopelman, R.; Tsang, A. W.; Swanson, J. A. *Anal. Chem.* **1999**, *71*, 1767.

(20) Varnes, A. W.; Dodson, R. B.; Wehry, E. L. *J. Am. Chem. Soc.* **1972**, *94*, 946.

(21) Franz, K. J.; Singh, N.; Spingler, B.; Lippard, S. J. *Inorg. Chem.* **2000**, *39*, 4081.

(22) Boyar, E. B.; Robinson, S. D. *Coord. Chem. Rev.* **1983**, *50*, 109.

(23) Johnson, S. A.; Hunt, H. R.; Neumann, H. M. *Inorg. Chem.* **1963**, *2*, 960.

(24) Koh, Y.-B. Metal-Metal Bonding in Dirhodium Tetracarboxylates Trans Influence and Dependence of the Rhodium-Rhodium Bond Distance Upon the Nature of Axial Ligands. Ph.D. Thesis, Columbus, OH, 1979. The Ohio State University: Columbus, 1979.

(25) Saavedra, J. E.; Booth, M. N.; Hrabie, J. A.; Davies, K. M.; Keefer, L. K. *J. Org. Chem.* **1999**, *64*, 5124.

(26) Kitchens, J.; Bear, J. L. *Thermochim. Acta* **1970**, *1*, 537.

(27) Drago, R. S.; Long, J. R.; Cosmano, R. *Inorg. Chem* **1981**, *20*, 2920.

(28) Pangborn, A. B.; Giardello, M. A.; Grubbs, R. H.; Rosen, R. K.; Timmers, F. J. *Organometallics* **1996**, *15*, 1518.

(29) Lorkovic, I. M.; Ford, P. C. *Inorg. Chem* **2000**, *39*, 632.

(30) *SMART: Software for the CCD Detector System*, version 5.626; Bruker AXS: Madison, WI, 2000.

(31) Kuzelka, J.; Mukhopadhyay, S.; Spingler, B.; Lippard, S. J. *Inorg. Chem* **2004**, *43*, in press.

(32) Sheldrick, G. M. *SADABS: Aera-Detector Absorption Correction*; University of Göttingen, Göttingen Germany, 2001.

(33) *SHELXTL: Program Library for Structure Solution and Molecular Graphics*, version 6.2; Bruker AXS: Madison, WI, 2001.

(34) *SAINTPLUS: Software for the CCD Detector System*, version 5.01; Bruker AXS: Madison, WI, 1998.

(35) Spek, A. L. *PLATON, A Multipurpose Crystallographic Tool*; Utrecht University: Utrecht, The Netherlands, 2000.

(36) Allen, F. H. *Acta Crystallogr., Sect. B* **2002**, *B58*, 380.

(37) Cotton, F. A.; Walton, R. A.; Dirhodium Compounds, *Multiple Bonds Between Metal Atoms*, 2nd ed.; Oxford University Press: Oxford, England, 1993.

(38) Christoph, G. G.; Koh, Y.-B. *J. Am. Chem. Soc.* **1979**, *101*, 1422.

(39) Enemark, J. H.; Feltham, R. D. *Coord. Chem. Rev.* **1974**, *13*, 339.

(40) Lindsay, A. J.; Wilkinson, G.; Motevalli, M.; Hursthouse, M. B. *J. Chem. Soc., Dalton Trans.* **1987**, 2723.

(41) Tesler, J.; Drago, R. S. *Inorg. Chem* **1984**, *23*, 2599.

(42) Wang, C.; Deen, W. M. *Ann. Biomed. Eng.* **2003**, *31*, 65.

Table 4.1. Summary of X-ray Crystallographic Data of **6** and **7**.

	6·2CHCl₃	7
formula	$C_{40}H_{44}N_6O_{12}S_2Rh_2$	$C_{40}H_{54}N_6O_{12}S_2Rh_2$
fw	1283.45	1080.83
space group	$P\bar{1}$	$P2_1/c$
a,Å	8.577(2)	11.387(2)
b Å	9.062(2)	16.431(3)
c Å	16.026(4)	12.395(2)
α, deg	94.218(5)	
β, deg	96.824(4)	101.224(3)
γ, deg	96.319(4)	
V, Å³	1219.8(5)	2274.6(7)
Z	1	2
ρ_{calc}, g/cm³	1.747	1.578
T, °C	-100	-100
μ(Mo Kα), mm⁻¹	1.157	0.883
total no. of data	10965	19856
no. of unique data	5553	5387
no. of params	311	288
R (%)[a]	4.56	7.99
wR² (%)[b]	10.045	9.67

[a] $R = \Sigma||F_o|-|F_c||/\Sigma|F_o|$, [b] $wR^2 = \{w(F_o^2-F_c^2)^2/\Sigma[w(F_o^2)^2]\}^{1/2}$

Table 4.2. Selected bond distances and angles for **6** and **7**.[a]

Compound	Distances	(Å)	Angles	(deg)
[Rh$_2$(O$_2$CMe)$_4$(Ds-im)$_2$]	Rh1-O1	2.040(3)	O1-Rh1-Rh1A	87.67(8)
(**6**)	Rh1-O2	2.032(3)	O2-Rh1-Rh1A	88.57(8)
	Rh1-O3	2.043(3)	O3-Rh1-Rh1A	87.48(8)
	Rh1-O4	2.038(3)	O4-Rh1-Rh1A	88.60(8)
	Rh1-N1	2.237(3)	O1-Rh1-N1	93.2(1)
	Rh1-Rh1A	2.3907(7)	O3-Rh1-N1	90.6(1)
			O3-Rh1-N1	91.8(1)
			O4-Rh1-N1	92.2(1)
[Rh$_2$(O$_2$CMe)$_4$(Ds-pip)$_2$]	Rh1-O1	2.036(5)	O1-Rh1-Rh1A	88.8(1)
(**7**)	Rh1-O2	2.013(5)	O2-Rh1-Rh1A	86.9(1)
	Rh1-O3	2.032(4)	O3-Rh1-Rh1A	89.1(1)
	Rh1-O4	2.024(4)	O4-Rh1-Rh1A	86.9(1)
	Rh1-N1	2.272(6)	O1-Rh1-N1	92.8(2)
	Rh1-Rh1A	2.398(1)	O3-Rh1-N1	91.4(2)
			O3-Rh1-N1	87.2(2)
			O4-Rh1-N1	96.8(2)
Literature values[b]	Rh-N	2.19-2.41		
	Rh-Rh	2.39-2.45		

[a]Numbers in parentheses are estimated standard deviations of the last significant figure. Atoms are labeled as indicated in Figure 1.

[b]Range of Rh-L and Rh-Rh distances for dirhodium tetracarboxylate complexes with axial nitrogen donor ligands reported in ref 37.

Table 4.3. Summary of X-ray Crystallographic Data for **8**, **9**, and **10**.

	8	**9**	**10**
formula	$C_8H_{12}N_2O_{10}Rh_2$	$C_{12}H_{20}N_2O_{10}Rh_2$	$C_{16}H_{28}N_2O_{10}Rh_2$
fw	502.02	558.12	614.22
space group	$P2_1/n$	$P2_1/c$	P-1
a, Å	8.142(2)	8.156(3)	8.440(3)
b Å	11.575(3)	13.112(5)	10.463(3)
c Å	9.278(2)	9.576(4)	14.299(4)
α, deg			105.43(1)
β, deg	123.87(2)	112.160(6)	106.84(2)
γ, deg			96.00(2)
V, Å^3	726.0(3)	948.4(7)	1142.2(6)
Z	2	2	2
ρ_{calc}, g/cm^3	2.296	1.954	1.786
T, °C	-100	-100	-100
μ(Mo Kα), mm^{-1}	2.326	1.791	1.496
total no. of data	6200	6697	10171
no. of unique data	1718	1665	5173
no. of params	106	120	275
R (%)[a]	2.70	2.50	3.42
wR^2 (%)[b]	5.28	6.51	7.18

[a] $R = \Sigma||F_o|-|F_c||/\Sigma|F_o|$, [b] $wR^2 = \{w(F_o^2-F_c^2)^2/\Sigma[w(F_o^2)^2]\}^{1/2}$

Table 4.4. Selected bond distances and angles for **8**, **9**, and **10**.[a]

Compound	Distances	(Å)	Angles	(deg)
8	Rh1-O1	2.037(2)	O1-Rh1-Rh1A	87.21(6)
	Rh1-O2	2.037(2)	O2-Rh1-Rh1A	85.62(6)
	Rh1-O3	2.035(2)	O3-Rh1-Rh1A	87.68(6)
	Rh1-O4	2.033(2)	O4-Rh1-Rh1A	85.21(6)
	Rh1-N1	1.947(3)	O1-Rh1-N1	96.1(1)
	Rh1-Rh1A	2.5134(8)	O2-Rh1-N1	91.0(1)
	N1-O5	1.147(3)	O3-Rh1-N1	97.0(1)
			O4-Rh1-N1	90.0(1)
			N1-Rh1-Rh1A	174.19(9)
			O5-N1-Rh1	121.0(2)
9	Rh1-O1	2.035(2)	O1-Rh1-Rh1A	84.96(6)
	Rh1-O2	2.039(2)	O2-Rh1-Rh1A	87.73(5)
	Rh1-O3	2.036(2)	O3-Rh1-Rh1A	87.44(5)
	Rh1-O4	2.035(2)	O4-Rh1-Rh1A	85.17(5)
	Rh1-N1	1.951(3)	O1-Rh1-N1	89.98(9)
	Rh1-Rh1A	2.512(2)	O2-Rh1-N1	97.32(9)
	N1-O5	1.150(3)	O3-Rh1-N1	95.38(9)
			O4-Rh1-N1	91.98(9)
			N1-Rh1-Rh1A	174.22(8)
			O5-N1-Rh1	120.8(2)
10	Rh1-O1	2.036(2)	O1-Rh1-Rh1A	87.32(7)
	Rh1-O2	2.035(2)	O2-Rh1-Rh1A	85.42(7)
	Rh1-O3	2.037(2)	O3-Rh1-Rh1A	86.72(7)
	Rh1-O4	2.034(2)	O4-Rh1-Rh1A	86.05(7)
	Rh1-N1	1.945(3)	O1-Rh1-N1	96.7(1)
	Rh1-Rh1A	2.5151(8)	O2-Rh1-N1	90.5(1)
	N1-O5	1.131(4)	O3-Rh1-N1	92.9(1)
			O4-Rh1-N1	94.4(1)
			N1-Rh1-Rh1A	175.91(9)
			O5-N1-Rh1	122.7(3)
	Rh2-O6	2.037(2)	O6-Rh2-Rh2A	87.63(7)
	Rh2-O7	2.032(2)	O7-Rh2-Rh2A	85.19(7)
	Rh2-O8	2.030(2)	O8-Rh2-Rh2A	85.40(7)
	Rh2-O9	2.035(2)	O9-Rh2-Rh2A	87.36(7)
	Rh2-N2	1.958(3)	O6-Rh2-N2	94.9(1)
	Rh2-Rh2A	2.5191(9)	O7-Rh2-N2	92.3(1)
	N2-O10	1.146(4)	O8-Rh2-N2	90.4(1)
			O9-Rh2-N2	96.8(1)
			N2-Rh2-Rh2A	175.1(1)
			O10-N2-Rh2	121.1(3)

[a]Numbers in parentheses are estimated standard deviations of the last significant figure. Atoms are labeled as indicated in Figures 2 and 3.

Table 4.5. Atomic coordinates (x 10^4) and equivalent isotropic displacement parameters (Å^2x 10^3) for [Rh$_2$(O$_2$CMe)$_4$(Ds-im)$_2$]·2(CHCl$_3$) (6·2CHCl$_3$). U(eq) is defined as one third of the trace of the orthogonalized U^{ij} tensor.

	x	y	z	U(eq)
Rh(1)	5521(1)	9526(1)	5639(1)	21(1)
S(1)	6611(1)	7726(1)	9143(1)	27(1)
O(1)	7479(3)	9174(3)	5078(2)	27(1)
O(2)	3506(3)	9917(3)	6124(2)	25(1)
O(3)	4543(3)	7446(3)	5120(2)	26(1)
O(4)	6444(3)	11655(3)	6079(2)	30(1)
N(2)	6765(4)	7866(4)	8105(2)	22(1)
O(6)	7836(3)	6870(3)	9413(2)	35(1)
C(3)	5920(5)	8666(5)	7566(3)	26(1)
N(1)	6449(4)	8613(4)	6835(2)	25(1)
O(5)	6640(4)	9223(3)	9498(2)	37(1)
C(5)	7917(5)	7312(5)	7684(3)	28(1)
C(10)	2721(5)	4605(4)	8876(2)	24(1)
C(4)	7680(5)	7787(4)	6904(3)	26(1)
C(2)	7549(5)	9495(4)	4324(3)	25(1)
N(3)	631(4)	2505(4)	8577(2)	32(1)
C(1)	3807(5)	7291(5)	4381(3)	26(1)
C(6)	4710(5)	6775(4)	9155(2)	26(1)
C(15)	2232(5)	3083(5)	8554(3)	27(1)
C(7)	3663(5)	7597(5)	9507(3)	33(1)
C(11)	4308(5)	5241(5)	8835(3)	26(1)
C(9)	1695(5)	5467(5)	9265(3)	28(1)
C(12)	5369(5)	4338(5)	8493(3)	34(1)
C(14)	3310(5)	2243(5)	8248(3)	35(1)
C(8)	2137(5)	6912(5)	9573(3)	33(1)
C(16)	319(6)	891(5)	8612(3)	44(1)
C(13)	4864(5)	2874(5)	8218(3)	39(1)
Cl(3)	1864(1)	7301(2)	7390(1)	44(1)
Cl(1)	748(1)	6724(2)	5606(1)	48(1)
Cl(2)	2705(3)	4734(2)	6450(1)	88(1)
C(17)	2304(5)	6580(5)	6398(3)	34(1)
C(18)	8978(5)	9164(5)	3930(3)	32(1)
C(19)	3209(6)	5739(5)	4008(3)	37(1)
C(20)	-531(5)	3059(6)	7984(3)	44(1)

Table 4.6. Atomic coordinates (x 10^4) and equivalent isotropic displacement parameters (Å^2x 10^3) for [Rh$_2$(O$_2$CMe)$_4$(Ds-pip)$_2$] (7). U(eq) is defined as one third of the trace of the orthogonalized U^{ij} tensor.

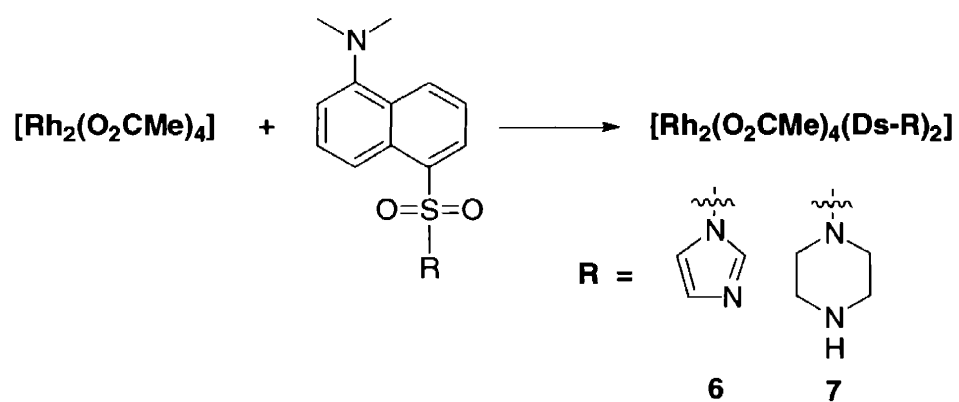|	x	y	z	U(eq)
Rh(1)	-61(1)	10072(1)	4028(1)	22(1)
S(1)	2578(2)	9167(2)	620(2)	43(1)
N(1)	-322(6)	10195(4)	2171(5)	43(2)
O(1)	474(4)	11250(3)	4285(4)	34(1)
O(3)	-1764(4)	10489(3)	3893(4)	30(1)
O(4)	1645(4)	9659(3)	4280(3)	31(1)
O(2)	-594(4)	8901(3)	3894(4)	33(1)
C(1)	4080(6)	8372(4)	2391(5)	28(2)
N(2)	1545(5)	9525(4)	1231(4)	33(2)
O(6)	2146(4)	8417(4)	137(4)	57(2)
O(5)	2858(4)	9791(4)	-74(4)	58(2)
C(2)	-2167(6)	10561(4)	4779(6)	31(2)
C(3)	3925(6)	9024(5)	1616(6)	36(2)
C(4)	5135(6)	8354(5)	3212(6)	36(2)
C(5)	519(7)	10708(5)	1734(6)	44(2)
C(6)	5874(7)	9524(5)	2386(7)	48(2)
N(3)	6316(6)	7765(4)	4904(6)	52(2)
C(7)	4811(6)	9586(4)	1622(6)	39(2)
C(8)	778(6)	8973(4)	1707(6)	36(2)
C(9)	5312(7)	7746(5)	4038(7)	41(2)
C(10)	-424(6)	9383(5)	1593(6)	38(2)
C(11)	1736(7)	10305(4)	1814(6)	42(2)
C(12)	4474(8)	7116(5)	3953(7)	58(3)
C(13)	6041(6)	8940(5)	3156(6)	37(2)
C(14)	-3380(6)	10958(5)	4677(6)	44(2)
C(15)	3451(8)	7116(5)	3099(8)	53(2)
C(16)	3226(7)	7706(5)	2352(7)	47(2)
C(17)	6385(7)	8463(6)	5645(6)	65(3)
C(18)	6594(8)	7021(6)	5507(8)	91(4)
C(19)	805(6)	12415(4)	5422(6)	49(2)
C(20)	613(6)	11519(4)	5260(7)	34(2)

Table 4.7. Atomic coordinates (x 10^4) and equivalent isotropic displacement parameters (Å^2x 10^3) for [Rh$_2$(O$_2$CMe)$_4$(NO)$_2$] (**8**). U(eq) is defined as one third of the trace of the orthogonalized U^{ij} tensor.

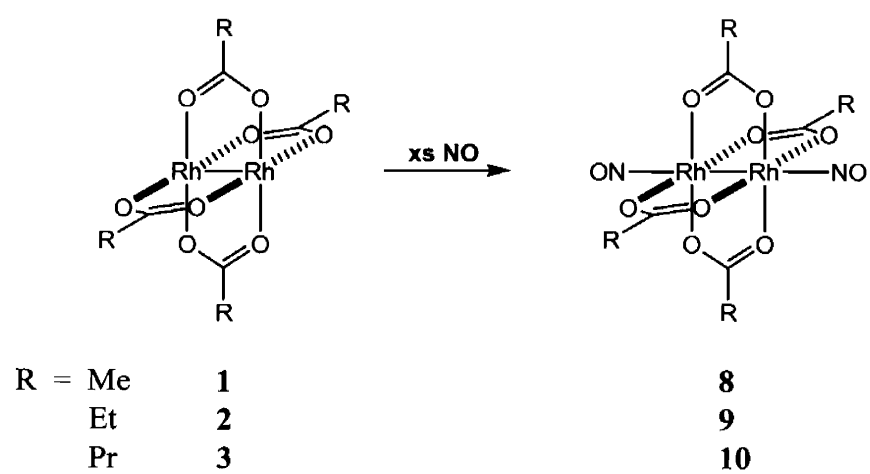|	x	y	z	U(eq)
Rh(1)	3750(1)	10270(1)	8444(1)	16(1)
O(5)	2653(4)	11255(2)	5367(3)	43(1)
O(1)	2026(3)	10876(2)	9236(3)	21(1)
O(3)	2602(3)	8654(2)	8099(3)	21(1)
O(2)	5741(3)	9632(2)	7975(3)	22(1)
O(4)	5150(3)	11823(2)	9098(3)	21(1)
N(1)	2028(4)	10778(3)	6045(3)	28(1)
C(1)	2632(4)	10801(3)	10823(4)	20(1)
C(2)	3403(4)	7953(3)	9364(4)	20(1)
C(3)	1308(5)	11274(3)	11331(4)	26(1)
C(4)	2592(5)	6755(3)	9049(5)	31(1)

Table 4.8. Atomic coordinates (x 10^4) and equivalent isotropic displacement parameters (Å^2x 10^3) for [Rh$_2$(O$_2$CEt)$_4$(NO)$_2$] **(9)**. U(eq) is defined as one third of the trace of the orthogonalized U^{ij} tensor.

	x	y	z	U(eq)
Rh(1)	11024(1)	52(1)	6360(1)	24(1)
O(4)	9994(2)	1472(1)	6304(2)	32(1)
O(2)	9038(2)	-557(1)	6899(2)	31(1)
O(1)	12787(2)	648(1)	5543(2)	33(1)
O(3)	11844(2)	-1383(1)	6130(2)	32(1)
C(4)	8838(3)	1838(2)	5121(3)	29(1)
C(1)	7588(3)	-781(2)	5851(3)	30(1)
C(2)	6143(4)	-1227(3)	6274(3)	50(1)
C(3)	6624(4)	-1547(3)	7875(4)	52(1)
N(1)	12726(3)	249(2)	8415(3)	38(1)
O(5)	13586(4)	972(2)	8740(3)	76(1)
C(5)	8205(4)	2901(2)	5229(3)	36(1)
C(6)	7793(7)	3519(3)	3827(4)	86(2)

Table 4.9. Atomic coordinates (x 10^4) and equivalent isotropic displacement parameters (Å^2x 10^3) for [Rh$_2$(O$_2$CPr)$_4$(NO)$_2$] (**10**). U(eq) is defined as one third of the trace of the orthogonalized U^{ij} tensor.

	x	y	z	U(eq)
Rh(1)	4727(1)	6142(1)	10404(1)	23(1)
O(4)	5302(3)	6690(2)	9260(2)	28(1)
O(3)	4196(3)	5357(2)	11463(2)	27(1)
O(2)	7226(3)	6593(2)	11250(2)	28(1)
O(1)	2270(3)	5444(2)	9492(2)	30(1)
N(1)	4471(4)	7940(3)	11095(2)	31(1)
C(1)	8183(4)	5755(4)	11118(3)	29(1)
C(2)	5695(4)	5859(4)	8580(3)	26(1)
O(5)	5013(4)	8424(3)	11958(2)	52(1)
C(3)	10031(4)	6207(4)	11747(3)	34(1)
C(4)	6049(5)	6344(4)	7751(3)	31(1)
C(5)	6518(5)	7863(4)	8010(3)	36(1)
C(6)	10537(5)	7951(4)	10885(3)	45(1)
C(7)	10716(5)	7686(4)	11900(3)	38(1)
C(8)	6674(5)	8281(4)	7095(3)	40(1)
Rh(2)	8635(1)	4482(1)	5064(1)	26(1)
O(6)	7562(3)	5890(2)	4493(2)	33(1)
O(9)	8109(3)	3249(2)	3602(2)	32(1)
O(7)	9978(3)	3184(2)	5619(2)	32(1)
N(2)	6613(4)	3712(3)	5290(2)	37(1)
O(10)	6694(4)	3492(3)	6044(2)	53(1)
C(9)	11541(5)	3251(4)	5716(3)	30(1)
C(13)	12389(5)	2194(4)	6083(3)	39(1)
C(14)	12340(7)	1016(4)	5159(3)	56(1)
C(16)	13121(7)	-101(5)	5484(4)	70(2)
O(8)	9442(3)	5808(2)	6510(2)	29(1)
C(10)	8659(5)	2478(3)	2036(3)	31(1)
C(11)	8097(5)	999(4)	1884(3)	39(1)
C(12)	9146(4)	3371(3)	3125(3)	28(1)
C(15)	7521(5)	184(4)	760(3)	47(1)

$[Rh_2(O_2CMe)_4]$ + $\longrightarrow$ $[Rh_2(O_2CMe)_4(Ds\text{-}R)_2]$

R =

6   7

Scheme 4.1.

$$R = \text{Me} \quad \mathbf{1} \qquad\qquad \mathbf{8}$$
$$\text{Et} \quad \mathbf{2} \qquad\qquad \mathbf{9}$$
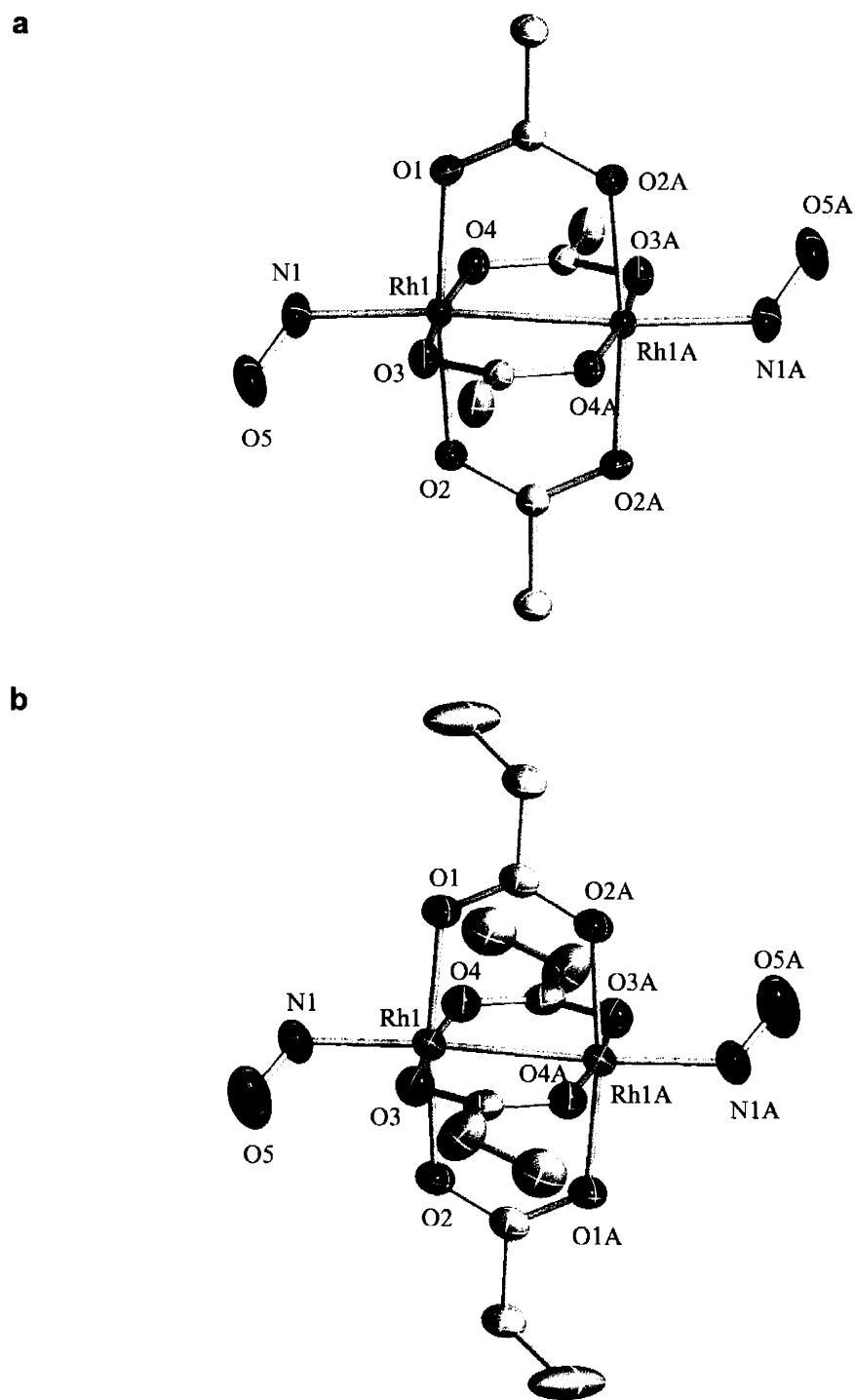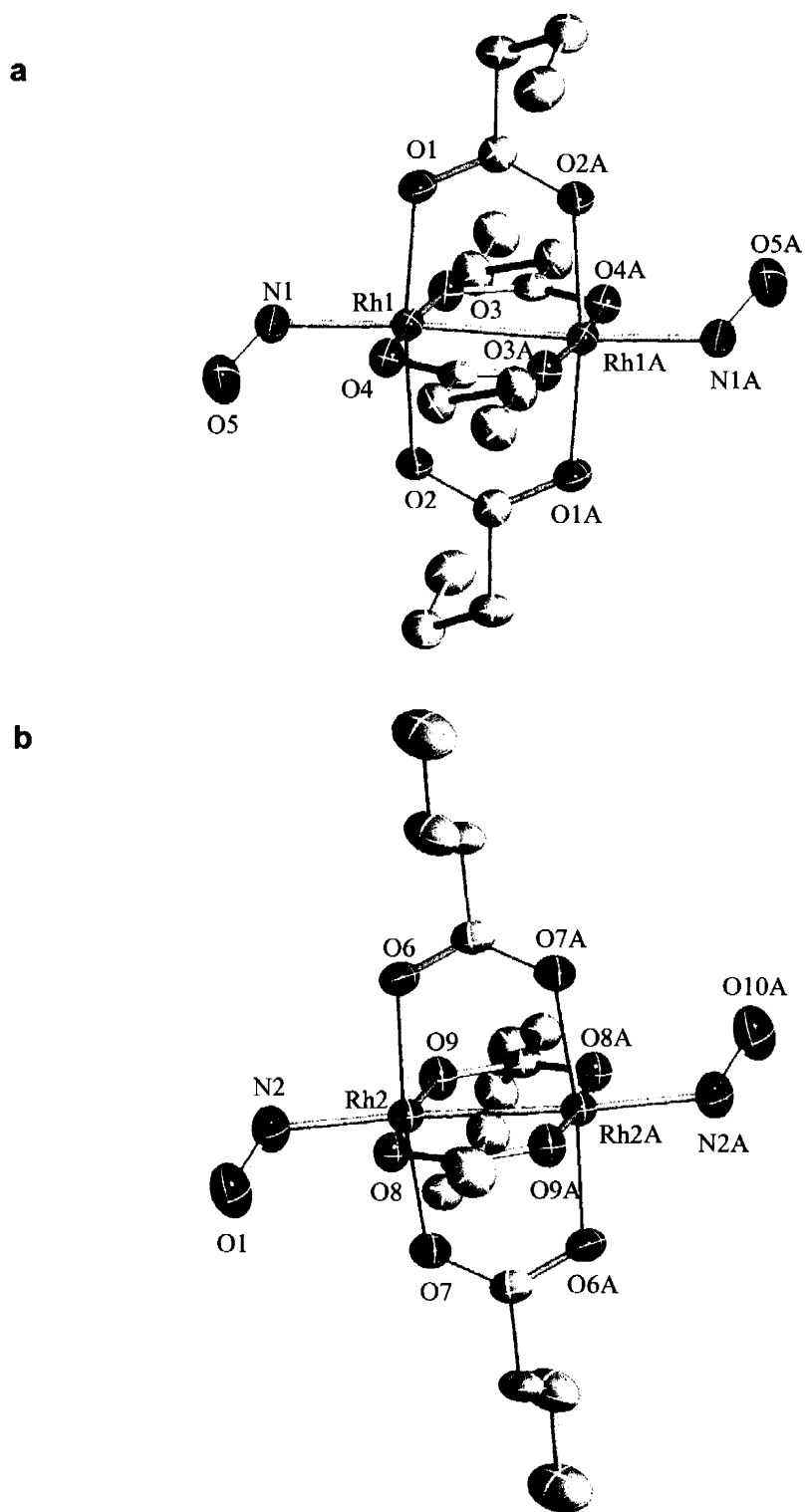$$\text{Pr} \quad \mathbf{3} \qquad\qquad \mathbf{10}$$
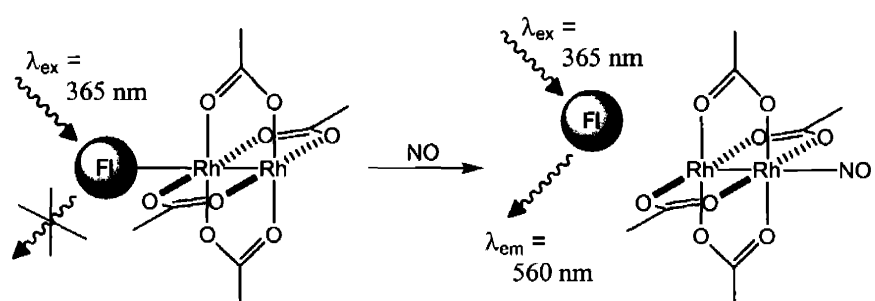
Scheme 4.2.

Scheme 4.3.

Figure 4.1. ORTEP diagrams showing 50% probability thermal ellipsoids and selected atom labels for (a) [Rh₂(O₂CMe)₄(Ds-im)₂] (**6**) and (b) [Rh₂(O₂CMe)₄(Ds-pip)₂] (**7**).

Figure 4.1. ORTEP diagrams showing 50% probability thermal ellipsoids and selected atom labels for (a) $[Rh_2(O_2CMe)_4(Ds\text{-}im)_2]$ (**6**) and (b) $[Rh_2(O_2CMe)_4(Ds\text{-}pip)_2]$ (**7**).

Figure 4.2. ORTEP diagrams showing 50% probability thermal ellipsoids and selected atom labels for (a) [Rh₂(O₂CMe)₄(NO)₂] (**8**) and (b) [Rh₂(O₂CEt)₄(NO)₂] (**9**).

Figure 4.3. ORTEP diagrams showing 50% probability thermal ellipsoids and selected atom labels for the two unique molecules of [Rh₂(O₂CEt)₄(NO)₂] (**10**) from the single crystal X-ray data.
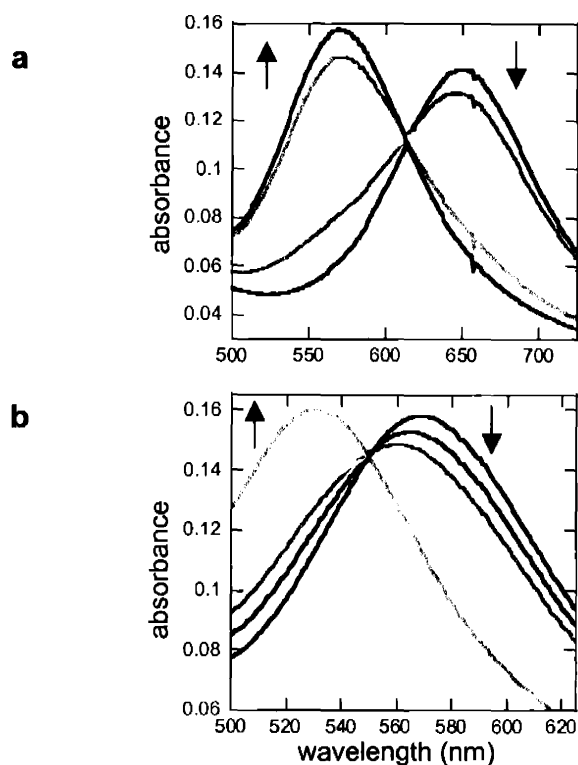
Figure 4.4. Absorbance spectra for the titration of 50 μM [Rh$_2$(O$_2$CMe)$_4$] (**1**) with dansyl-piperazine (**5**) in DCE at 25.0±0.1° C. As **5** is added to **1**, as shown in **a**, the initial absorbance maximum at 648 nm decreases as a new feature at 568 nm, which corresponds to the 1:1 adduct forms. In **a**, starting with the first trace with an absorbance maximum at 648 nm, the traces correspond to 0, 5, 10, 15, 20, 25, 30, 35, and 45 μM **5**. In **b**, after additional aliquots of **5** are administered, the 568 nm absorbance is replaced by a third feature at 530 nm that indicates formation of [Rh$_2$(O$_2$CMe)$_4$(Ds-pip)$_2$] (**7**). Starting with the 568 nm absorbance maximum trace the spectra correspond to 50, 60, 70, 80, 90, 100, 150, 200, and 250 μM **5**.
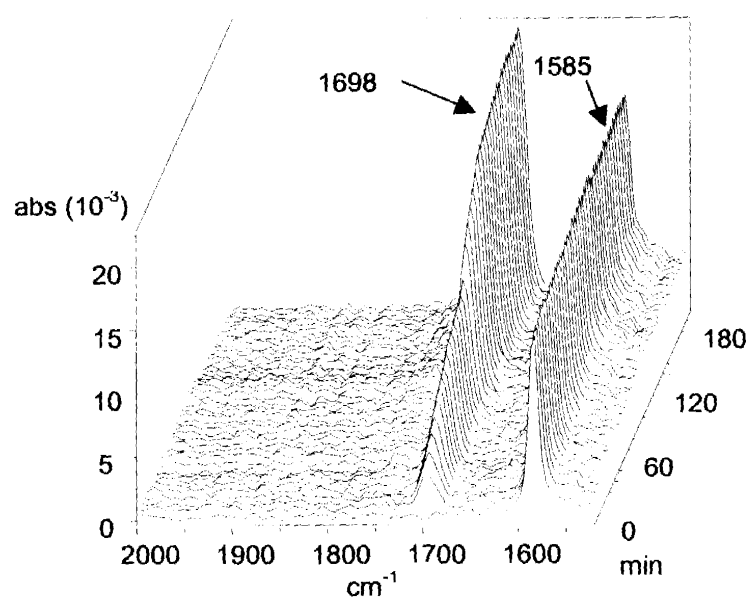
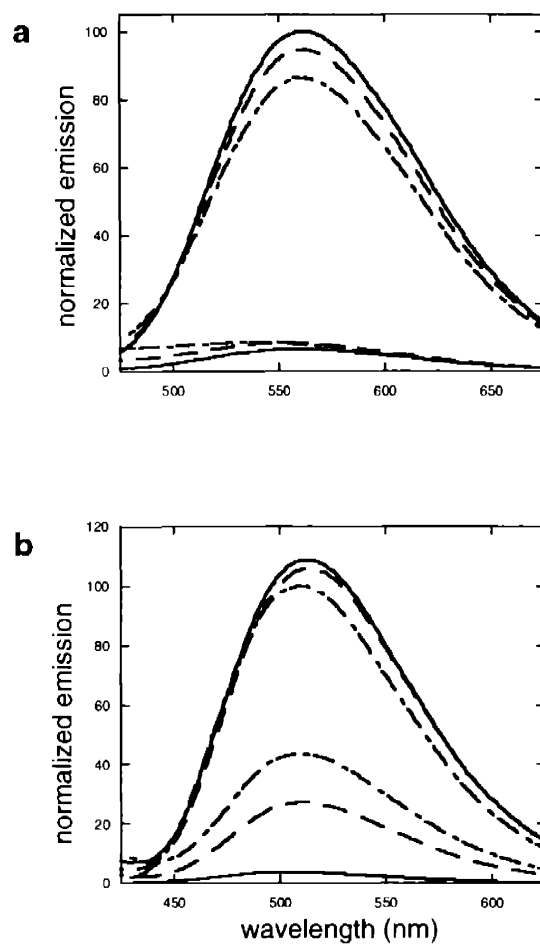**Figure 4.5.** Solution IR spectra of the reaction of [Rh$_2$(O$_2$CPr)$_4$] with NO in DCE at room temperature. The first aliquot of 1 equiv NO was added at t = 0 min and a second equiv was added at t = 60 min.
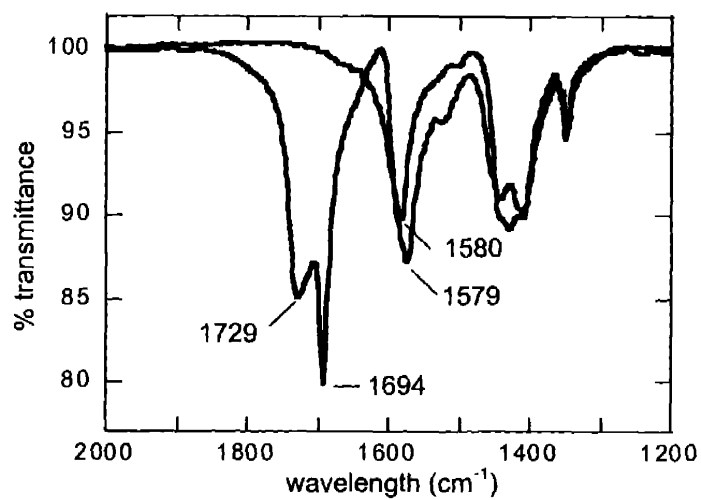
Figure 4.6. IR spectra (KBr) of [Rh₂(O₂CMe)₄(NO)₂] (**8**), blue trace, and [Rh₂(O₂CMe)₄] (**1**), red trace, formed by allowing a DCE solution of **8** to stand in air.

Figure 4.7. Fluorescence emission intensity spectra showing the reversible fluorescence response of 10 μM Ds-im and 40 μM [Rh$_2$(O$_2$CMe)$_4$] (a) and 10 μM Ds-pip with 20 μM [Rh$_2$(O$_2$CMe)$_4$] (b) in DCE. The upper set of solid, dashed, and dashed-dot lines are after the first, second and third additions of 100 equiv of NO, respectively. The lower set of corresponding lines are before admission of NO and after the first and second 30 min Ar purges. Excitation is at 365 nm for the Ds-im system and 350 nm for the Ds-pip system.
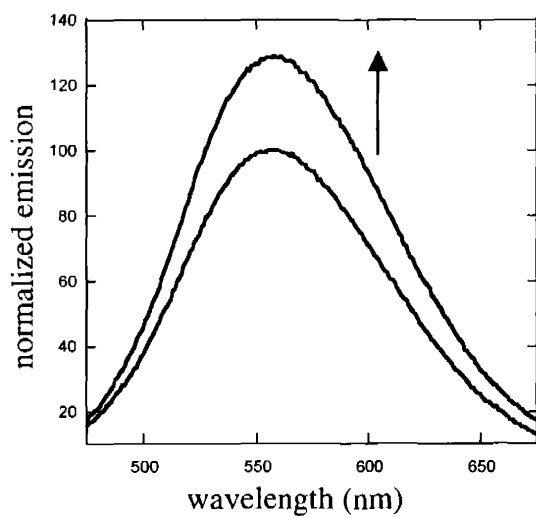
Figure 4.8. Fluorescence spectra of 10 μM Ds-im (**4**) and 40 μM [Rh₂(O₂CMe)₄] (**1**) in DCE after exposure to 1 equiv of NO showing a 27% increase in integrated fluorescence emission intensity.
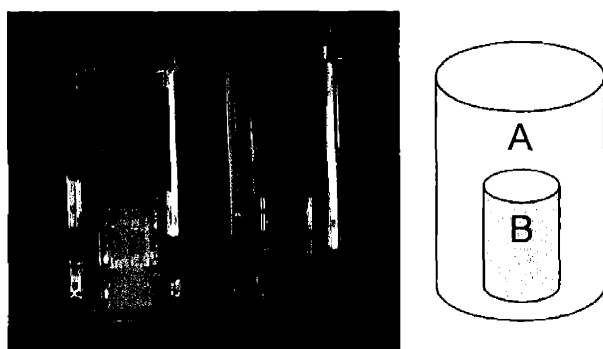
Figure 4.9. Left: a photo monitoring the fluorescence response in the reaction of [Rh₂(O₂CMe)₄(Ds-pip)] and NO. Vials from left to right: saturated aqueous NO solution and aqueous control. Right: experimental apparatus with the Silastic© membrane separating vial A and B. Vial B contains 15 mL aqueous solution saturated with NO, and vial B contains a DCE solution of 40 μM [Rh₂(O₂CMe)₄] and 20 μM Ds-pip.

Scott Hilderbrand

OBJECTIVE

A research position with an emphasis on creativity where I can use my background in inorganic chemistry and gain exposure to new research areas.

HIGHLIGHTS

- Highly knowledgeable of fluorescence-based sensor technologies for small molecule analytes
- Skilled with air-sensitive inorganic and multi-step organic synthesis
- Extensive experience in nitric oxide handling, purification, and reactivity with transition metal complexes

EDUCATION

Massachusetts Institute of Technology, Cambridge, MA
Ph.D., Inorganic Chemistry, degree expected February, 2004
Thesis title: "Fluorescence-Based Detection Methodologies for Nitric Oxide using Transition Metal Scaffolds"
Advisor: Professor Stephen J. Lippard

New College of Florida, Sarasota, FL
B.A., Chemistry, 1998
Thesis title: "Magnesium Complexes of 1,4,7-Triazacyclononane-N-acetate as Models for the Active Site of RuBisCO"
Advisor: Associate Professor Suzanne E. Sherman

RESEARCH EXPERIENCE

1998-Present   Research Assistant, Massachusetts Institute of Technology
                Advisor: Professor Stephen J. Lippard

- Developed new asymmetric fluoresceins for use as building blocks to prepare fluorescent sensors
- Designed and synthesized new air-stable mono- and di-nuclear fluorophore-containing metal complexes for use as nitric oxide sensors
- Mounted single crystals on an X-ray diffractometer and solved crystal structures routinely
- Performed system administration and maintenance on a cluster of SGI, Linux, and Windows NT workstations

1997-1998   Undergraduate Research Assistant, New College of Florida
                Advisor: Associate Professor Suzanne E. Sherman

- Prepared small molecule magnesium complexes and investigated their ability to mimic reactivity observed at the active site of RuBisCO
- Monitored reaction kinetics by ^{1}H NMR

1997   Summer REU (Research Experiences for Undergraduates) Research Assistant, University of Utah
                Supervisor: Professor Peter J. Stang

- Prepared icosahedral supra-molecular cages
- Modeled supra-molecular cages with Spartan on SGI workstations

1994, 1995   Summer Intern, University of Missouri
                Supervisor: Professor William Folk

- Developed protein purification protocols

ADDITIONAL EXPERIENCE

2002-2003   Undergraduate Research Supervisor, Massachusetts Institute of Technology
                Supervised two undergraduate students performing research directed towards development of nitric oxide sensors.

1998-1999	Teaching Assistant, Massachusetts Institute of Technology Laboratory instructor in general chemistry and recitation instructor in general chemistry
1996	Teaching Assistant, New College of Florida Laboratory instructor in general and organic chemistry

ACADEMIC SCHOLARSHIPS AND AWARDS

1994-1998	New College Foundation Scholarship
1994-1998	Out-of-State Tuition Award

AFFILIATIONS

American Chemical Society

PUBLICATIONS, PATENTS, AND PRESENTATIONS

Hilderbrand, S. A.; Lim, M. H.; Lippard, S. J. Dirhodium Tetracarboxylate Scaffolds as Reversible Fluorescence-Based Nitric Oxide Sensors. *J. Am. Chem. Soc.* Submitted.

Hilderbrand, S. A.; Lippard, S. J. Carboxylate-Bridged Dimetallic Complexes as Potential Nitric Oxide Sensors. *Inorg. Chem.* Manuscript in preparation.

Hilderbrand, S. A.; Lippard. S. J. Cobalt Chemistry with Mixed Aminotroponimine Salicylaldimine Ligands: Synthesis, Characterization and Nitric Oxide Reactivity. *Inorg. Chem.* Manuscript in preparation.

Hilderbrand, S. A.; Lippard, S. J. Dinuclear Transition-Metal Complexes as Nitric Oxide Sensors. Presented at the 225th ACS National Meeting, New Orleans, LA, USA, March 23-27, 2003; Oral Presentation INOR-870.

Lippard, S. J.; Hilderbrand, S. A. Coordination Complexes for Detecting Analytes, and Methods of Making and Using the Same. US Pat. Appl. 20030068275, Aug. 27, 2002.

Lippard, S. J.; Burdette, S.; Hilderbrand, S.; Tsien, R. Y.; Walkup, G. K. Fluorescein-Based Metal Sensors and Methods of Making and Using the Same. US Pat. Appl. 20020106697, July 9, 2001.

Odom, D.; Gramer, C. J.; Young, V. G.; Hilderbrand, S. A.; Sherman, S. E. Synthesis and Characterization of Magnesium and Zinc Complexes of 1,4,7-Triazacyclononane-N-acetate. Potential Models for the Active Site of RuBisCO. *Inorg. Chim. Acta.* **2000**, 297, 404-410.

REFERENCES

Professor Stephen J. Lippard
Department of Chemistry
Massachusetts Institute of Technology
Cambridge, MA 02139
(617) 253-1892
lippard@lippard.mit.edu

Professor Alan Davison
Department of Chemistry
Massachusetts Institute of Technology
Cambridge, MA 02139
(617) 253-1794
adavison@mit.edu

Associate Professor Suzanne E. Sherman
Division of Natural Sciences
New College of Florida
Sarasota, FL 34243
(941) 359-4376
sherman@ncf.edu